DOE/CE/90029---8

DE92 016597

HEAT TRANSFER AND PRESSURE DROP FOR AIR FLOW THROUGH ENHANCED PASSAGES

FINAL REPORT
FHMT REPORT No. 007

N. T. Obot and E. B. Esen
Fluid Mechanics, Heat and Mass Transfer Laboratory
Clarkson University
Potsdam, New York 13676-5705

JUNE 1992

Prepared for

THE U.S. DEPARTMENT OF ENERGY
AGREEMENT NO. DE-FG02-89CE90029.A000

SUMMARY

An extensive experimental investigation was carried out to determine the pressure drop and heat transfer characteristics for laminar, transitional and turbulent flow of air through a smooth passage and twenty-three enhanced passages. The internal surfaces of all enhanced passages had spirally shaped geometries; these included fluted, finned/ribbed and indented surfaces. The Reynolds number (Re) was varied between 400 and 50000.

The effect of heat transfer (wall cooling or fluid heating) on pressure drop is most significant within the transition region; the recorded pressure drop with heat transfer is much higher than that without heat transfer. The magnitude of this effect depends markedly on the average surface temperature and, to a lesser extent, on the geometric characteristics of the enhanced surfaces. When the pressure drop data are reduced as values of the Fanning friction factor (f), the results are about the same with and without heat transfer for turbulent flow, with moderate differences in the laminar and transition regions.

For any enhanced passage, the friction factor and the nondimensional heat transfer coefficient (Nusselt number, Nu) are, respectively, no more than 4.5 and 3 times the corresponding values for the smooth passage. In laminar flow, the largest increases in both friction factor and Nusselt number over the smooth tube values are obtained with passages of the spirally fluted type. Within the transition region and in turbulent flow, a straightforward comparison between the smooth tube and any enhanced passage is complicated by the transition process.

In laminar flow, the nondimensional heat transfer coefficient (Nu) is proportional to the square-root of the Reynolds number (Re); the friction factor is inversely proportional to Re for all passages. Based on these findings, an analogy between friction and heat transfer is developed. Explicit relationships between f and Nu are formulated for laminar flow as well as for the transition and turbulent regimes. The reduced forms of these relations afford direct calculations of the Nusselt number for smooth and enhanced passages from the friction factor data, provided the critical parameters f_c, Nu_c and Re_c at the onset of transition to turbulent flow are known. The relationship between the

critical parameters is given by $Nu_c/(Re_c^{3/2} f_c) = 0.0075$ for all passages, with errors that are within 12%.

The *frictional law of corresponding states* is validated conclusively for smooth and enhanced passages. Several forms of the reduced correlations are presented and discussed. In particular, it is established that the reduced friction factor-heat transfer relation for turbulent flow is in complete agreement with the well known Reynolds analogy. These predictive equations give errors that, for the most part, under $\pm 10\%$ for laminar flow, and under $\pm 20\%$ for both transitional and turbulent flow.

At the same reduced conditions, that account for variations in the critical parameters at the onset of transition to turbulence, the thermal performance (defined as the increase in nondimensional heat transfer coefficient over that for frictional pressure coefficient) is unity in laminar flow. This is a clear indication that the best thermal performance is obtained in laminar flow under dynamically similar conditions. For transitional and turbulent flow, the performance index is practically constant at a value close to unity or decreases with increasing similarity parameter (Re_m), depending on the geometric characteristics of the enhanced surface.

Table of Contents

List of Figures

List of Tables

Nomenclature

A_h	=	heat transfer area, $\pi D_i L_h$, m^2
A_x	=	cross-sectional flow area, m^2
C_f	=	friction parameter, $f \times Re$
$C_{f,m}$	=	reduced friction parameter, $f_m \times Re_m$
C_h	=	heat transfer parameter, $Nu/Re^{1/2}$
$C_{h,m}$	=	reduced heat transfer parameter, $Nu_m/Re_m^{1/2}$
C_p	=	specific heat, J/kg°C
D_i	=	maximum internal diameter, m
D_h	=	hydraulic diameter, $4A_x/P_w$, m
e	=	roughness height, m
e^+	=	roughness Reynolds number, $(e/D_i)Re(f_e/2)^{1/2}$
f	=	Fanning friction factor, $\Delta p \rho_w A_x^2 D_i / 2\dot{m}^2 L_p$
f_m	=	reduced friction factor, $\psi_f f_a$
$\bar{h}$	=	average heat transfer coefficient, $W/m^2°C$
k_b	=	fluid thermal conductivity at T_b, W/m°C
L_e	=	smooth entrance length, m
$L_{e,r}$	=	rough entrance length, m
L_h	=	length of heated section, m
L_p	=	distance between pressure taps, m
l	=	lead, pN_s, m
$\dot{m}$	=	mass flow rate, kg/s
N_s	=	number of starts, $\pi D_i / p tan\alpha$
Nu	=	Nusselt number, $\bar{h} D_i / k_b$
Nu_m	=	reduced Nusselt number, $\psi_N Nu_a$
p	=	roughness pitch, m
Pr	=	Prandtl Number, $\mu C_p / k_b$
P_w	=	wetted perimeter, m
Δp	=	pressure drop, Pa
Δp_w	=	pressure drop without heat transfer, Pa

Δp_{wh}	=	pressure drop with heat transfer, Pa
Q_L	=	total electrical power without flow at T_w, W
Q_T	=	total electrical power with flow at T_w, W
Re	=	Reynolds number, $4\dot{m}/\pi D_i\mu$
Re_m	=	similarity parameter or reduced Reynolds Number, $\psi_R Re_a$
St	=	Stanton number, $\bar{h}/\rho C_p \overline{V}$
St_m	=	reduced Stanton number, $Nu_m/Re_m Pr$
T	=	temperature, °C
T_b	=	bulk mean temperature, $(T_i + T_o)/2$, °C
T_w	=	average surface temperature, °C
t	=	wall thickness, m
$\overline{V}$	=	average flow velocity, m/s

Greek Symbols

α	=	helix angle, degrees
ϵ_m	=	efficiency index at reduced conditions, $(Nu_m/Nu_s)/(f_m/f_s)$
η	=	efficiency index, $(Nu_e/Nu_s)/(f_e/f_s)$
μ	=	fluid viscosity, Pa-s
ρ_w	=	fluid density evaluated at T_w, kg/m^3
ψ_f	=	ratio of critical friction factor, $f_{c,r}/f_{c,a}$
ψ_N	=	ratio of critical Nusselt number, $Nu_{c,r}/Nu_{c,a}$
ψ_R	=	ratio of critical Reynolds number, $Re_{c,r}/Re_{c,a}$

Additional Subscripts

a	=	arbitrary condition
c,a	=	critical parameters for arbitrary condition
c,r	=	critical parameters for reference condition

e	=	enhanced passage
i	=	condition at inlet to test section
o	=	condition at test section exit
s	=	smooth passage

1. INTRODUCTION

The subject of friction and heat transfer enhancement is a very active one and extensive experimental studies on the pressure drop and heat transfer characteristics for a wide range of enhanced surface geometries have been published by numerous researchers. Reviews of the widespread literature have been carried out recently (Reay, 1991; Obot *et al.* 1990a,b; Rabas, 1988; Webb, 1987; Ravigururajan and Bergles, 1986). It is of general knowledge that varying amounts of pressure drop and heat transfer increases can be realized with enhanced passages depending on the geometric characteristics of the surfaces.

Enhanced passages of simple as well as complicated design are available commercially. A search of the literature reveals very limited studies with these practical flow passages over the entire range of flow conditions extending from laminar through turbulent flow. For example, virtually all the studies with passages of the spirally fluted type were confined to turbulent flow (Yampolsky *et al.*, 1984; Panchal and France, 1986; Ravigururajan and Bergles, 1986). Similarly, for corrugated surfaces of single and multiple helix (Withers, 1980a,b) or three-dimensional spiral ribs (Takahashi *et al.*, 1985), pressure drop and heat transfer data were reported for turbulent flow. In general, limited experimental data on pressure drop and heat transfer in laminar flow and the transition region exist for enhanced passages (Marner and Bergles, 1978; Watkinson *et al.*, 1974; Koch, 1960; Nunner, 1956).

Most of the available data for smooth and enhanced tube friction factor were obtained in the absence of heat transfer. Of the studies that provided data with heat transfer, only few gave results for the laminar and transition regions (Marner and Bergles, 1978; Nunner, 1956). The results of Marner and Bergles for forge-fin tubes indicated a significant increase in friction factor due to wall cooling while the results for heating were 10-20% below those without heat transfer. Nunner found a negligible effect of heat transfer on turbulent friction factors, but the laminar results were higher than those obtained without heat transfer. For spirally fluted passages, limited pressure drop data were obtained with heat transfer (Ravigururajan and Bergles, 1986) and these were for turbulent flow. There is the need for a study of the effect of heat transfer on pressure

drop with the commercially available passages.

Besides the limited studies on the effect of heat transfer on pressure drop and the almost total neglect of the laminar and transition regions, the length scale used by previous investigators to reduce the pressure drop, flowrate and heat transfer data to nondimensional form has complicated a comparative evaluation of the data obtained on enhanced passages. For single-phase flow through smooth passages, it is customary to use the hydraulic diameter (D_h), defined as four times the flow area divided by the wetted perimeter. For enhanced passages of circular cross section, the hydraulic diameter is smaller than the maximum internal diameter of the passage due primarily to the increase in the wetted perimeter . Consequently, the use of D_h can result in enhanced tube friction factors and Nusselt numbers that are much lower than those for a smooth passage of comparable internal diameter, even though the actual enhanced tube pressure drop and heat transfer data may be considerably higher than those for a smooth passage (Yampolsky *et al.*, 1984; Watkinson *et al.*, 1974).

Although numerous studies on pressure drop and heat transfer for enhanced passages have been made for more than half a century, the mechanism whereby roughness affects surface friction or heat transfer is not well understood. Even the generally known fact that the increases in pressure drop due to roughness far exceed those for heat transfer has been open to speculation. In a recent study (Obot, 1988), it was demonstrated that the differences in friction factor between circular and noncircular smooth passages were the direct result of the inseparable effects of transition to turbulent flow and the length scale used to reduce the data. The results of subsequent studies (Obot *et al.*, 1990a,b; 1991a,b) suggest that there is some connection between transition and friction/heat transfer enhancement, supporting the need for a comprehensive investigation of the problem.

In summary, there is the need for experimental data for a wide range of enhancement geometries to fill the gaps in the existing literature; notably, laminar and transitional flow data are needed because these regions have received very meager treatment in the past. Also, detailed studies of the effect of heat transfer (i.e., wall heating or fluid cooling) on pressure drop, including its influence on transition to turbulent flow, are

needed for smooth and enhanced passages.

2. OBJECTIVES OF THE RESEARCH PROGRAM

Overall Objectives

1. To carry out an extensive and consistent experimental investigation of pressure drop and heat transfer for laminar, transitional and turbulent flow with smooth and internally enhanced passages.

2. To develop a general method that will aid data correlation as well as prediction, and to validate same using the present experimental data; both aspects of which will provide better understanding of the friction and heat transfer characteristics for smooth and enhanced passages.

The development of the general method, referred to as the *frictional law of corresponding states*, was given in Obot *et al.* (1990a,b). Preliminary verification of the frictional law was carried out using literature data. In this report, the experimental results obtained with air as the working fluid are presented and discussed. The validation of the *frictional law of corresponding states* is also given.

3. EXPERIMENTAL FACILITY AND TEST PROCEDURES

3.1 General Description of Apparatus.

The experimental facility is shown schematically in Fig. 1. The air is generated with a blower, metered by one of three rotameters and a calibrated nozzle designed according to ASME standards (1984). The air then passes through a smooth or enhanced flow passage that contains a test section. Located downstream of the test section is a mixing chamber. The pressure and temperature at the inlet to the rotameter are measured by a U-tube manometer and chromel-alumel thermocouple, respectively. The pressure drop

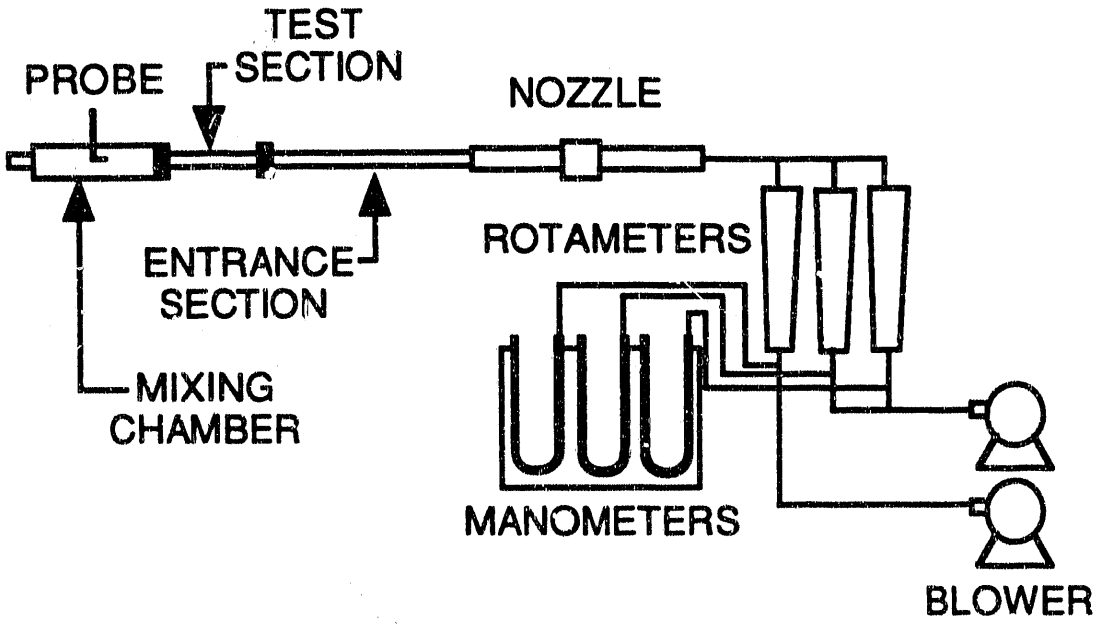

Fig. 1 Schematic of experimental facility.

across the nozzle and the air temperature downstream of the nozzle are measured with a pressure transducer and thermocouple, respectively. The mixing chamber is equipped with a thermocouple probe that can be used to traverse the duct cross-section to obtain average air temperature under heat transfer conditions.

3.2 General Description of Enhanced Passages.

Twenty-three enhanced passages and a smooth passage were tested in this study. The geometric characteristics of the smooth passage and the enhanced surfaces are given in Table 1, while Table 2 gives a summary of the test conditions. In the first column of Tables 1 and 2, S, GA, HC, W, and Y denote smooth, General Atomic, Hitachi Cable, Wieland-Werke AG, and IMI Yorkshire Alloy, respectively. The last four are the suppliers of the passages used in this study. A close-up photograph of all flow passages is given in Fig. 2.

In this study, the characteristic dimension in the definition of the nondimensional pressure drop, flowrate and heat transfer coefficient is the maximum internal diameter of the flow passages; the mean values determined in our laboratory are given in Tables 1 and 2. For helix angle, the values for the Hitachi tubes (HC-4 - HC-6) are the manufacturer's data; the values for the remaining passages were calculated from the relation $tan\alpha = \pi D_i/pN_s$, where p is the axial pitch and N_s is the number of starts.

It is evident from Tables 1 and 2 that the twenty-three enhanced passages have a common feature, that is, the internal surface geometries are spirally shaped. For each of the spirally fluted passages (GA-1 through GA-3, Y-22 and Y-23), the internal surface contour is basically the same as that on the outside surface. The HC-4 and the W-7 - W-13 passages are basically spirally ribbed surfaces. The latter are also referred to by the manufacturer as spirally finned passages, hence both terminologies are used interchangeably in this report.

The two Hitachi passages (H-5 and H-6) complement one another in that the the surface protrusions are cross-cut to provide multi-start three-dimensional spiral ribs. Details of the procedures used to generate these surface contours are given by Takahashi *et al.* (1985). Suffice it state here that the primary ribs form an angle α_1 with the tube

TABLE 1. Geometric Characteristics of the Flow Passages.

Tube	D_i (mm)	t (mm)	e (mm)	N_s	l (mm)	p (mm)	α (degrees)	e/D_i	p/e	Material	Roughness Description
S-0	13.39	1.2								Copper	Smooth
GA-1	21.45	0.7	0.95	20	82.0	4.1	39.4	0.044	4.3	Stainless Steel	Spirally fluted
GA-2	23.96	0.98	1.33	25	141	5.6	28.1	0.056	4.2	Stainless Steel	Spirally fluted
GA-3	28.49	1.89	1.58	31	160	5.2	29.2	0.055	3.3	Aluminum	Spirally fluted
HC-4	13.87	1.0	0.3	10	82.0	8.2	28.0	0.022	27.3	Copper	Spirally ribbed
HC-5	17.78	0.64	0.5 (0.3)	25 (25)	142.5 (93.0)	5.7 (3.7)	21.5 (-31.0)	0.028 (0.017)	11.4 (12.3)	Copper	3-D Spirally ribbed
HC-6	17.61	0.72	0.26 (0.14)	25 (25)	140.0 (92.1)	5.6 (3.7)	21.5 (-31)	0.015 (0.008)	21.5 (26.4)	Copper	3-D Spirally ribbed
W-7	14.10	1.07	0.42	1	2.2	2.2	87.2	0.030	5.2	Copper	Spirally ribbed
W-8	14.40	1.12	0.10	1	1.0	1.0	88.7	0.007	10.0	Copper	Spirally ribbed
W-9	15.90	1.52	0.5	41	102.5	2.5	26.0	0.032	5.0	Copper	Spirally ribbed
W-10	14.95	1.48	0.55	25	100.0	4.0	25.2	0.037	7.3	Copper	Spirally ribbed
W-11	14.45	1.49	0.45	20	76.0	3.8	30.9	0.031	8.5	Copper	Spirally ribbed
W-12	14.56	1.59	0.50	10	40.0	4.0	48.8	0.034	8.0	Copper	Spirally ribbed
W-13	14.45	1.50	0.51	25	120.0	4.8	20.7	0.035	9.4	Copper	Spirally ribbed
Y-14	12.68	1.08	0.38	3	15.0	5.0	69.4	0.030	13.2	Copper	Spirally indented
Y-15	19.16	1.24	1.27	3	30.0	10.0	63.5	0.066	7.9	Copper	Spirally indented
Y-16	19.53	1.23	0.51	3	30.0	10.0	63.9	0.026	19.6	Copper	Spirally indented
Y-17	24.22	1.67	0.31	3	15.0	5.0	78.8	0.013	16.1	Copper	Spirally indented
Y-18	18.81	1.66	0.36	3	7.6	2.6	82.7	0.019	7.2	Copper	Spirally indented
Y-19	22.88	1.04	1.5	6	19.8	3.3	74.6	0.066	2.2	K10	Spirally indented
Y-20	16.05	1.36	1.0	3	30.0	10.0	59.2	0.062	10.0	Copper	Spirally indented
Y-21	23.45	0.93	0.52	1(6)	6.0	6.0	85.3	0.022	11.5	K10	Spirally indented Doubly enhanced
Y-22	48.65	0.87	2.0	43	273.1	6.35	29.2	0.041	3.2	YAB	Spirally fluted
Y-23	47.67	1.29	2.96	25	277.5	11.1	28.4	0.062	3.8	Copper	Spirally fluted

TABLE 2. Test Conditions for the Flow Passages.

Tube	D_i (mm)	L_e (mm)	$L_{e,r}$ (mm)	L_h (mm)	L_p (mm)	A_h (mm^2)	A_x (mm^2)	L_e/D_i	$L_{e,r}/D_i$	L_h/D_i	L_p/D_i
S-0	13.39	2019			381		140.8	150.8			
		1969		458.0	381	19266		147.1		34.2	28.5
					1565.3		361.4				73.0
GA-1	21.45	254			1354.1			11.8			63.1
		1016			920.8			47.4			42.9
GA-2	23.96				1587.5		450.9				
		254			1343			10.6			56.1
		254			2773.4			8.9			97.3
GA-3	28.49	1089			920.75			38.2			32.3
		1089	38.1		838.2			38.2	1.3		29.4
			1524	381.0	304.8	34101	637.5		53.5	13.4	10.7
HC-4	13.87		1968.5	441.1	365.0	19221	151.1		141.9	31.8	26.3
HC-5	17.78		1968.5	344.2	268.0	19224	248.3		110.7	19.4	15.1
HC-6	17.61		1968.5	347.5	271.3	19224	243.6		111.8	19.7	15.4
W-7	14.10		1165.2	434.1	357.9	19229	156.2		82.7	30.8	25.4
W-8	14.40		1968.5	424.9	348.7	19224	162.9		136.7	29.5	24.2
W-9	15.90		1644.7	384.8	308.6	19222	198.6		103.4	24.2	19.4
W-10	14.95		2087.6	410.5	333.5	19278	175.5		139.6	27.4	22.3
W-11	14.45		2089.2	423.4	347.2	19222	164.0		144.6	29.3	24.0
W-12	14.56		2133.6	420.4	344.2	19228	166.5		146.6	28.9	23.7
W-13	14.45		2133.6	423.4	347.2	19222	164.0		147.6	29.3	24.0
Y-14	12.68		1651	482.9	406.7	19227	126.2		130.3	38.9	32.1
Y-15	19.16		1651	319.6	243.4	19231	288.2		86.2	16.7	12.7
Y-16	19.53		1651	313.3	237.1	19223	299.6		84.5	16.0	12.1
Y-17	24.22		1651	448.6	372.4	34131	460.7		68.2	18.5	15.4
Y-18	18.81		1651	325.3	249.1	19224	277.9		87.8	17.3	13.2
Y-19	22.88		1651	474.5	398.3	34110	411.2		72.2	20.7	17.4
Y-20	16.05		1651	381.2	330.4	19223	202.3		102.9	23.8	20.6
Y-21	23.45		838.2	463.1	386.9	34113	431.7		35.8	19.8	16.5
Y-22	48.65		522.3	457.2	381.0	69878	1859		10.7	9.4	7.8
Y-23	47.67		1622.4	466.5	390.2	69855	1785		34.0	9.8	8.2

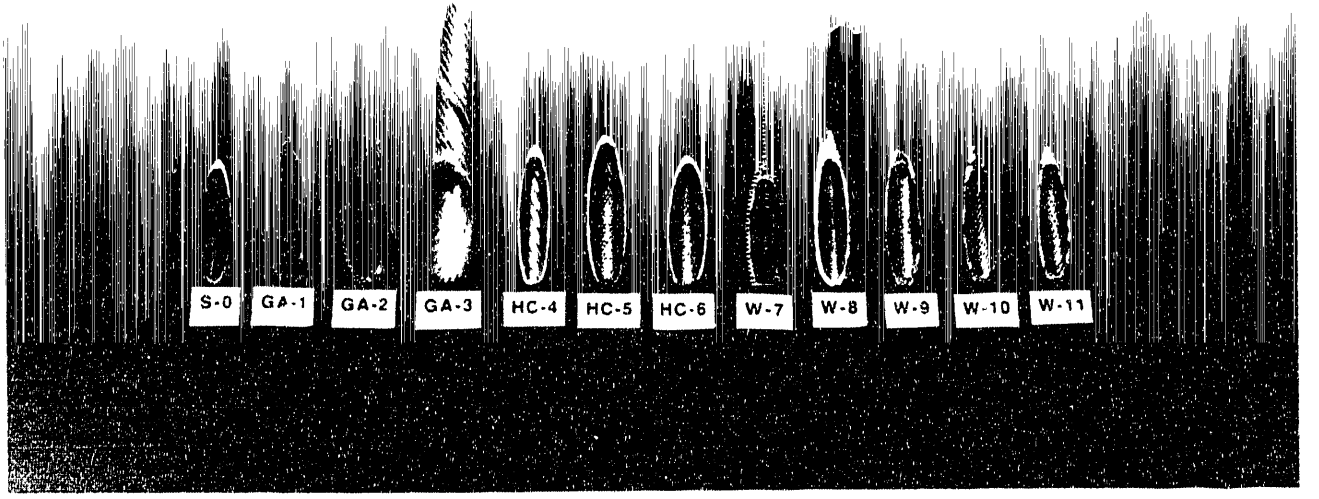

Fig. 2 Close-up photograph of surface contours for all passages.

axis, the row of dents on the primary ribs form a different angle α_2 against the tube axis. When the ribs are oriented in the same rotational direction as the primary rib, α_2 is positive, and negative when the orientation of the dents counters that of the primary ribs. The height of the primary rib is e_1 while the depth of the dents is e_2. The axial pitch of the primary rib measured along the tube axis is p_1 and that of the dents is p_2. The above features are illustrated in Fig. 3.

The remaining eight passages (Y-14 - Y-21), supplied by IMI Yorkshire Alloys and referred to as spirally roped tubes by the supplier, are characterized by indentations on the outside surfaces with ridges on the inner surfaces. These are termed spirally indented passages in this report.

3.3 Test Procedures.

For each tube, the pressure drop data were obtained in the presence of, as well as in the absence of, heat transfer thus affording an extensive documentation of the effect of heat transfer on pressure drop. The frictional pressure coefficients (or values of the Fanning friction factor) were computed from the relation

$$f = \Delta P \rho_w A^2 D_i / 2\dot{m}^2 L \tag{1}$$

where ρ_w is the air density evaluated at the average surface temperature.

For heat transfer, each test section was heated with nichrome wire, located in small grooves machined on the outside surface of a flow passage, using a direct current power source. The temperatures close to the inner surface of a test section were measured with twenty-four chromel-alumel thermocouples (36 guage) located at six axial stations; four were equally spaced circumferentially at a location. The convective heat transfer rates to the air flow were determined from the total electrical power input to a test section with appropriate corrections for heat losses.

Results for the average heat transfer coefficient, expressed in nondimensional form as the values of average Nusselt number (Nu), were computed from

$$Nu = D_i(Q_T - Q_L)/(k_b A)(T_w - T_b) \tag{2}$$

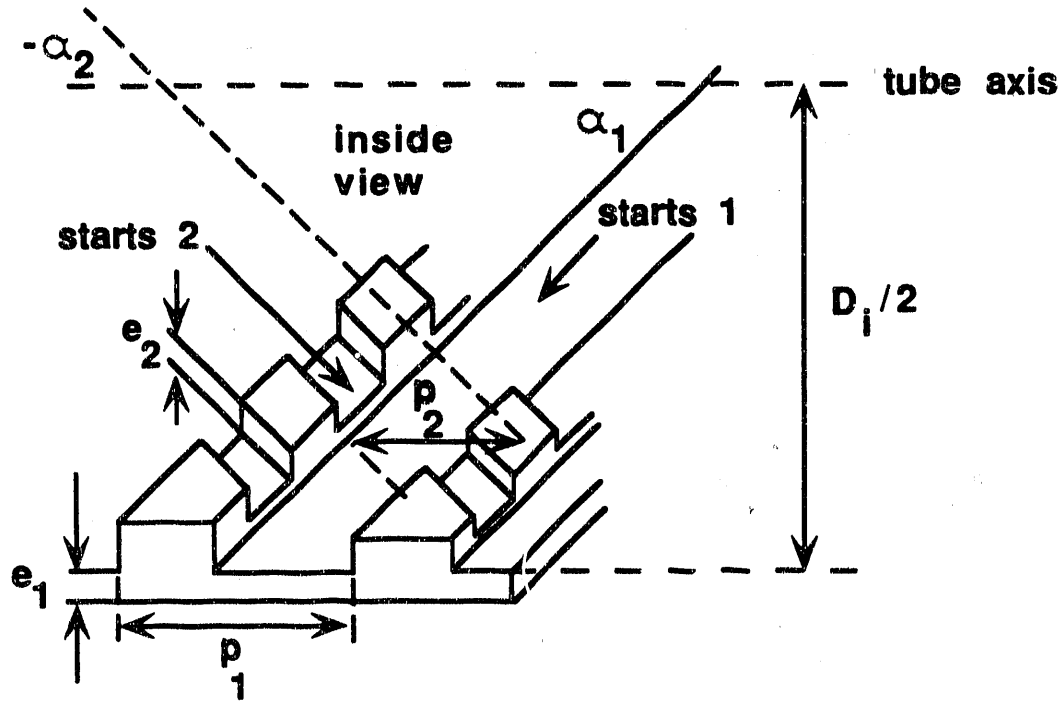

Fig. 3 Definitions of the geometric details of the 3D spiral ribs.

where Q_T and Q_L represent the total electrical power input with air flow and the heat losses, respectively. The losses, determined experimentally in the absence of the air flow, corresponded to the total electrical power input required to maintain the test section at the same average surface temperature as in tests with flow. The convective heat transfer rate, calculated as the difference between Q_T and Q_L, was within $\pm 10\%$ of the value computed from the enthalpy change for a given Reynolds number (Obot and Esen, 1992a, Appendix 1).

Additional details on the design of the test sections, instrumentation for pressure drop, surface thermocouple installation, and the test procedures are given in Obot *et al.* (1991b).

4. RESULTS AND DISCUSSION

The presentation and discussion of results are divided into six main sections. The first three sections, 4.1 through 4.3, consider the effect of heat transfer (wall cooling or fluid heating) on pressure drop, the friction factor and the heat transfer characteristics of the enhanced passages, respectively. In Section 4.4, the validation of the *frictional law of corresponding states* is presented in great detail, followed by an evaluation of the thermal performance of the various enhanced passages in Section 4.5. Comparison of the present results with published data is given in Section 4.6.

The results for the first ten flow passages of Tables 1 and 2 (S-0 through W-9) were presented and discussed in some detail in a previous report (DOE/CE/90029-5, Obot *et al.*, 1991a), but validation of the role of transition was provided only for the GA-3 passage (Obot *et al.*, 1991b). For the sake of completeness, the results for all enhanced passages are presented in this report along with those for the smooth passage. A more detailed discussion of the results obtained with the latter is given in a recent publication (Obot and Esen, 1992a) which is appended to this report (Appendix 1). It is worthy of note that heat transfer tests were not carried out with the GA-1 and GA-2 flow passages.

It is noted at the outset that, due to the large amount of experimental informa-

tion, a compact format is adopted for the graphical presentation of the results shown subsequently for all enhanced passages. Since this format may not lend itself to very accurate extraction of the data from the figures, a complete tabulation of the friction factor, Nusselt and Reynolds number data is given in Appendix 2.

4.1 Effect of Heat Transfer on Pressure Drop

The magnitude of the effect of heat transfer (wall cooling or fluid heating) on pressure drop is best illustrated using plots of the pressure drop ratio ($\Delta p_{wh}/\Delta p_w$) versus the Reynolds number (Re), and these are presented in compact form on Figs. 4 and 5. In each figure, Δp_{wh} is the steady state pressure drop with heat transfer at the average surface temperature of the experiment, while Δp_w is the corresponding value recorded in the absence of heat transfer, that is, just before the onset of heating of the test section. For the smooth passage, the results are given in Appendix 1 for three values of total electrical power input.

For any particular passage, the results show that the largest effects of wall cooling or fluid heating on pressure drop occur within the transition region; the recorded pressure drop with heat transfer is much higher than that without for a given Re. The indication is that the behavior of the $\Delta p_{wh}/\Delta p_w$ data may be used to determine the onset of transition to turbulence. Another feature is the sharp decline in the value of this ratio at the onset of fully turbulent flow, an indication that the onset of fully turbulent flow can also be determined from the trends depicted in these figures for the pressure drop ratio. In turbulent flow, the effect of heat transfer on pressure drop is minimal.

It is evident from these results as well as those in Appendix 1 that the pressure drop ratio depends on, among other things, the magnitude of the total electrical power input and the geometric characteristics of the enhanced passage. Specifically, the pressure drop ratio increases markedly with increasing average surface temperature within the transition region, with moderate effects of surface temperature in laminar and turbulent flow. Interestingly, of the twenty-one enhanced passages for which the ratios are given on Figs. 4 and 5, the peak values are largest (on the order of 1.4) for the three-dimensional enhanced geometries (HC-5 and HC-6). Within the laminar-transition

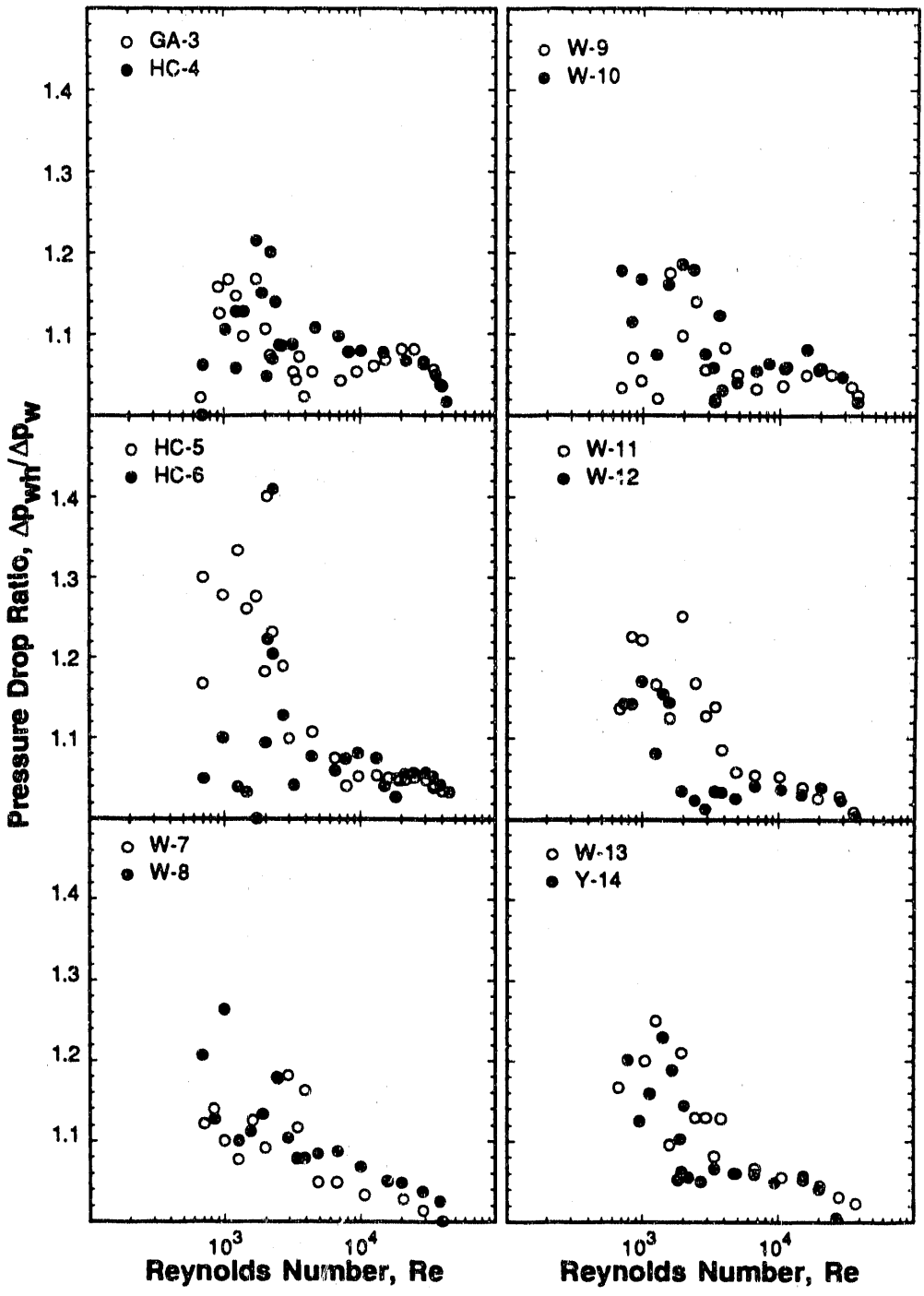

Fig. 4 Pressure drop ratio vs. *Re* for GA-3 - Y-14.

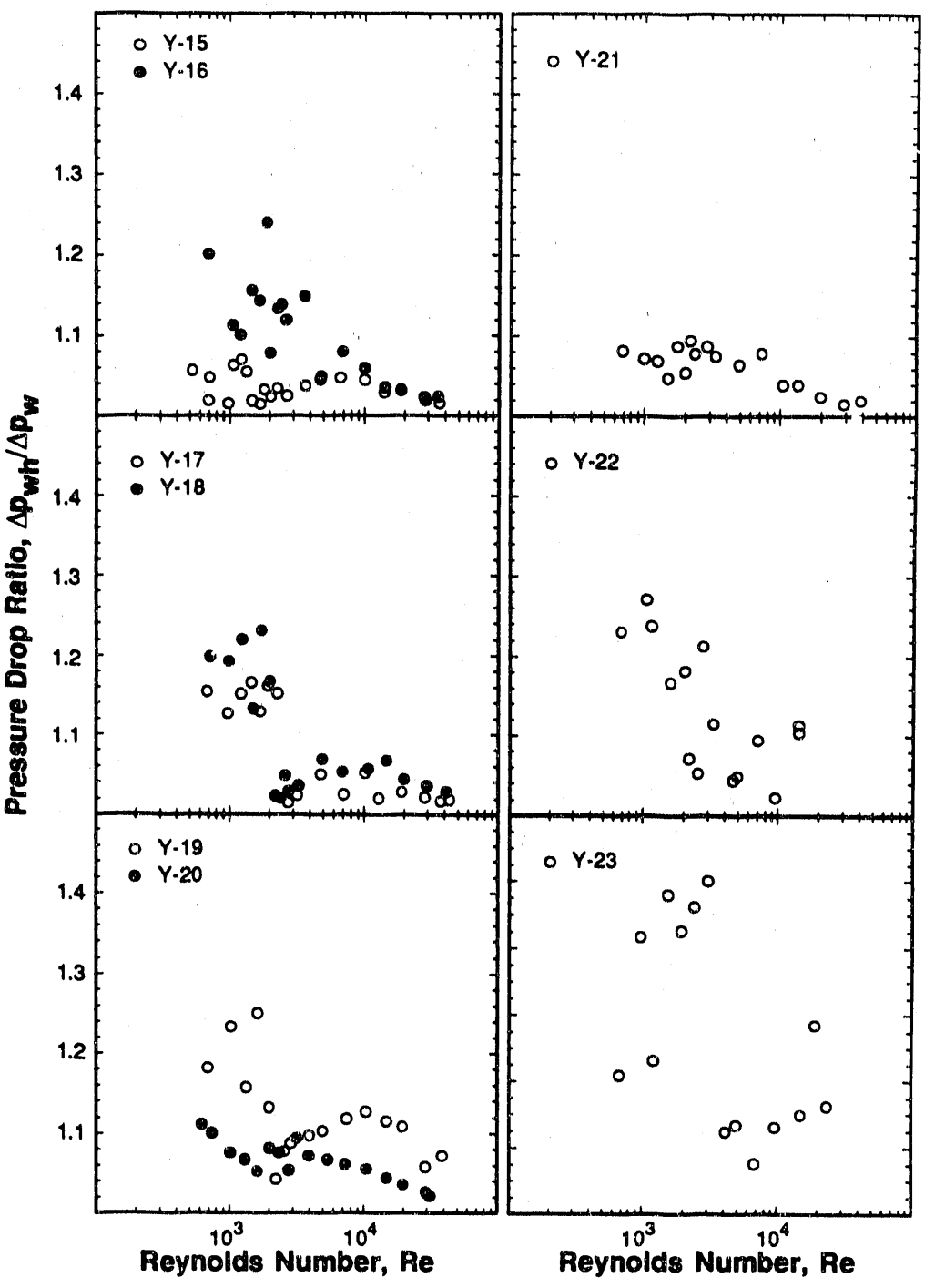

Fig. 5 Pressure drop ratio vs. *Re* for Y-15 - Y-23.

region, the $\Delta p_{wh}/\Delta p_w$ values for the other passages lie between 1.1 and 1.30.

On the basis of the results that are charted here for the pressure drop ratio, it is reasonable to conclude that the effect of heat transfer on pressure drop is greatest within the transition region, the effect is moderate in laminar flow and least in turbulent flow. For the latter flow region, the ratios are generally below 1.1, an indication that turbulent friction factor is insensitive to heat transfer.

4.2 Friction Factor for Enhanced Passages

The pressure drop data reduced as values of the Fanning friction factor (f) are given compactly in Figs. 6-8, where the abscissa is the Reynolds number based on the maximum internal diameter. The data for each enhanced passage are compared with those for the smooth passage. With the exceptions of the GA-1 and GA-3 passages that were not tested with heat transfer, the results obtained with and without heating are given for each of the remaining passages. Since the effects of heat transfer on friction factor are small for all passages, the results obtained in the presence of heat transfer are used in all subsequent illustrations, unless stated otherwise.

The alternative representations of the same friction factor-Reynolds number data as plots of the friction factor ratio f_e/f_s versus Re_m are given on Figs. 9 and 10. Here, the abscissa is the similarity parameter, Re_m, the values of which were calculated from the relation

$$Re_m = (Re_{c,r}/Re_{c,a})Re_a$$

where $Re_{c,r}$ (= 2093) and $Re_{c,a}$ respectively are the values of the critical Reynolds number at the onset of transition to turbulent flow for the reference and arbitrary conditions. The use of these empirical corrections locates the onset of transition to turbulent flow at the same point as the reference, in line with the formulation of the *frictional law of corresponding states*. Recall that the GA-1 and GA-2 data of Fig. 9 were obtained in the absence of heat neat transfer.

In laminar flow, the general behavior of the data with increasing Re is the same for all passages; f is inversely proportional to Re or the product $f \times Re$ is constant. The departure from the smooth passage data depends on the geometric characteristics

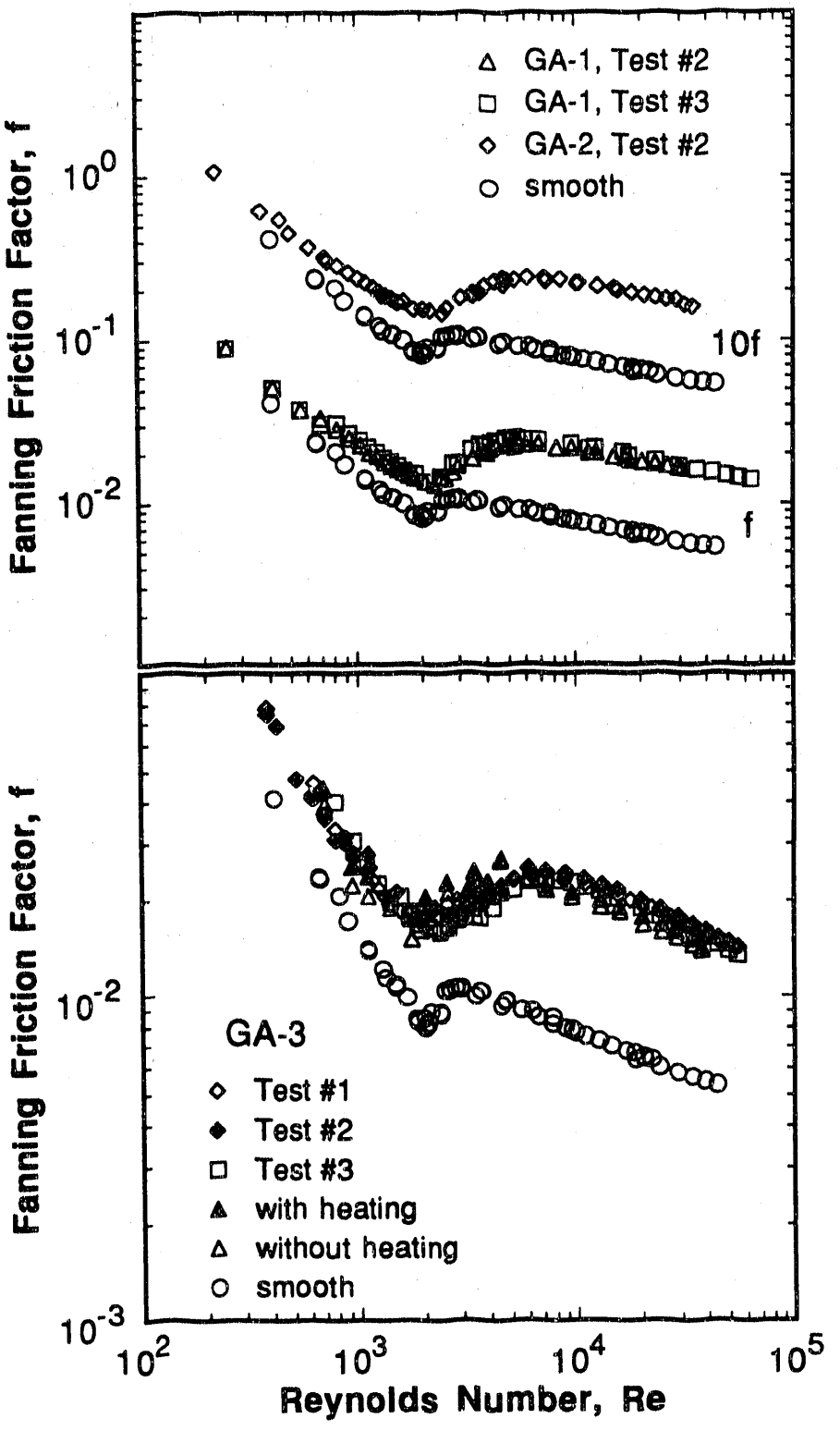

Fig. 6 Friction factor vs. Reynolds number for GA-1 to GA-3.

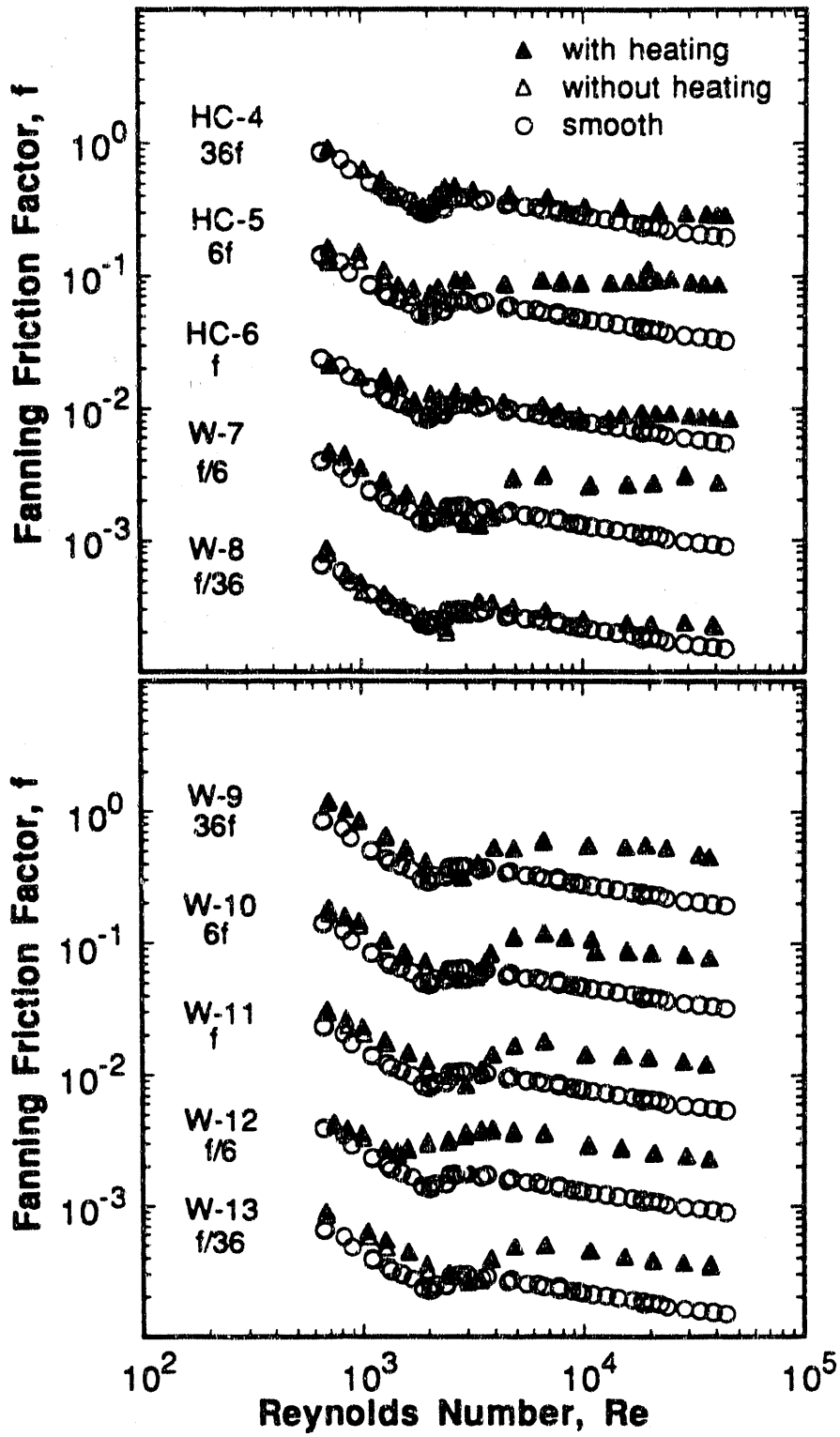

Fig. 7 Friction factor vs. Reynolds number for HC-4 to W-13.

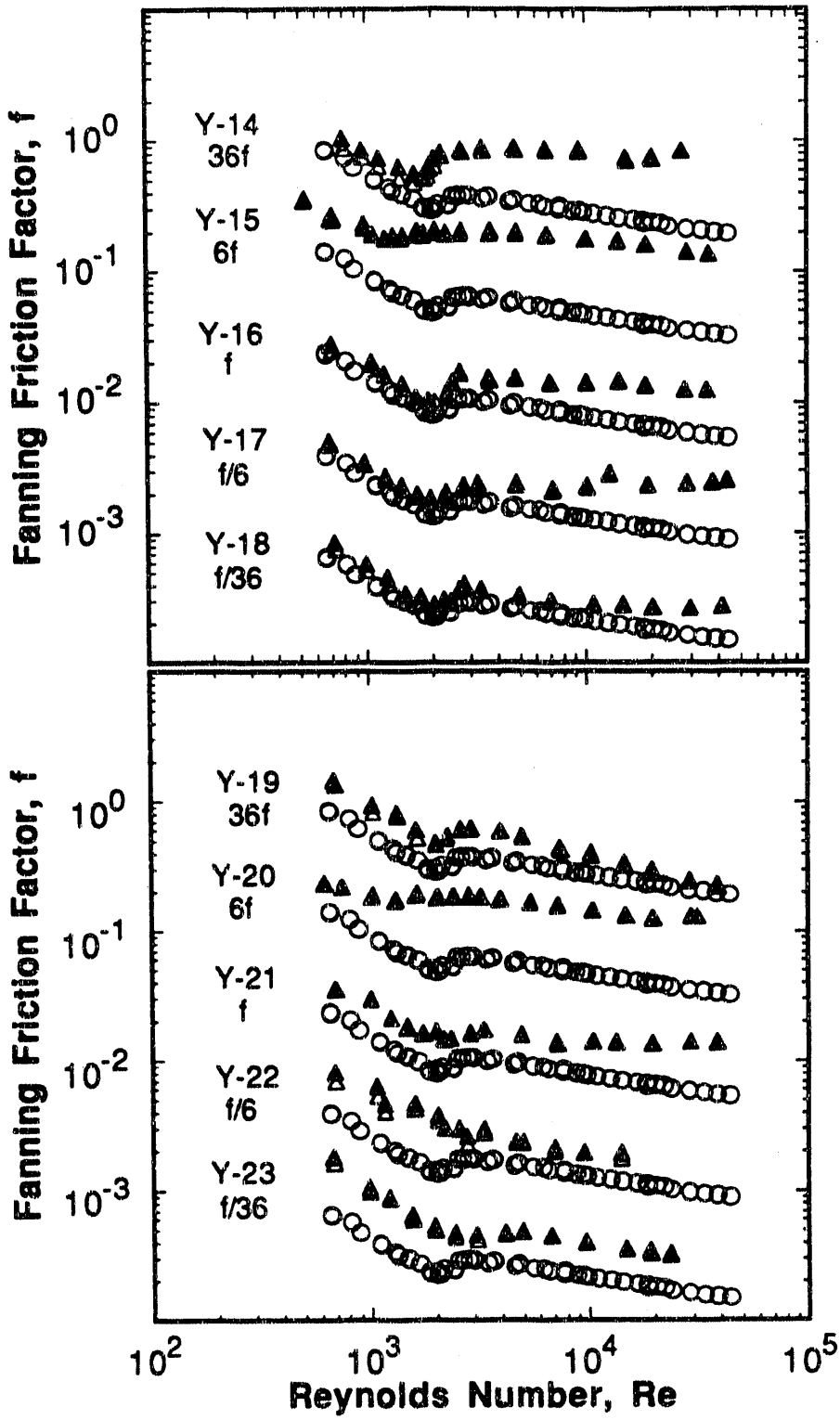

Fig. 8 Friction factor vs. Reynolds number for Y-14 - Y-23.

of the enhanced passage, and is most pronounced for passages of the spirally fluted type (GA-1 through GA-3, Y-22 and Y-23).

The results indicate a rather complex effect of enhancement geometries on transition to turbulent flow. All but three of the passages have critical Reynolds number values that are either about the same as, or significantly greater than, those for the smooth passage. As a result, crossings of the enhanced and the smooth passage f versus Re curves are observed within the transition region. The critical friction factor at transition also varies with the passage geometry. The trend is one of decreasing critical friction factor with increasing critical Reynolds number, in line with the behavior established previously for transverse repeated-rib disruptions (Obot *et al.*, 1990a,b). The range of conditions tested preclude definite statements on the effects of geometric parameters (e/D_i, p/e, α, etc.) on the critical friction factor and Reynolds number. A summary of the critical parameters is given in Table 3.

In turbulent flow, values of friction factor for any particular enhanced passage are generally greater than those for the smooth passage. Of the twenty-three enhanced passages tested, only three (Y-14, Y-15 and Y-20) are characterized by f_e/f_s values that are greater than 3 but under 4.5; $f_e/f_s \leq 3$ for the other passages. For the three passages with spirally indented disruptions, Table 1 shows that $N_s = 3$ for each; $\alpha =$ 69.4, 63.5 and 59.2 degrees; $e/D_i = 0.033$, 0.066 and 0.062; and $p/e = 13.2$, 7.9 and 10.0, respectively. Also, Table 3 shows that the critical Reynolds numbers are 1836, 1228 and 1021 for Y-14, Y-15 and Y-20, respectively. So, the unique behavior of these three passages is most likely the result of the inseparable effects of α, e/D_i and p/e.

The friction factor trends for the three-dimensional spiral ribs (HC-5 and HC-6, Fig. 7) are remarkably similar to those for sand-grain roughness (Nikuradse, 1933). For small e/D_i (HC-6), the data are close to those for the smooth tube but depart from the smooth tube line for $Re > 10000$. With the larger e/D_i (HC-5), the data are generally higher than those for the smooth tube, and the turbulent flow trend parallels that established by Nikuradse for large relative height of sand-grain roughness. Comparison of the present data with those of Takahashi *et al.* (1985) for comparable surface geometry will be given in Section 4.6.

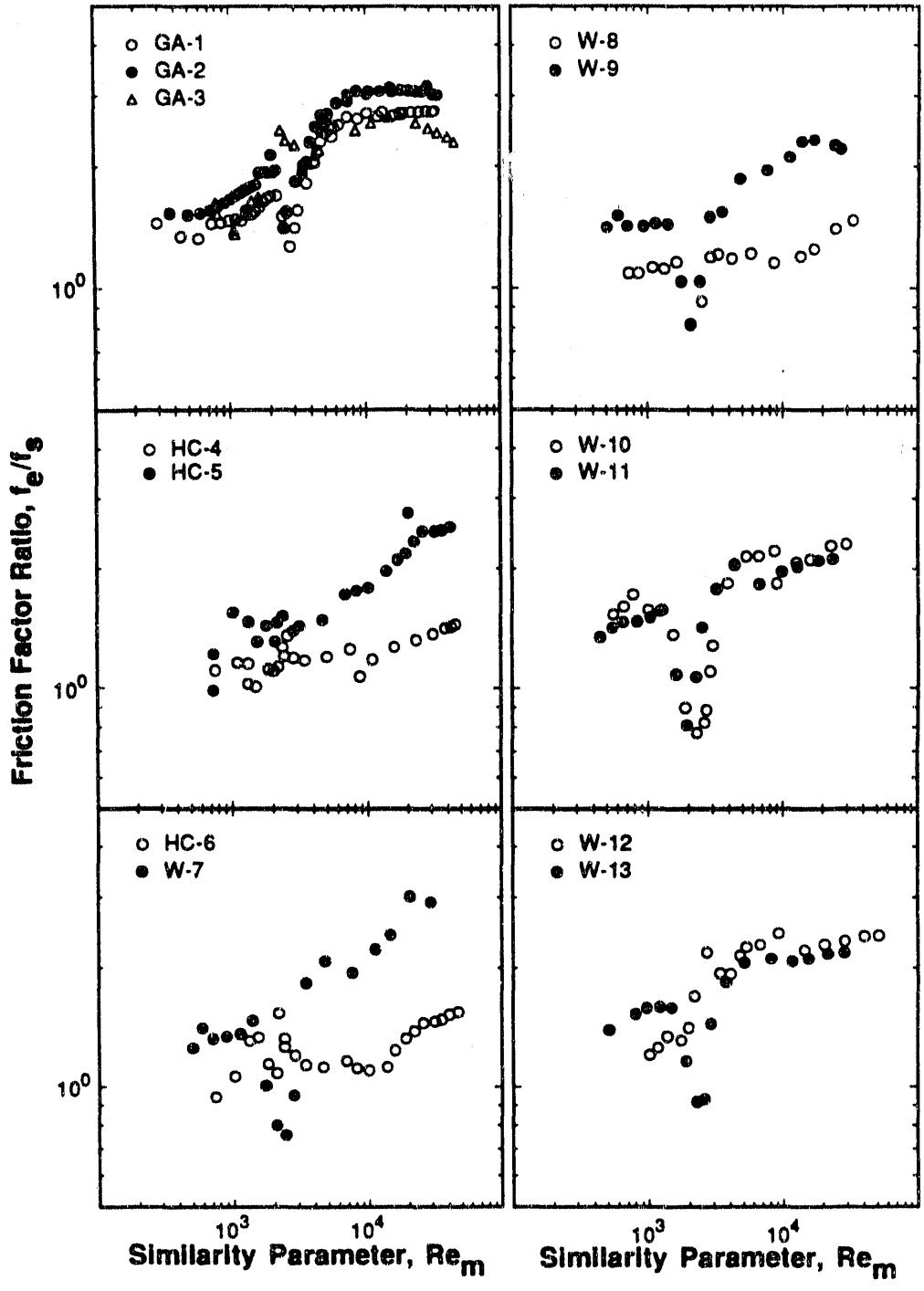

Fig. 9 Friction factor ratio vs. similarity parameter, Re_m, for GA-1 - W-13.

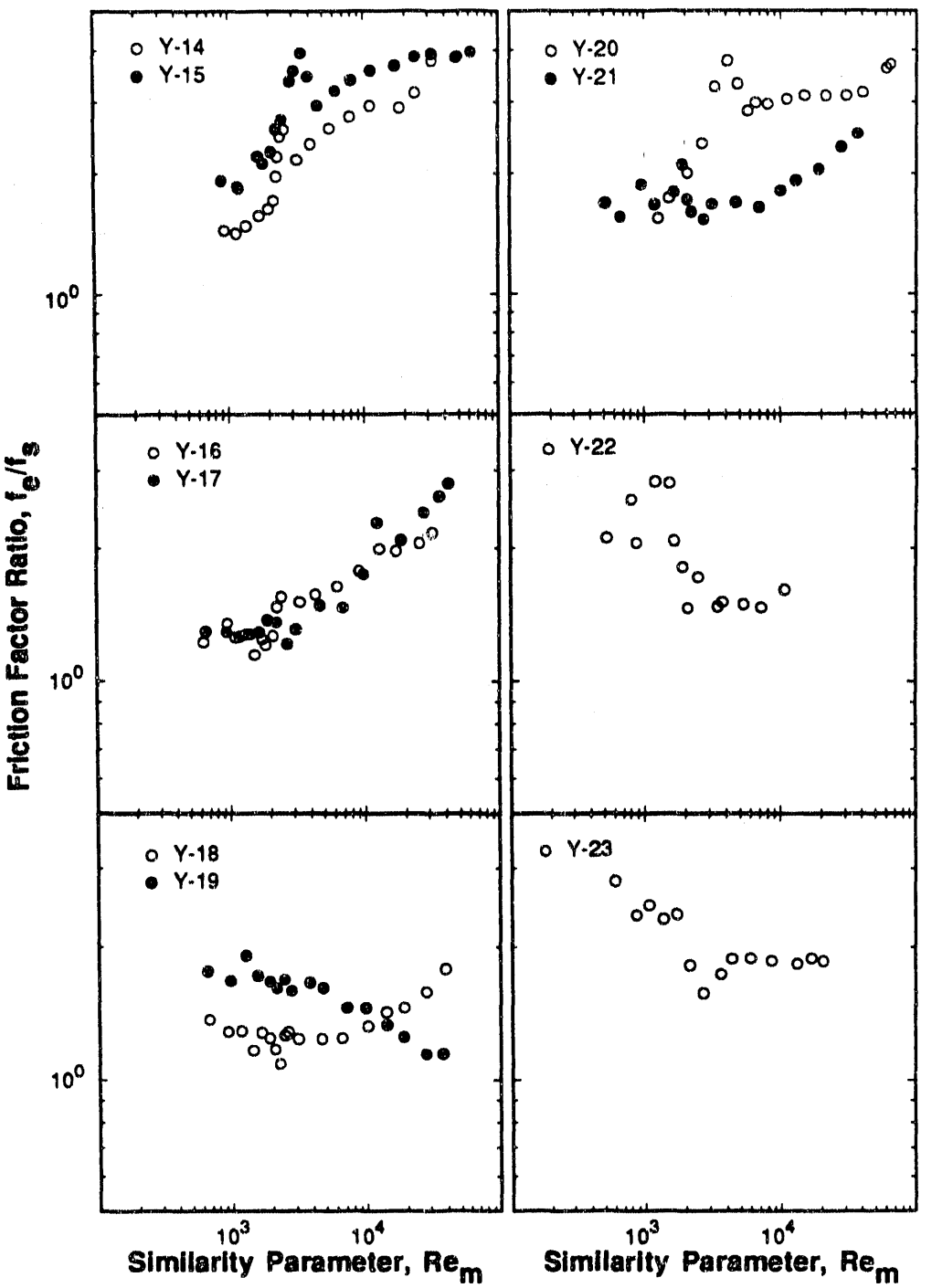

Fig. 10 Friction factor ratio vs. Re_m for Y-14 - Y-23.

TABLE 3. Critical Data for all Flow Passages.

Tube	T_w (°C)	Re_c	f_c	Nu_c
S-0		2004[1]	0.0086[1]	
	52.7±0.4	1843	0.0084	5.5
	variable[2]	1970	0.0080	5.6
	variable[3]	2060	0.0100	5.6
	variable[4]	2093	0.0093	6.1
GA-1		1874	0.0144	
GA-2		1851	0.0154	
GA-3		1861[1]	0.0179[1]	
	45.5±0.3	1786	0.0142	9.2
HC-4	47.5±0.3	1965	0.0089	6.4
HC-5	47.6±0.3	1997	0.0109	7.0
HC-6	47.5±0.3	2017	0.0091	7.1
W-7	45.4±0.3	2963	0.0076	8.6
W-8	45.7±0.2	2434	0.0071	7.4
W-9	45.5±0.2	2873	0.0082	9.0
W-10	45.5±0.2	2614	0.0088	7.7
W-11	45.6±0.3	2968	0.0081	9.2
W-12	45.6±0.3	1504	0.0133	5.0
W-13	45.6±0.2	2724	0.0094	8.3
Y-14	45.5±0.3	1753	0.0134	6.6
Y-15	45.6±0.3	1228	0.0264	7.6
Y-16	45.4±0.2	2065	0.0099	8.4
Y-17	45.4±0.3	1868	0.0110	7.5
Y-18	45.3±0.2	1983	0.0105	7.9
Y-19	45.5±0.3	2200	0.0127	10.4
Y-20	45.4±0.2	825	0.0317	5.0
Y-21	45.5±0.2	2171	0.0131	10.2
Y-22	45.6±0.2	2770	0.0149	15.7
Y-23	45.4±0.2	2371	0.0166	12.8

[1] Test without heating.
[2] q_T = 773 W/m^2, 42$\leq T_w \leq$ 75°C.
[3] q_T = 1708 W/m^2, 46$\leq T_w \leq$ 131°C.
[4] q_T = 2509 W/m^2, 68$\leq T_w \leq$ 158°C.

It is evident from Table 1 that the upper limit to the range of e/D_i tested is 0.066 and, for this case, $p/e = 2.2$ (Y-19); this value of e/D_i can be considered to be on the high side. Despite this fact, the friction factor for this flow passage are no more than 2 times those for the smooth passage. This contrasts sharply with the friction factor trends for surfaces having transverse disruptions. For instance, the f_e/f_s values at comparable Re for the transverse inserts of Koch (1960) with $e/D_i = 0.045$ and 0.075 ($p/e = 9.8$ in each case) are about 17.5 and 20, respectively. These values, even that for the lower e/D_i of 0.045, are considerably greater than those for the spiral disruptions. Differences of these magnitude in the pressure drop characteristics between the two types of surface disruptions cannot be explained in terms of the difference in p/e, because the f_e/f_s values for Y-20 ($e/D_i = 0.062$ and $p/e = 10$) are equally much lower than those deduced from Koch's data for transverse ribs of $e/D_i = 0.045$.

In summary, the results indicate that, unlike transverse ribs or inserts, spirally shaped disruptions result in very moderate increases in pressure drop. Although the effects of transition on friction factor are not accounted for in the aforegoing presentation and discussion, the use of the reduced friction factor as dictated by the corresponding states method does not modify the above observation.

4.3 Heat Transfer for Enhanced Passages

The convective heat transfer rates reduced as values of the average Nusselt number (Nu) are presented compactly on Figs. 11 and 12; the abscissa is the Reynolds number, Re. Consistent with the treatment of friction factor, the alternative representations as plots of the Nusselt number ratio Nu_e/Nu_s versus Re_m are given in Figs. 13 and 14.

Figures 11 and 12 show that Nu increases steadily in laminar flow for all passages, the curves rise sharply after the point of transition, in line with the friction factor behavior, and then changes direction at the onset of fully turbulent flow. It was established in previous publications (Obot and co-workers, 1991a,b; 1992a,b) that Nu varies as the 1/2 power on Re in laminar flow for the smooth and the GA-3 spirally fluted passages. This dependence of Nu on Re in laminar flow holds for all passages and this will be evident from the subsequent discussion of data correlation.

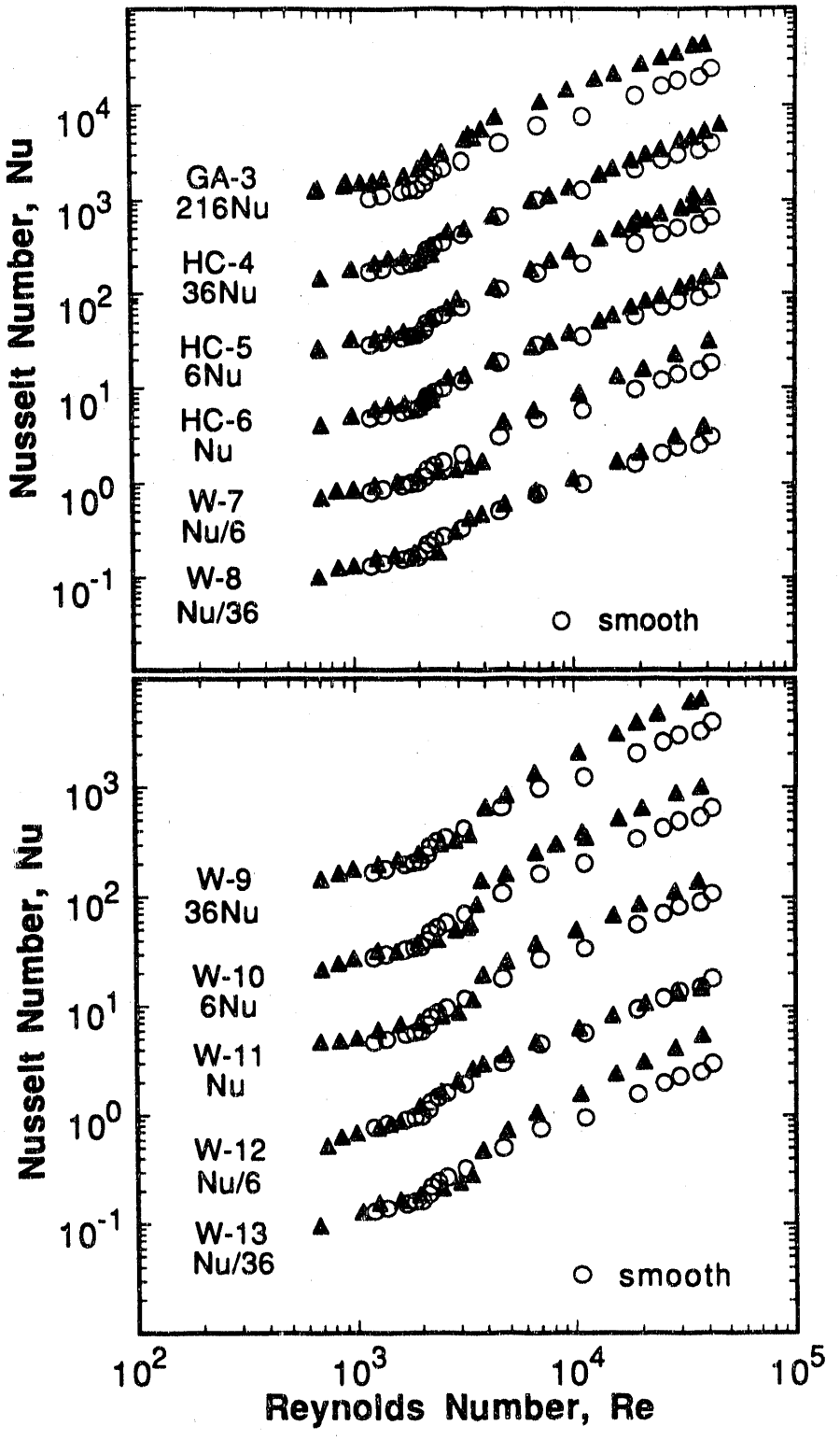

Fig. 11 Nusselt number vs. Reynolds number for GA-3 - W-13.

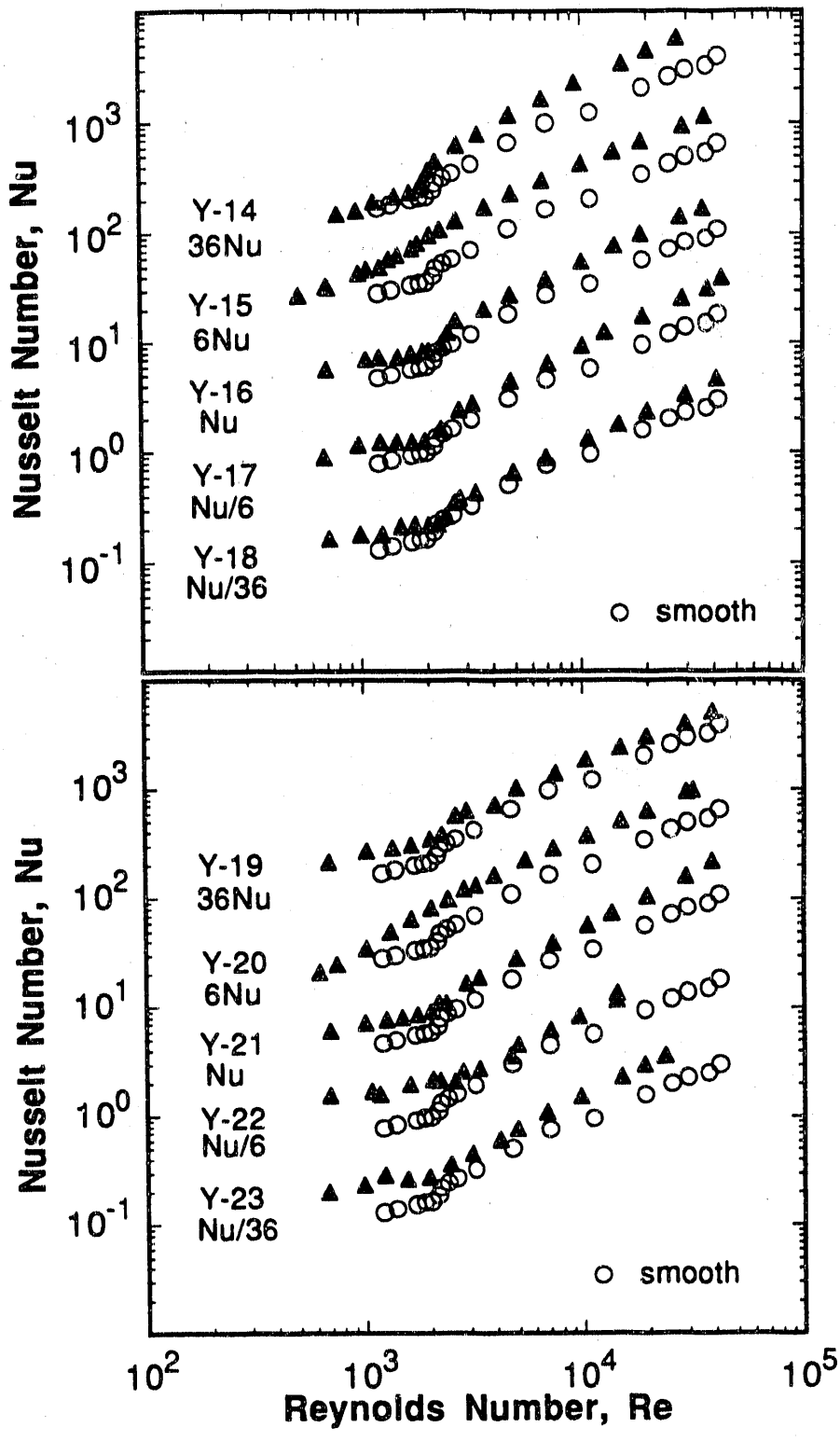

Fig. 12 Nusselt number vs. *Re* for Y-14 - Y-23.

The results on these series of figures, in particular those on Figs. 13 and 14, indicate varying amounts of enhancement in laminar flow. The ratio Nu_e/Nu_s varies from slightly above unity to about 2.5, depending on the geometric details of the enhanced passage. The only exception to this consistent trend is observed for the W-12 passage; there is practically no improvement in heat transfer in laminar flow. The attainable values of Nu_e/Nu_s in laminar flow are greatest for enhanced passages of the spirally fluted type (GA-3, Y-22, and Y-23); these passages are also characterized by the largest values of the friction factor ratio f_e/f_s in laminar flow. Figs. 13 and 14 show that Nu_e/Nu_s is essentially independent of Re_m in laminar flow, a clear indication that the dependence of Nu on the Reynolds number is the same for all passages. Note that in terms of Re_m the onset of transition is located at $Re_m = 2093$.

In the transition region, the trend for the most part is one of a drop in the Nu_e/Nu_s value, beginning at the onset of transition to turbulent flow. An exception to this consistent behavior occurs for the spirally indented passages (Y-14, Y-15 and Y-20), the only passages for which $f_e/f_s > 3$ but < 4.5. For these passages, each Nu_e/Nu_s curve rises steeply over the narrow $2000 < Re_m < 2300$ region, drops slightly and then rises moderately with increasing Re_m. These trends are entirely due to transition because, as noted already in connection with the discussion of the f_e/f_s data, the critical Reynolds numbers for these passages are much lower than the smooth tube values.

For most of the spirally ribbed/finned passages, the Nusselt number ratios are considerably lower than one within the transition region. This is a reflection of the crossing of the Nu versus Re curves and the fact that the transition Reynolds numbers for the enhanced passages are much higher than the smooth tube value (Table 3). The W-12 passage is the only exception as the ratio is slightly higher than one within the transition region.

Figures 11 and 12 show that $Nu \propto Re^n$ in turbulent flow. For a specified Re range, the empirically determined value for n depends on the geometric details of the flow passage. Although this dependence of the Reynolds number exponent on the type of surface disruptions is well documented in the literature (see, for example, Carnavos, 1980), no satisfactory explanation of the causative phenomena has been provided.

A careful study of these Nu versus Re curves reveals that, over the same Re, the Re exponent for an enhanced passage is practically the same as or different from that of the smooth passage according to whether the critical Re at transition is lower or higher than the smooth tube value. The results for GA-1, Y-12, Y-15 and Y-20 give almost the same exponent as the smooth passage; the exponents for the other passages are different. So, variations in the Reynolds number exponent appear to be intimately associated with the transition process.

In turbulent flow, the results on Figs. 13 and 14 indicate varying amounts of enhancement depending on the geometric characteristics of the enhanced passage. The upper limit to the range of Nu_e/Nu_s values is 2.5. The Nu_e/Nu_s versus Re_m curves for nearly one-half of the enhanced passages tested exhibit maxima for some range of Re_m. The fact that a plot of Nu_e/Nu_s against the conventional Reynolds number or any appropriately defined parameter (such as the roughness Reynolds number, e^+ or Re_m) may pass through a maximum in turbulent is well documented in the literature (Webb *et al.*, 1971; Rabas, 1988; Obot *et al.*, 1990a).

A comparison of the f_e/f_s versus Re_m curves (Figs. 9 and 10) with the Nusselt number ratios of Figs. 13 and 14 reveals complete similarity in behavior between the two sets of data for any particular passage. For instance, the existence of a maximum in the f_e/f_s versus Re_m curve is also reflected in a maximum in the Nu_e/Nu_s versus Re_m plot. Also, when f_e/f_s increases with increasing Re_m, Figs. 13 and 14 show that the same trend is exhibited by Nu_e/Nu_s. Although there are quantitative differences between the magnitude of f_e/f_s and Nu_e/Nu_s, the similarity in the general features of the curves begins in laminar flow and continues in the transition and turbulent flow regimes.

In summary, $Nu \propto Re^{1/2}$ in laminar flow for all passages; the Nu versus Re curves rise sharply after the onset of transition to turbulent flow and then change direction at the onset of fully turbulent flow. Consistent with the low pressure drop characteristics of the flow passages, the increases in heat transfer coefficient can be as much as 2.5 times the smooth tube values depending, of course, on the geometric configurations of

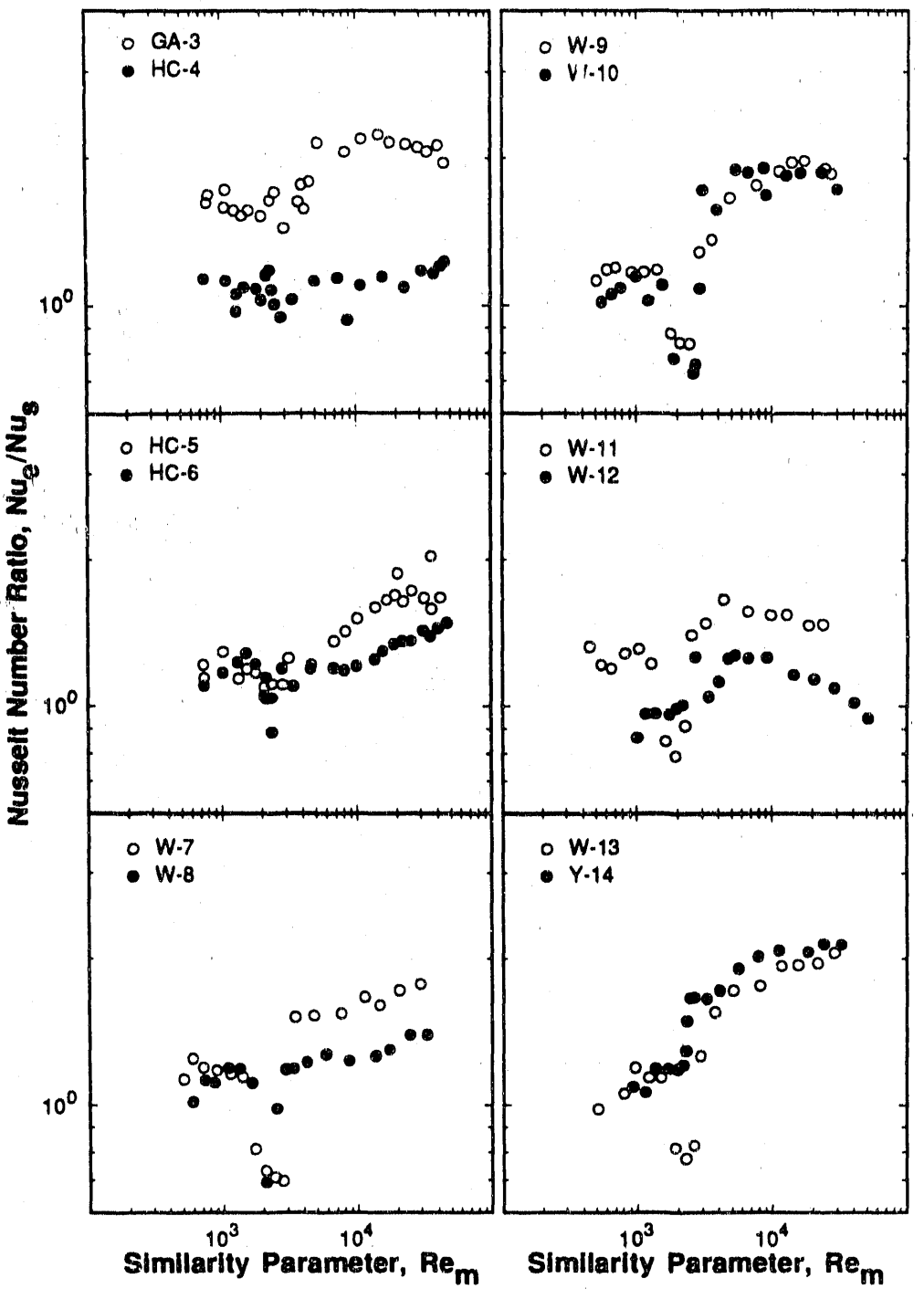

Fig. 13 Nusselt number ratio vs. Re_m for GA-3 - Y-14.

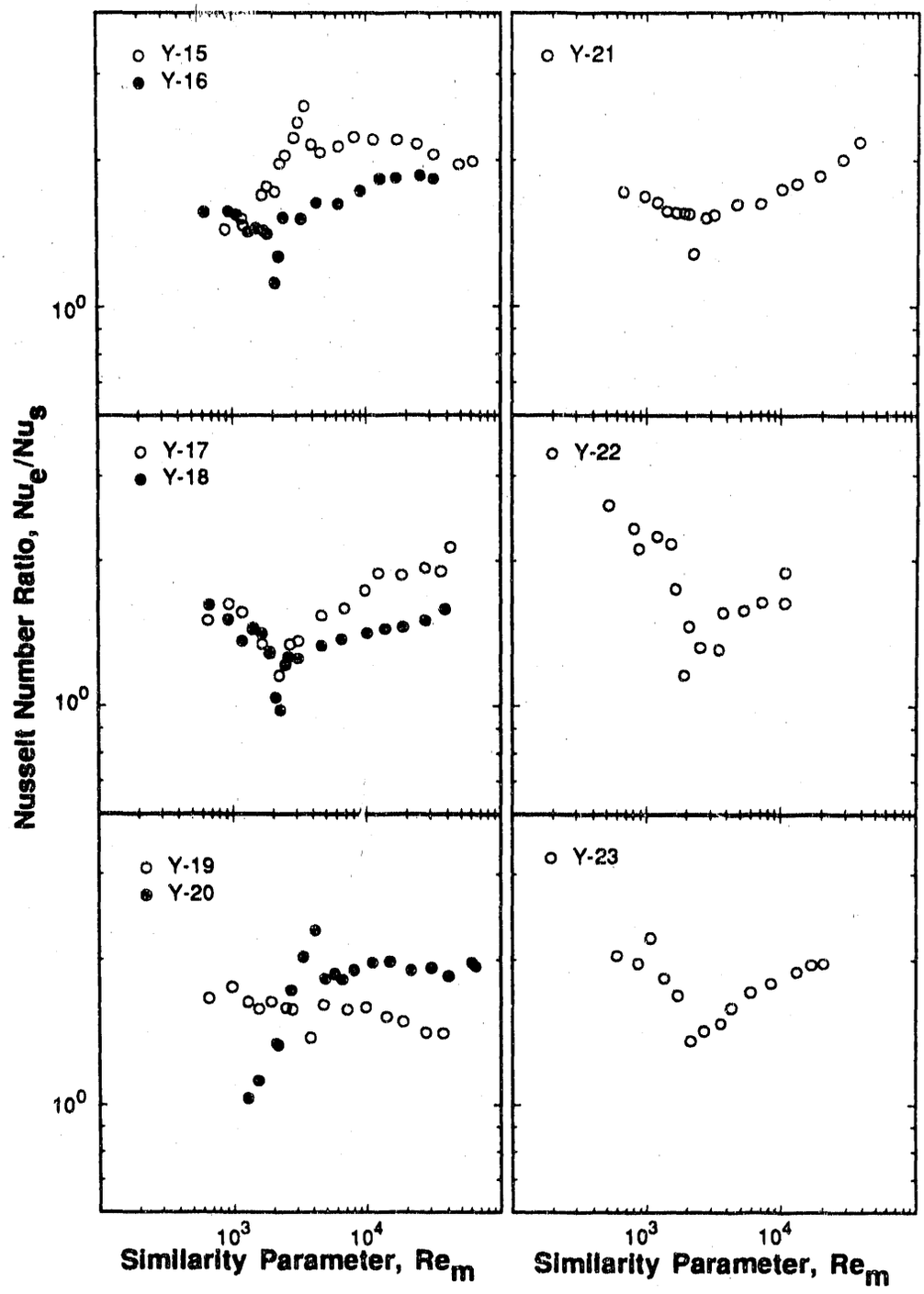

Fig. 14 Nusselt number ratio vs. Re_m for Y-15 to Y-23.

the enhanced surfaces.

4.4 Validation of the *Frictional Law of Corresponding States*

This section is divided into five sub-sections. The presentation begins with the discussion of the role of transition, followed in sequence by analysis and data correlation, validation of the friction-heat transfer analogy, the consistency of the friction-heat transfer relation with the well known Reynolds analogy, and the calculation of Nusselt number or friction factor using the proposed correlations.

4.4.1 The Role of Transition

Because the transition process is central to the formulation of the frictional law, this presentation is intended to shed further light on its complicated influence on friction and heat transfer. The friction factor results of Section 4.2 show conclusively that the data trend is basically the same in laminar flow for all passages; the departure from the smooth passage trend occurs after the onset of transition to turbulent flow. For heat transfer, the general shape of the curves is clearly universal with well defined laminar, transition and turbulent flow regions; the departure from the laminar trend also occurs after the onset of transition. In the absence of transition, it may indeed be argued that f and Nu are always proportional to Re^{-1} and $Re^{1/2}$, respectively; the deviations from these consistent laminar trends are entirely the result of transition.

It is of particular importance to the present considerations to note that the critical values of friction factor, Nusselt and Reynolds numbers vary widely at the onset of transition (Table 3). These variations, which are due to the inseparable effect of the transition process itself (*i.e.*, variations in values of the critical velocity) and the selected length scale for data reduction, imply that the flows are not similar for equal Reynolds number, Re.

Direct experimental methods were detailed recently for the determination of the onset of transition in flow passages (Obot *et al.*, 1991c). It was established that the characteristic features at transition include the sudden change from steady to oscillating wall static pressure readings, the distinctive change in profile for the power spectral

density representations of the wall pressure fluctuations, and the sharp rise in the root-mean-square values of the wall pressure fluctuations. The critical Reynolds numbers obtained with a 7.75 mm stainless steel smooth passage ranged from about 2600 to 3300. Since this range of Re_c is much greater than that uncovered in the literature for comparable D_i (see, for example, Lindgren, 1957), and since the experimental methods are rather straightforward and easily implemented, the Re_c values were determined for five smooth copper tubings with diameters ranging from 7.85 mm to 25.27 mm.

Figure 15[1] shows the variation of Re_c with D_i for geometrically similar entrance configuration. Note that the flow passages were similarly supported. The flow phenomena causing such a complex Re_c versus D_i trend is not so readily explained. The important observation here relates to the variability of Re_c with D_i for smooth passages; it is indicative of the differences in heat transfer or friction factor trends that can result from variations in D_i. The effect of D_i on the friction factor trend was confirmed in that study. Interestingly, two smooth passages of comparable D_i give vastly different Re_c values, 2600-3300 and 2100 for the stainless steel (D_i = 7.75 mm) and copper (D_i = 7.85 mm) tubings, respectively.

A review of the literature reveals significant quantitative differences among the Re_c values of various investigators. For instance, the smooth passage Re_c values deduced from the data of Kaupas *et al.* (1989, D_i = 36.3 mm) range from about 3500 to 5000; the values based on the data of Watkinson *et al.* (1974, D_i = 26.0 mm) and Marner and Bergles (1978, D_i = 23.0 mm) are about 1300 and 2370, respectively. Even for smooth passages, the fact that these variations in the critical parameters also give rise to differences in values of f and Nu for equal Re is documented in Appendix 1.

There are other implications of the observations noted in this section for smooth passages. For a given enhanced passage, the relative increases in both friction factor (f_e/f_s) and Nusselt number (Nu_e/Nu_s) depend on the transition characteristics of the smooth passage. Also, the crossings of the smooth and enhanced passage f or Nu versus Re curves, as documented already for several cases, may not exist when the smooth

[1]These results were obtained as part of the research directed by Dr. M. W. Wambsganss at Argonne National Laboratory

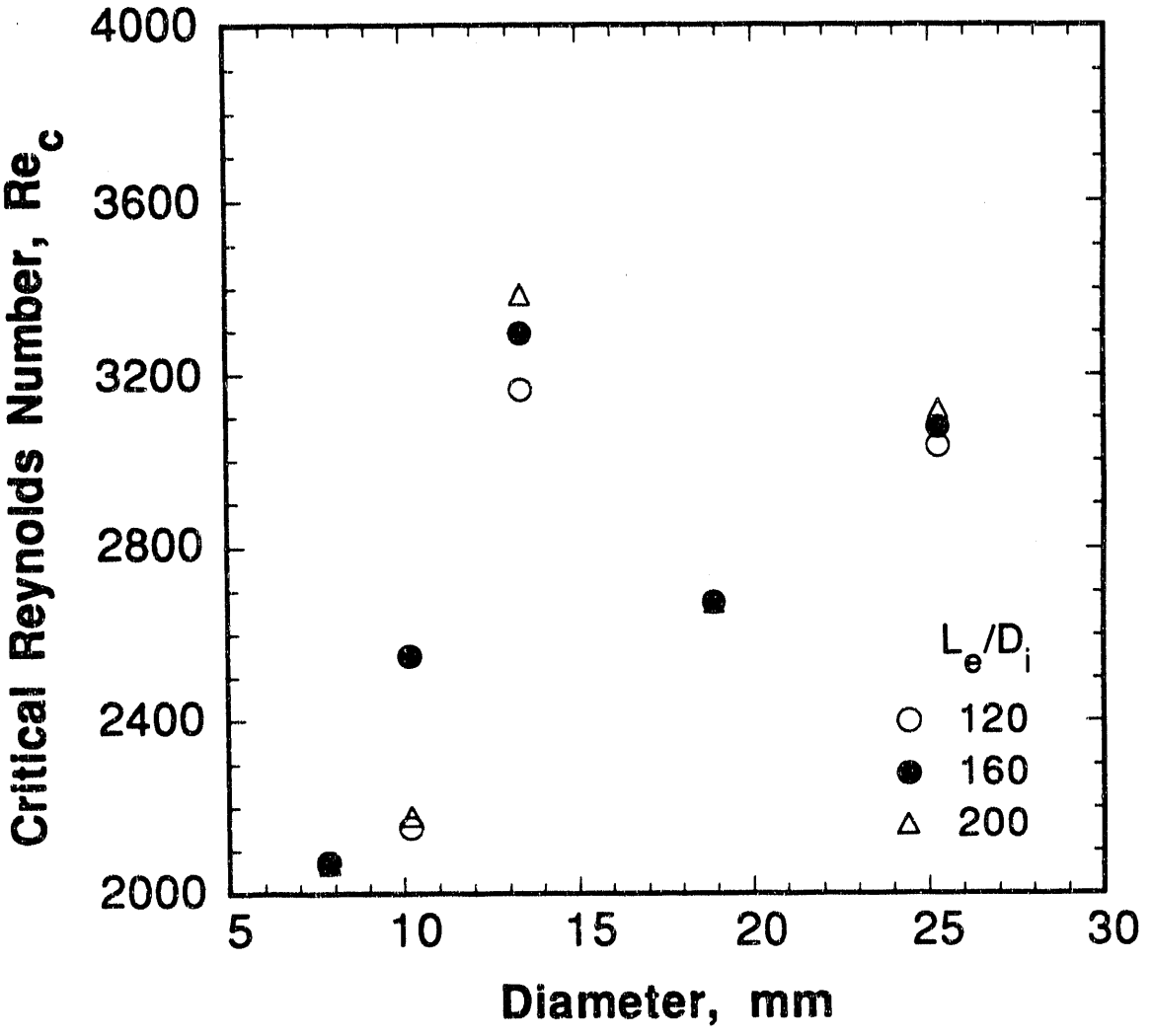

Fig. 15 Variation of critical Reynolds number with smooth passage diameter.

passage Re_c value is greater than that of the enhanced passage. From the point of view of friction and heat transfer enhancement, it is clear that transition is very important because it gives rise to vastly different f and Nu values for equal Re. Attempts to account for its effect in a systematic manner is the subject of the presentation that follows.

4.4.2 Analysis and Data Correlation

The results of empirical studies (Obot *et al.*, 1990a,b) indicated that there is a definite connection between the transition process and enhancement for both friction and heat transfer. Given the variability of the critical parameters (friction factor, Nusselt and Reynolds numbers) at the onset of transition to turbulent flow, the *frictional law of corresponding states* was formulated according to the following relations:

$$Re_m = (Re_{c,r}/Re_{c,a})Re_a = \psi_R Re_a \tag{3}$$

$$f_m = (f_{c,r}/f_{c,a})f_a = \psi_f f_a \tag{4}$$

$$Nu_m = (Nu_{c,r}/Nu_{c,a})Nu_a = \psi_N Nu_a \tag{5}$$

Equations (3)-(5) provide a generalized reference state of a physical nature for problem analysis; specifically, the onset of transition to turbulent flow is located at a particular Re_m for all passages.

A more useful form of the corresponding states relations, insofar as the relationship between friction factor and Nusselt number is concerned, is developed as follows. For laminar flow, it is well known that the relationship between friction factor and the Reynolds number takes the form

$$f \times Re = C_f \tag{6}$$

where C_f is a constant for any particular passage. For heat transfer, the laminar flow results for the smooth tube and the enhanced passages support the functional relation

$$Nu/Re^{1/2} = C_h \tag{7}$$

where C_h is a constant for any particular flow passage. It follows that the ratio C_h/C_f, which is given by equation (8), must be independent of Reynolds number in laminar

flow for a given flow passage.

$$C_h/C_f = Nu/(Re^{3/2}f) \tag{8}$$

Since equation (8) contains the three parameters, f, Nu and Re, its reduced form which accounts for the critical parameter variations can be readily written down as:

$$C_{h,m}/C_{f,m} = Nu_m/(Re_m^{3/2}f_m) \tag{9}$$

Prior to the presentation and discussion of these alternative representations of the experimental data, there are several comments. Equation (7), one of the two relations that are used here to develop the friction-heat transfer analogy, is supported by the smooth passage results of other investigators. This is demonstrated in Obot and Esen (1992a) which is appended to this report (Appendix 1). Another significance of equation (7) is that it brings the laminar heat transfer behavior for passages in line with the well known Nu versus Re trend for laminar boundary layers, just as there is consistency in the Nu dependence on Re in turbulent flow for incompressible boundary layer flows and flow through passages.

Figures 16 and 17 respectively are similarity plots of f_m and Nu_m versus Re_m for the twenty-one enhanced passages tested with heat transfer. The four sets of data obtained with the smooth passage are also included in both figures. For the latter, the average surface temperature was held fixed with increasing Re for one set, while the remaining three sets were obtained with three different values of Q_T (Obot and Esen, 1992a, Appendix 1). The smooth passage critical parameters ($f_{c,r} = 0.0093$, $Nu_{c,r} = 6.1$ and $Re_{c,r} = 2093$, Table 3) for one of the four sets are the reference values used in connection with equations (3)-(5).

Since f is inversely proportional to Re in laminar flow, the use of the empirically determined corrections to locate the departure from laminar flow at the same point as for the reference results in exact coincidence of the laminar f_m versus Re_m data for all passages. In the transition and turbulent flow regions, the general trend is one of a dependence of f_m on the geometric details of the enhanced passages. This is an experimental verification of the *frictional law of corresponding states* as discussed in

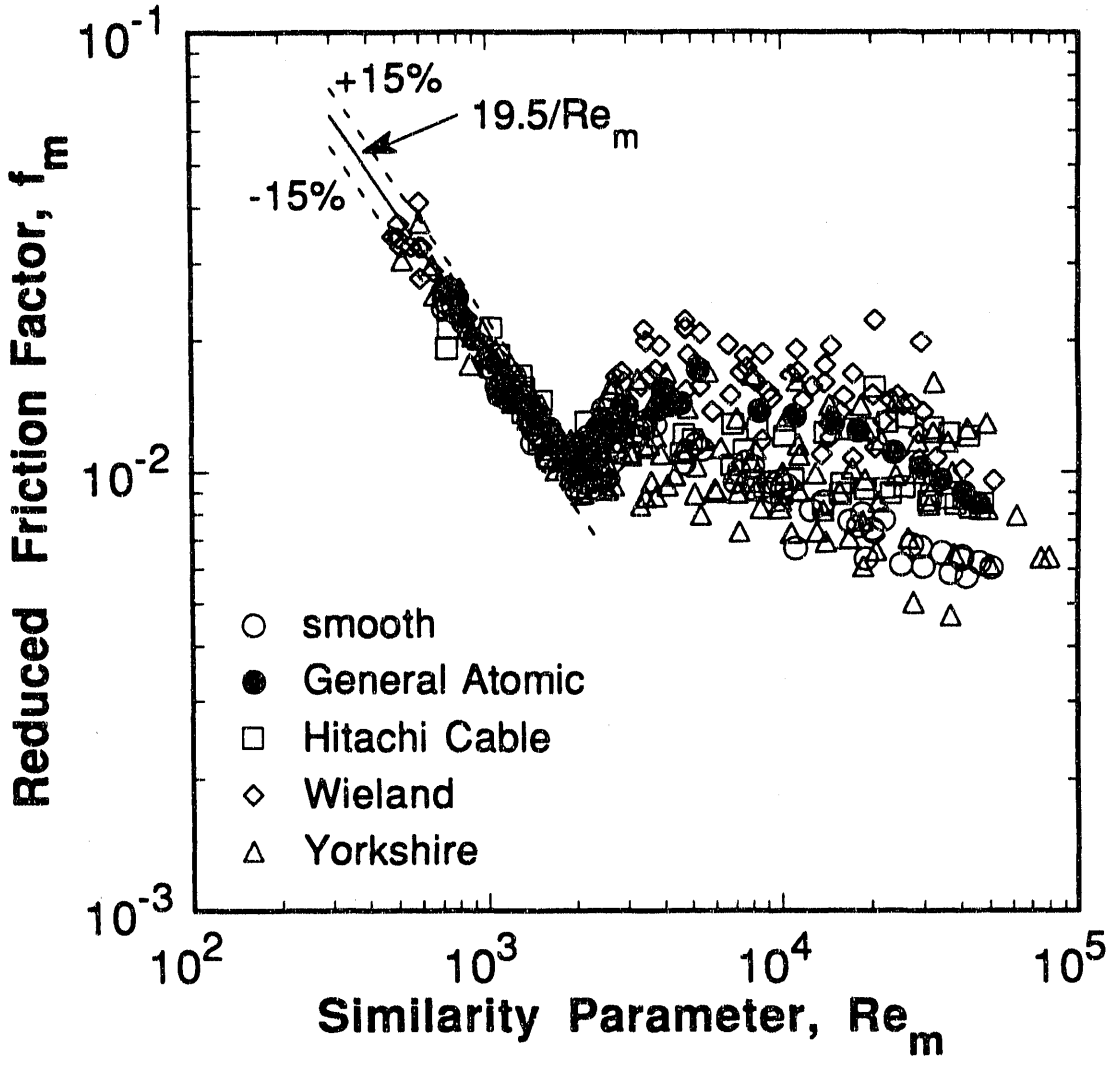

Fig. 16 Reduced friction factor vs. similarity parameter, Re_m.

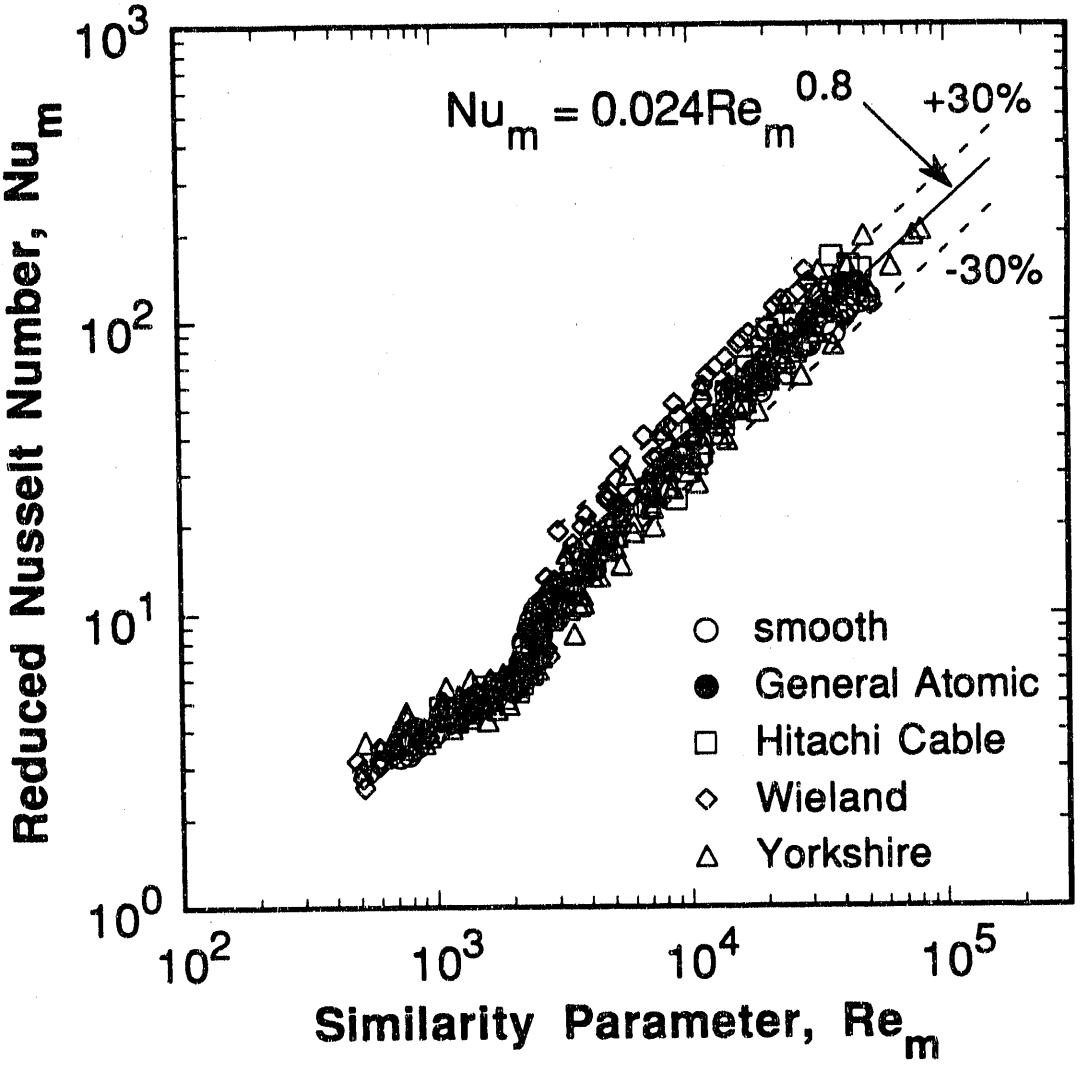

Fig. 17 Reduced Nusselt number vs. Re_m.

Obot *et al.* (1990a,b); the general behavior of the reduced friction factor is the same as presented therein using the results of other investigators. In passing, it is noted that, when the reference critical parameters are those without heating, the general behavior is exactly the same as on Fig. 16; but the laminar data for all passages are approximated by $f_m = 16/Re_m$.

Figure 17 shows that, despite the marked variation of Nu with Re over the entire range of conditions tested, the data sets for all enhanced and the smooth passages collapse into in a narrow band, with errors that are, for the most, under ±20%. The proposition that the average heat transfer coefficients for enhanced passages may be calculated from the data for a smooth passage (Obot *et al.*, 1990a,b) is hereby completely verified.

For $Re_m \geq 3000$, the data in Fig. 17 are approximated by the relation

$$Nu_m = 0.024 Re_m^{0.8} \tag{10}$$

where the exponent on Re_m has been rounded to the widely used value of 0.8. With this exponent, the mean value for the coefficient is insensitive to the Re_m range over which the data are fitted. For instance, the mean values obtained for the $5000 \leq Re_m \leq 80000$ and $10000 \leq Re_m \leq 80000$ ranges are 0.025±0.053 and 0.026±0.053, respectively; the standard errors are practically the same. At the same reduced conditions, the turbulent flow data are correlated essentially with the same exponent on Re_m, just as the laminar flow data are closely correlated with a 1/2 exponent on Re_m. This supports the contention in Section 4.3 that the widely observed variations in the Reynolds number exponent are associated with the transition process.

4.4.3 Validation of Friction-Heat Transfer Analogy

There was a temptation to give this section the title "A Generalized Friction-Heat Transfer Analogy" because there are clear indications that the outcome of the analysis is of general validity. It is demonstrated conclusively in the preceding section that heat transfer coefficients for smooth and enhanced passages can be computed from a reference set of data provided the critical transition parameters are known. A similar conclusion is valid for friction factor in laminar flow. The fact that the f_m versus Re_m data in

the transition and turbulent regimes consists of a family of geometry dependent curves is a reflection of the need for a more general treatment, especially since correlation of the turbulent flow f_m data in terms of Re_m and the disruption geometric variables is unlikely to result in generally valid equations.

For smooth passages, it was established that C_h $(= Nu/Re^{1/2})$ in laminar flow varied markedly with the Prandtl number (Obot and Esen, 1992a, see Appendix 1), but it was possible to reconcile all such data at the same reduced conditions, that is, when $C_{h,m}$ $(=Nu_m/Re_m^{1/2})$ was plotted against Re_m. When the four sets of smooth passage data were presented as C_h/C_f $(= Nu/(Re^{3/2}f))$ versus Re and as $C_{h,m}/C_{f,m}$ $(=Nu_m/(Re_m^{3/2}f_m))$ versus Re_m, the value of C_h/C_f was practically the same as that for $C_{h,m}/C_{f,m}$, this in spite of the differences in the critical parameters (Table 3). These considerations prompted analysis of the friction and heat transfer data to determine if a general analogy can be established. The discussion of the results of this development effort follows.

Figures. 18 and 19 respectively are plots of C_f and C_h versus Re. In both figures, results are given for the entire Re range covered in the experiments. The trend with increasing Re for C_h/C_f is illustrated in Fig. 20. Due to the large amount of information and for the sake of clarity, a common symbol is used for each set of passage in these figures.

The general features on each of Figs. 18-20 appear somewhat confused. In each figure, there is considerable spread of the experimental data, but this must be expected considering the differences in the geometric details of the flow passages as well as the attendant effect of transition to turbulence. In laminar flow, C_f, C_h, and hence C_h/C_f, are independent of the Reynolds number for a given flow passage, regardless of whether it is smooth or enhanced. However, the trend in each figure is obscured by the consolidation of all data into a single plot. The C_f trend with increasing Re and the shape of the curves are very similar to those for C_h; the main difference between the two sets of data is that C_f is considerably greater than C_h. As a result, C_h/C_f decreases markedly with increasing Re for smooth and enhanced passages for $Re > 2100$ (Fig. 20).

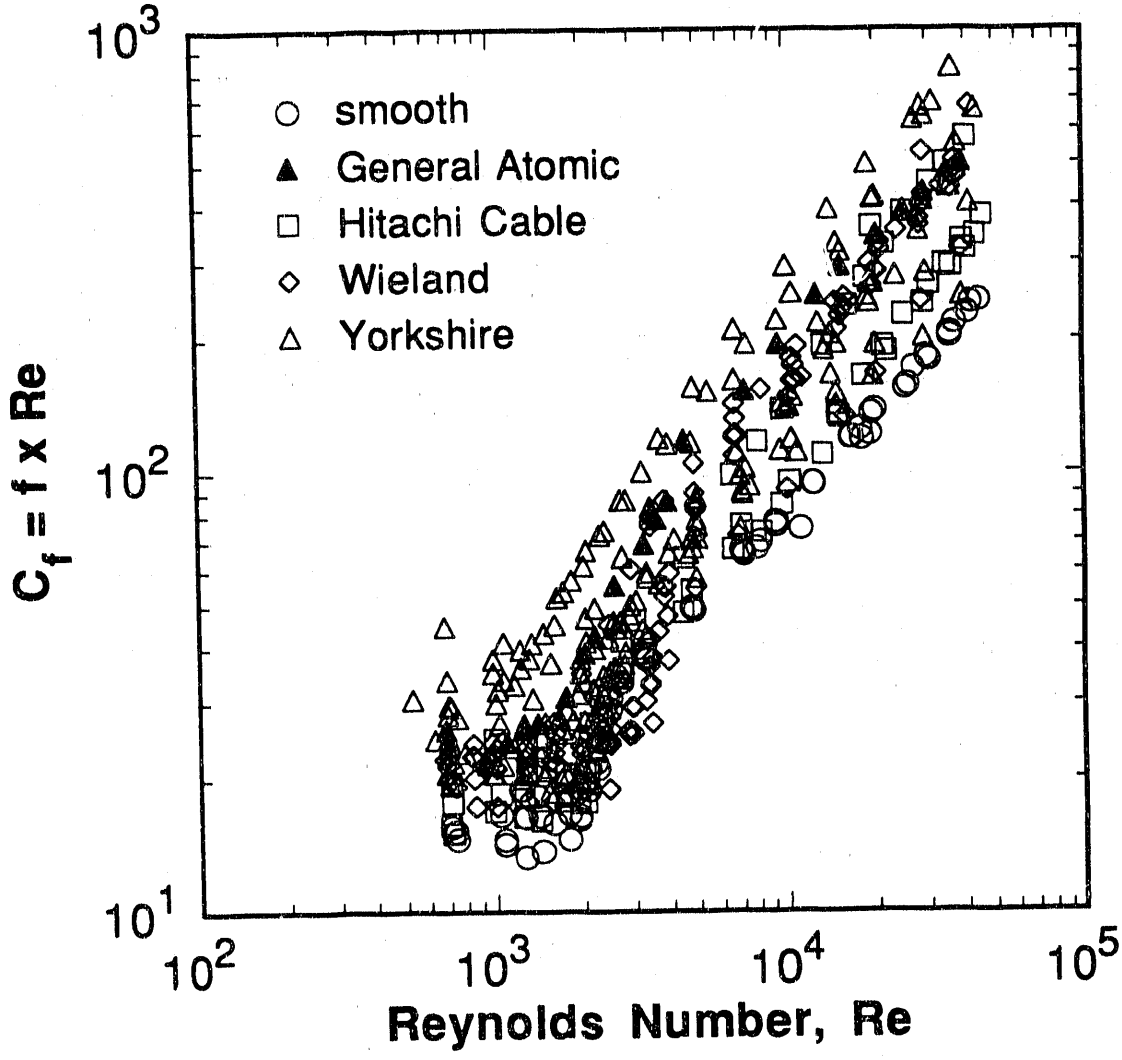

Fig. 18 Friction parameter C_f vs. Reynolds number.

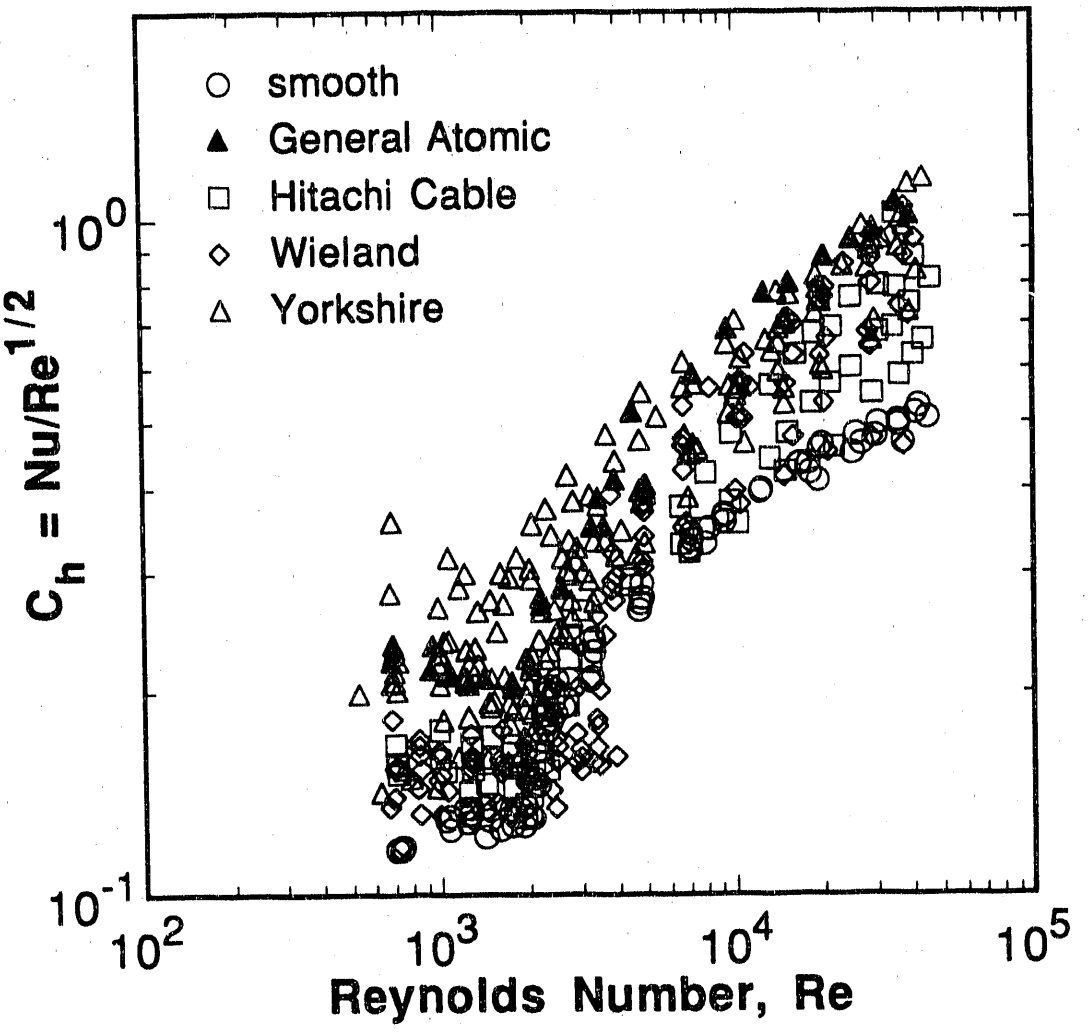

Fig. 19 Heat transfer parameter C_h vs. Reynolds number.

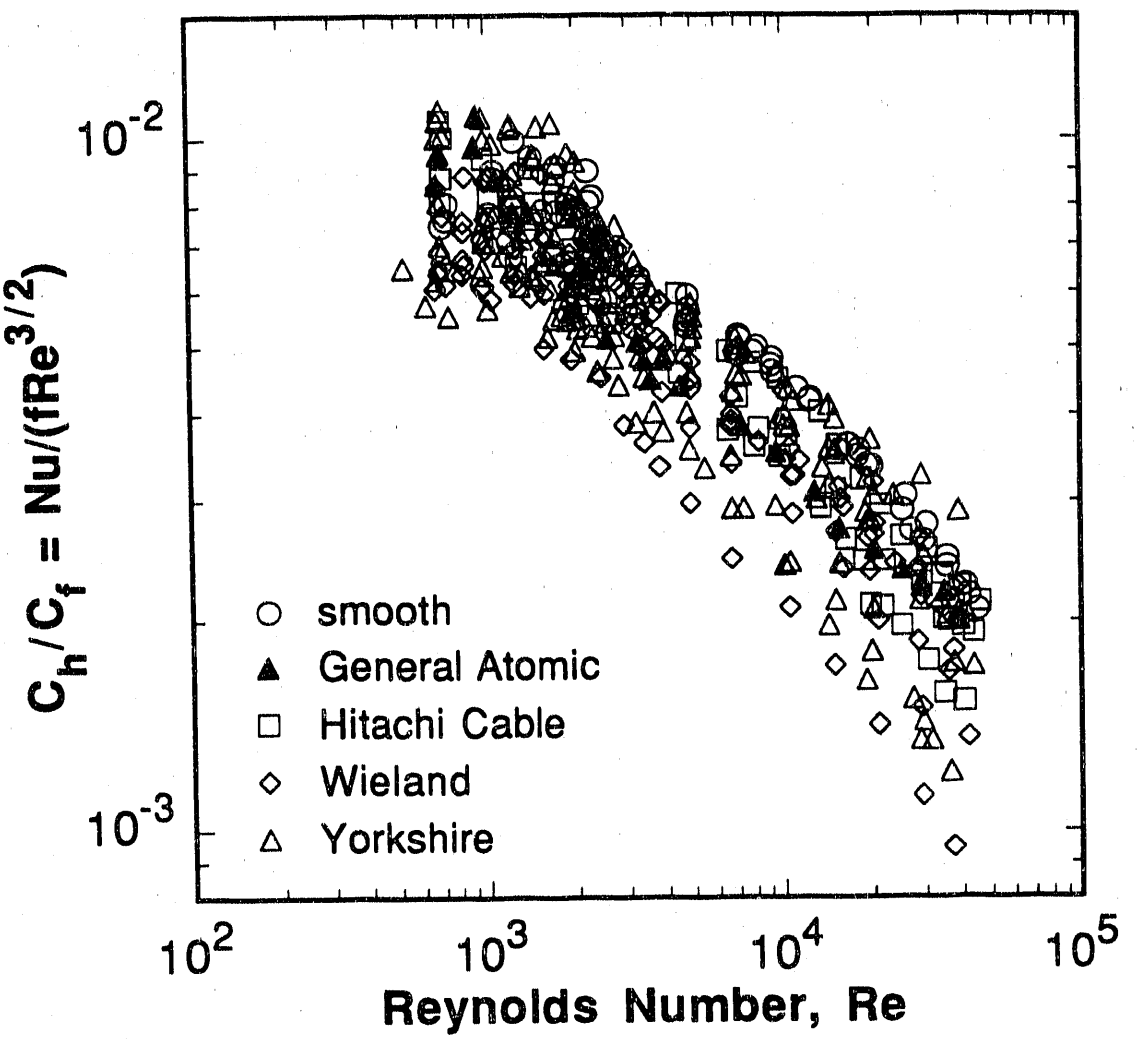

Fig. 20 Plot of C_h/C_f vs. Reynolds number.

Fig. 21, a plot of (Nu_c/f_c) versus Re_c using the data of Table 3, shows the relationship between the three critical parameters. The data are approximated by the relation

$$Nu_c/(Re_c^{3/2} f_c) = 0.0075 \tag{11}$$

The 1.5 exponent on Re_c is not the result of a regression analysis but rather the value occurring in the ratio C_h/C_f. The constant 0.0075, based on all experimental data, is somewhat higher than the value of 0.0061 deduced from the smooth passage data (Obot and Esen, 1992a, Appendix 1).

Equation (11) is of particular importance for several reasons. First, it affords direct calculation of the critical Nusselt number at the onset of transition from known critical values of f_c and Re_c, and vice versa. This, in turn, permits computation of heat transfer coefficients for any particular passage (smooth or enhanced) from the pressure drop data as outlined subsequently. Also, as demonstrated in the presentation which follows, this equation is central to the calculation of pressure drop for smooth and enhanced passages using heat transfer data.

Figures 22 and 23 respectively are plots of $C_{h,m}$ and $C_{h,m}/C_{f,m}$ versus Re_m. The reduced enhanced tube data of Watkinson *et al.* (1974, $Pr = 289$), and of Smith and Gowen (1965, $Pr = 349$) are also included in Fig. 22 for the purpose of comparison. In laminar flow, the data on both figures are closely approximated by the relations

$$C_{h,m} = Nu_m/Re_m^{1/2} = 0.13 \tag{12}$$

and

$$C_{h,m}/C_{f,m} = Nu_m/(Re_m^{3/2} f_m) = 0.0068 \tag{13}$$

Both equations are valid for $Re_m \leq 2100$ with $f_{c,r} = 0.0093$, $Nu_{c,r} = 6.1$ and $Re_{c,r} = 2093$ as the reference critical parameters. For equation (13), $C_{f,m} = 19.5$ (Fig. 16). Since the slightly adjusted values of $f_{c,r} = 0.009$, $Nu_{c,r} = 6.0$ and $Re_{c,r} = 2100$ give basically the same results, these are the recommended values for friction factor and heat transfer calculations.

The value of 0.13 with a $\pm 6\%$ error band is higher than the 0.09 quoted in the recent paper (Obot and Esen, 1992, Appendix 1). This is a direct consequence of the use of

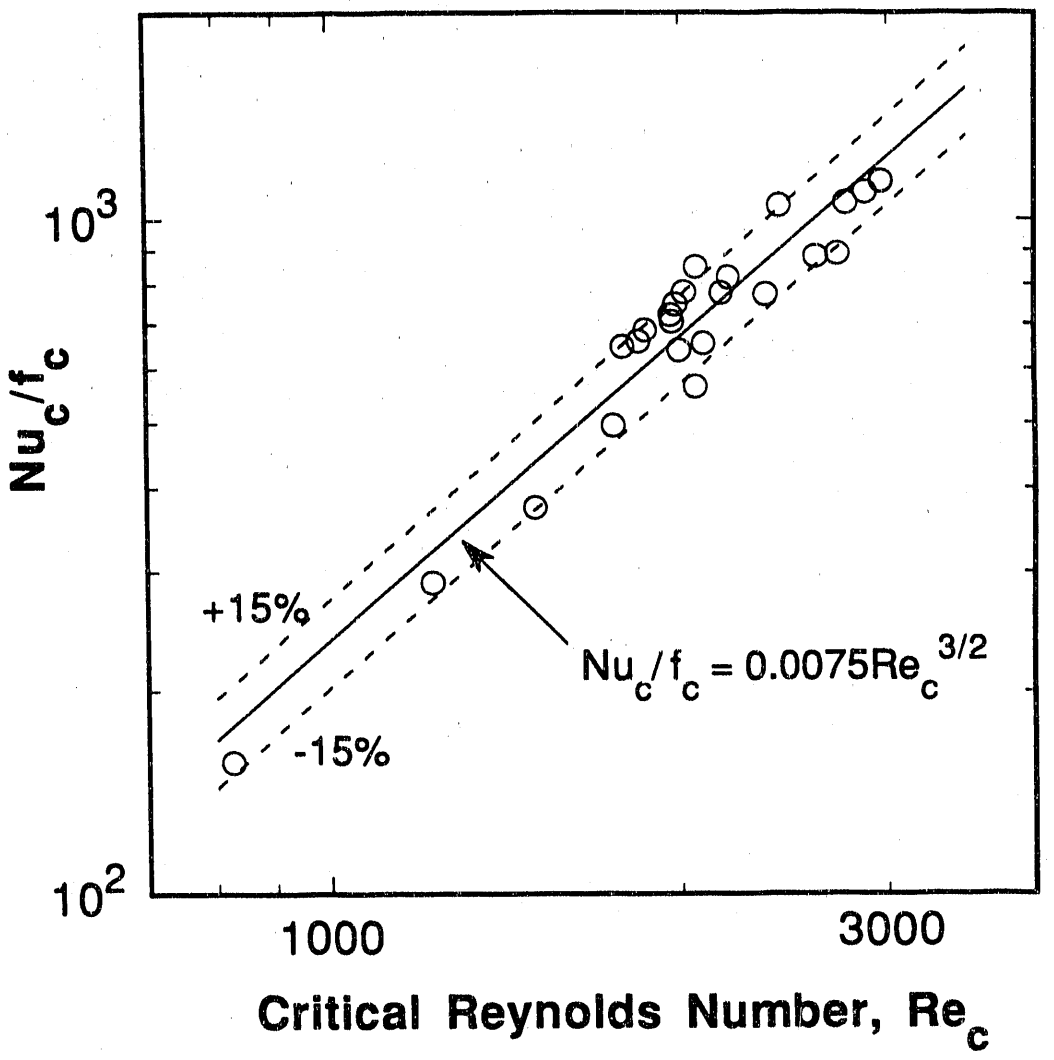

Fig. 21 Relationship between the critical parameters at the onset of transition.

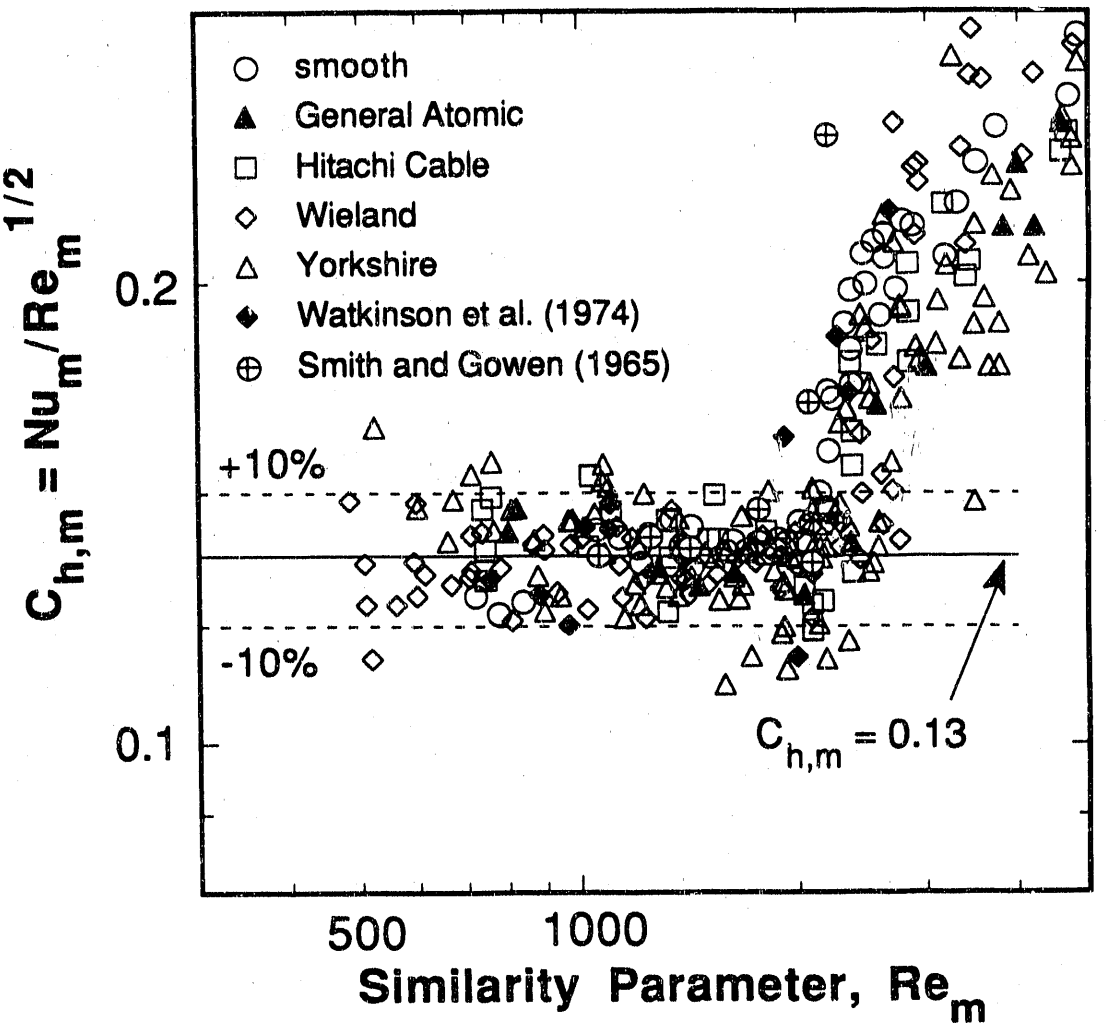

Fig. 22 Plot of $C_{h,m}$ vs. similarity parameter Re_m.

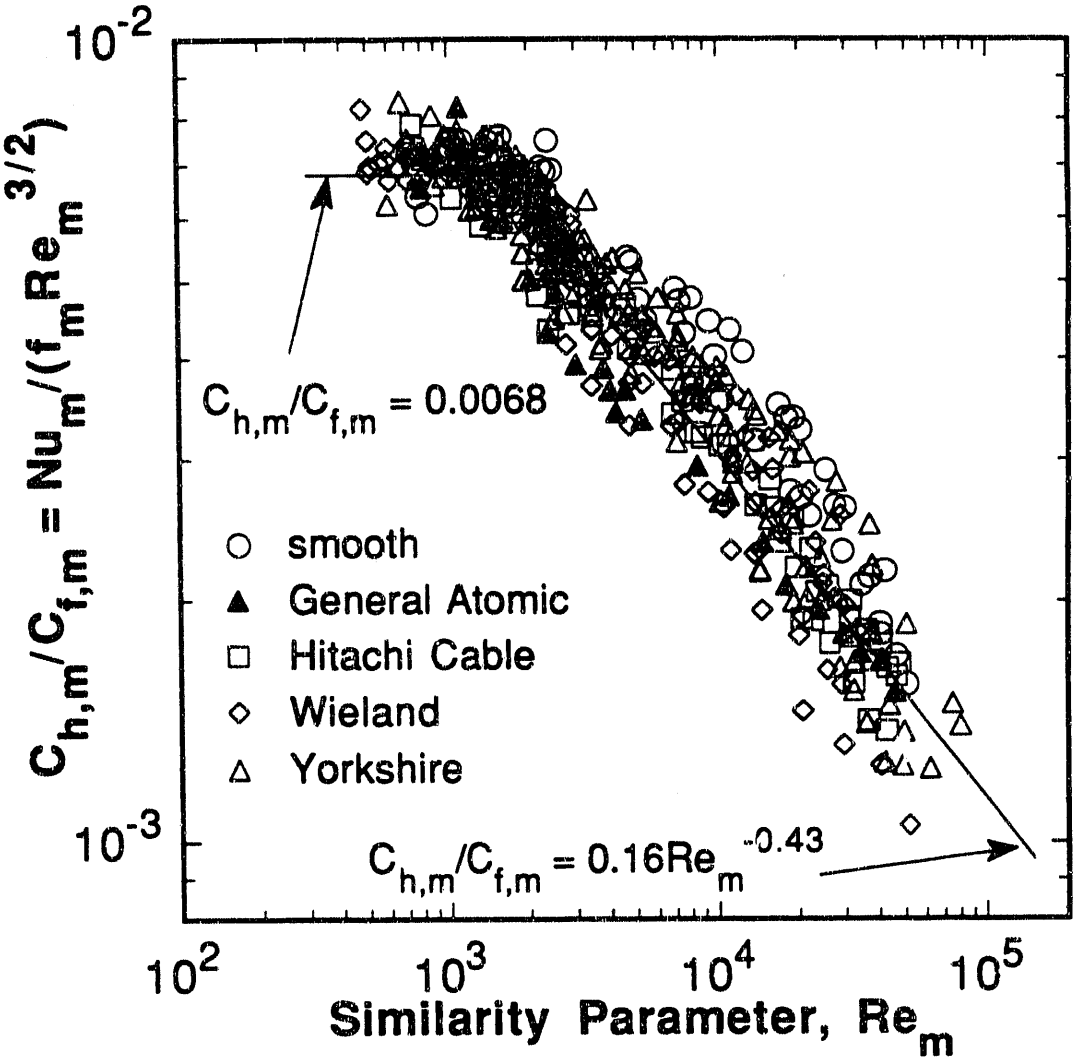

Fig. 23 Plot of $C_{h,m}/C_{f,m}$ vs. Re_m.

the smooth passage $f_{c,r}$ and $Nu_{c,r}$ values for which the critical Re is nearly 2100 ($Re_{c,r}$ = 2093) as the reference values. In the paper cited above, the critical parameters were those corresponding to Re_c = 1843 (Table 3). It is especially noticeable that, despite the marked variations in C_f, C_h and C_h/C_f in laminar flow, the error bands on $C_{h,m}$ and $C_{h,m}/C_{f,m}$ are, for the most part, under ±6% and ±10% respectively, that is, about the same as the overall experimental uncertainty. In Fig. 22, the data of Watkinson *et al.* and Smith and Gowen also lie within the ±6% error band.

For transitional and turbulent flow ($Re_m \geq 2100$), the data on Fig. 23 are satisfactorily correlated by

$$C_{h,m}/C_{f,m} = Nu_m/(Re_m^{3/2} f_m) = 0.16 Re_m^{-0.43} \tag{14}$$

Despite the marked dependence of f_m on the enhanced geometries (Fig. 16) and the spread of the experimental data on Fig. 20, equation (14) predicts nearly 95% of the data with errors that are under ±30%. This is illustrated in the typical scatter plot on Fig. 24. Equations (13) and (14) taken together serve two purposes: first, they provide alternative validation of the frictional law of corresponding states; and second, they are statements of the friction-heat transfer analogy for smooth and enhanced passages.

For $Re_m \geq 2100$, numerous attempts were made to correlate the data. For instance, the use of two separate relations, one for the transition and the intermediate regions which encompass the $2100 \leq Re_m \leq 5000$ range and the other for $Re_m \geq 5000$, did not give very accurate predictions. Suffice it to state that, of the numerous relations developed, the most accurate even for Re_m up to 10^5 is given by equation (14). Another useful information from the analysis is that the dependence of Nu_m/f_m on Re_m is essentially the same in both the transition and turbulent regimes. In passing, it is noted that the choice had to be made between the use of several correlations or one relation for $Re_m \geq 2100$. The latter was adopted by virtue of simplicity and the fact that it provides the basis for practical comparison with published results. Clearly, further refinements will be made as more data become available.

Equation (14) is in complete agreement with the existing literature. For instance, the Blasius equation gives $f = 0.079\ Re^{-0.25}$, while the relation for Nusselt number is

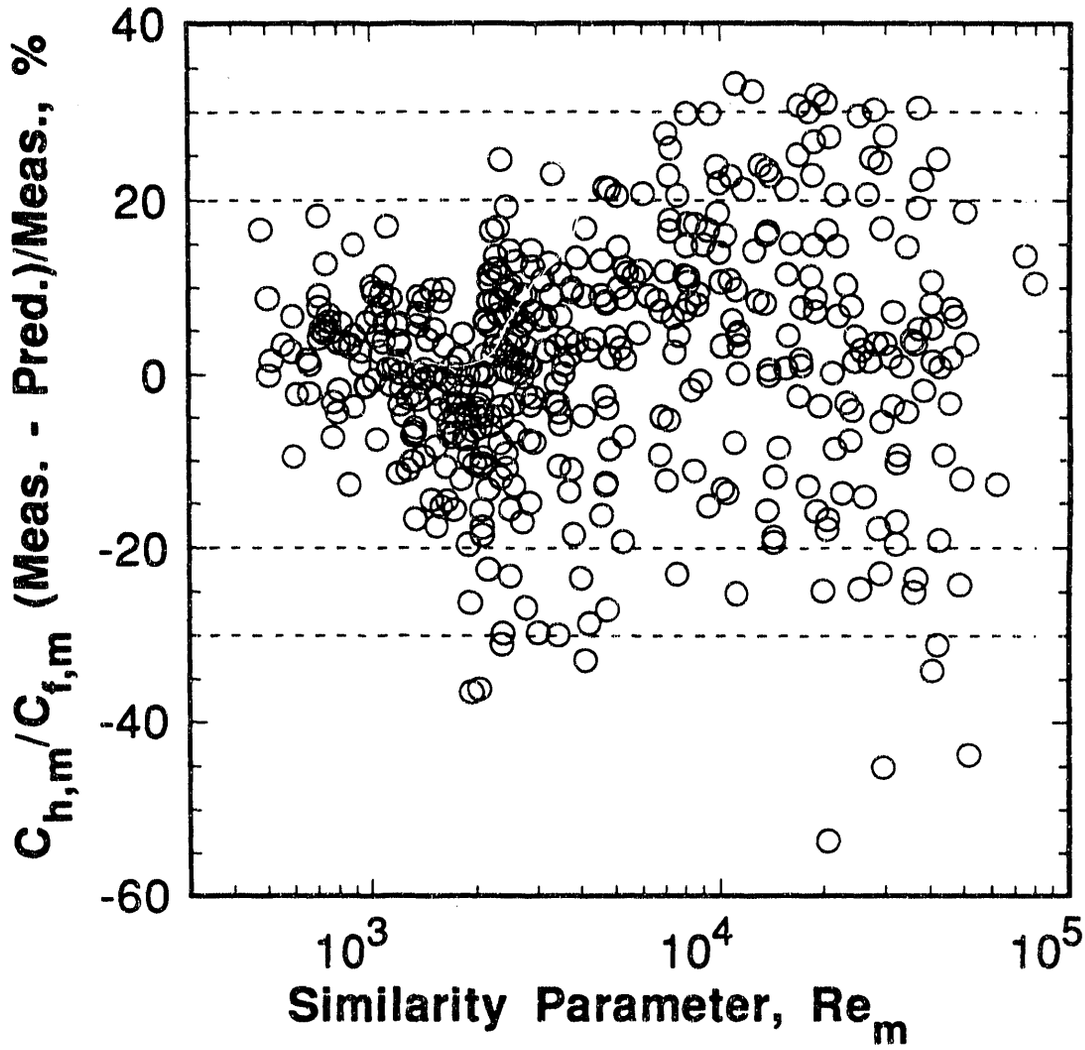

Fig. 24 Scatter plot of proposed correlation.

$Nu = 0.02Re^{0.8}$ based on the Dittus-Boelter equation ($Pr = 0.7$). It follows that $Nu/f = 0.25Re^{1.05}$ in turbulent flow. This can be compared with $Nu_m/f_m = 0.16Re_m^{1.07}$ from equation (14). Clearly, there are differences: 1) the use of f_m, Nu_m and Re_m instead of the usual f, Nu and Re; and 2) the value of 0.16 for the regression coefficient is smaller than that deduced from published data. It is of interest to note that the relation established for $Re_m \geq 5000$ is $Nu_m/f_m = 0.25Re^{1.02}$; the regression coefficient is the same as that based on the Dittus-Boelter and Blasius equations but the data were not adequately represented by this correlation. The remarkable agreement with respect to the effect of flow velocity provides further support for the C_h behavior in laminar flow because the 3/2 exponent on Re derives from the C_h/C_f ratio, with $C_h = Nu/Re^{1/2}$.

There is another comment, especially since it was suggested in previous publications (Obot *et al.*, 1991a,b) that values of Nu_m could be computed from the Petukhov-Popov (1963) correlation by replacing Re and f with Re_m and f_m. For the entire $10^4 \leq Re_m \leq 10^5$, the differences in the calculated Nu_m values between the Petukhov-Popov correlation and equation (14) are (on an average basis) under 10%. Specifically, the largest difference of about 18% occurs for $Re_m = 10^4$; the percentage difference decreases with increasing Re_m to under 2% for both $Re_m = 80000$ and 10^5. The values deduced from equation (14) are always the lower set. The results of this comparative evaluation support the original suggestion. Also, it is worthy of note that, since the denominator in the Petukhov-Popov correlation is a mild function of the Reynolds number (varying from about 0.9 for $Re = 10^4$ to 0.94 for $Re = 10^5$), their correlation gives $Nu/f \propto Re$. Again, the exponent on Re is not significantly different from that of this study, equation (14).

In summary, a general analogy between friction and heat transfer is developed and validated using air data for laminar, transitional and turbulent flow. This alternative treatment of turbulent flow supports the conclusion that the nondimensional heat transfer coefficient (Nu) varies as the 1/2 power of the Reynolds number in laminar flow. The results show conclusively that there is a definite connection between transition and the enhancement for friction and heat transfer. From a practical standpoint, the results afford direct calculation of heat transfer coefficients for smooth and enhanced passages

from friction factor data, and vice versa.

4.4.4 Consistency with the Reynolds Analogy

By definition, the Stanton number (St) is given by

$$St = Nu/RePr$$

Using this relationship and for $Pr = 0.7$, it is easily established that the alternative form of equation (13) for laminar flow is

$$St_m/f_m = 0.0095Re_m^{1/2} \tag{15}$$

or

$$St_m = 0095C_{f,m}/Re_m^{1/2} \tag{16}$$

where $C_{f,m} = f_m \times Re_m$. With $C_{f,m} = 19.5$ based on the $Re_c = 2100$ data as the reference, the reduced Stanton number relation becomes

$$St_m = 0.186/Re_m^{1/2} \tag{17}$$

For transitional and turbulent flow, a rather interesting result is obtained when equation (14) is re-written in terms of the reduced Stanton number, St_m. For $Pr = 0.7$, it is readily determined that the resulting equation is

$$St_m = 0.23f_m Re_m^{0.07} \tag{18}$$

The $Re_m^{0.07}$ term is practically constant over a wide Re_m range. For example, the computed values for $Re_m = 10000$, 40000, 80000 and 10^5 are 1.91, 2.10, 2.20 and 2.24, respectively; the average value is 2.11 ± 0.13. The use of this mean value in equation (18) gives

$$St_m = 0.49f_m \simeq \frac{1}{2}f_m \tag{19}$$

Equation (19) is a statement of the well known Reynolds analogy. However, unlike the conventional Reynolds analogy, the relation holds for both smooth and enhanced passages at the same reduced conditions which account for transition. Again, the outcome of the analysis fully supports the 1/2 power dependence of the Nusselt number

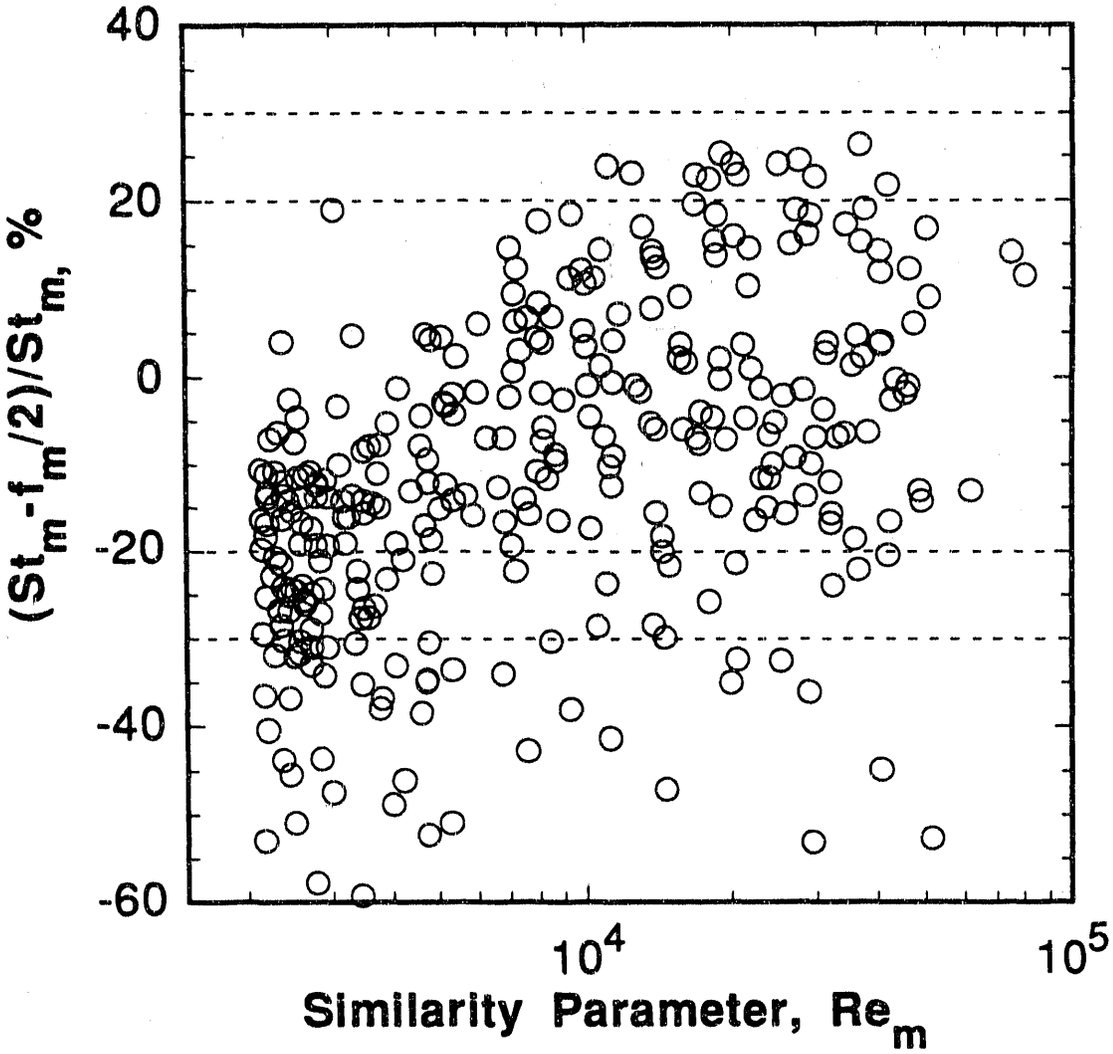

Fig. 25 Scatter plot of the Reynolds analogy at reduced conditions.

on the Reynolds number in laminar flow as well as the validity of the frictional law. For laminar, transitional and turbulent flow, the relations developed here also afford calculation of heat transfer coefficients from the friction factor data.

Figure 25 shows the scatter plot for equation (19). The calculated values are within ±30% for most of the data; the equation overpredicts about 15 data points by 30 to 50% for $Re_m \geq 5000$. About ten of the 15 points are associated with the W-11 and W-12 passages; these passages also account for most of the larger deviations over the $2100 < Re_m < 5000$ range.

4.4.5 Calculation of Nusselt Number or Friction Factor

We conclude the discussion of the validation of the *frictional law of corresponding states* by considering the calculation of nondimensional heat transfer coefficients from the friction factor data, and vice versa.

In laminar flow, plots of f_m and Nu_m versus Re_m are completely generalized. As a result, equations (12) and (13) give basically the same value of Nu_m. By contrast, whereas reasonable collapse of the Nu_m versus Re_m data is realized in the transition and turbulent regimes for all passages (Fig. 17), there is considerable spread of the f_m versus Re_m data (Fig. 16). In other words, a generalized Nu_m versus Re_m curve can be associated with an infinite number of f_m-Re_m curves. The consequence of this largely unacknowledged anomaly is that the Nu_m values determined from equation (10) (based solely in terms of Re_m) are generally higher than those deduced from the relation given in terms of f_m and Re_m (equation (14)), even though the error bands for both correlations are roughly about the same.

For turbulent flow, the results of comparative evaluations of existing correlations are consistent with the above observation. For instance, the Petukhov-Popov correlation gives consistently lower Nu values with $Pr = 0.7$ than the Dittus-Boelter relation for $Re \geq 20000$. In this regard, it is worthy of note that equation (10) is essentially the reduced form of the latter based, of course, on our data, while reasonable agreement with the Petukhov-Popov correlation at the same reduced conditions was established in Section 4.4.3.

From this alternative analysis of the same experimental data, there are several comments. For turbulent flow, the relation $Nu_m = f(Re_m)$ or the conventional $Nu = f(Re, Pr)$ considers the effect of flow velocity or Re and Prandtl number on heat transfer; the well known connection between friction and heat transfer as verified in this study is totally neglected. As a result, equation (10) as well as similar conventional representations do not give accurate estimates of Nusselt number. For turbulent friction factor and heat transfer calculations, equations (14) and (19) are recommended. Finally, to calculate friction factor and heat transfer coefficient using the present method, the procedural steps can be outlined as follows:

1. Determine the critical parameters, $f_{c,a}$ and $Re_{c,a}$, from the arbitrary data set, and compute $Nu_{c,a}$ from equation (11).

2. Calculate f_m and Re_m using $f_m = (f_{c,r}/f_{c,a})f_a$ and $Re_m = (Re_{c,r}/Re_{c,a})Re_a$, respectively, where $f_{c,r} = 0.009$ and $Re_{c,r} = 2100$.

3. Compute Nu_m from equation (12) or (13) for laminar flow and from (14) for $Re_m > 2100$, and then the desired Nusselt number Nu_a using $Nu_a = Nu_m(Nu_{c,a}/Nu_{c,r})$ with $Nu_{c,r} = 6.0$. Alternatively, estimates of Nu_m can be obtained from equations (15)-(17) for laminar flow and from $Nu_m = f_m/2$ for $Re_m > 2100$.

4. To calculate friction factor from known values of $Nu_{c,a}$ and $Re_{c,a}$, compute $f_{c,a}$ from equation (11), determine Nu_m from $Nu_m = (Nu_{c,r}/Nu_{c,a})Nu_a$ and Re_m, and then f_m from the appropriate equations given above. The desired friction factor f_a is calculated from $f_a = f_m(f_{c,a}/f_{c,r})$.

Although the effects of heat transfer on pressure drop can be significant, these manifest themselves through small variations in the critical parameters. Even when there are quantitative differences in values of friction factor due to large physical property variations, these can always be reconciled using the corresponding states relations. As a result, friction factor-Reynolds number data obtained in the absence of heat transfer can be used for heat transfer calculations using the procedures outlined above. In this regard it should be noted that the values of friction factor (Section 4.2) are practically

the same for tests with and without heat transfer at moderate surface temperatures.

4.5 Thermal Performance of Enhanced Tubes

A number of methods are used to effect comparisons of the performance of different types of enhanced surfaces. Of these, the efficiency index, η, defined as the ratio $(St_e/St_s)/(f_e/f_s)$ or $(Nu_e/Nu_s)/(f_e/f_s)$ has been used frequently in the literature (Webb *et al.*, 1971; Gee and Webb, 1980; Rabas, 1988). The index is usually plotted against the roughness Reynolds number $e^+ = (e/D_i)Re(f_e/2)^{1/2}$. For the presentation that follows, the η concept is adopted. However, instead of e^+, we will continue to use the similarity parameter, Re_m.

Figures 26 and 27 are compact plots of η versus Re_m. In laminar flow, many of the passages give η values that lie between 1 and 2. For a number of cases, the η values lie well below one within the transition region. In turbulent flow, at least three distinct trends are observed in Figs. 26 and 27: 1) η decreases with Re_m; 2) it is essentially independent of Re_m; and 3) it increases with Re_m.

It is difficult to draw an accurate conclusion from the results on Figs. 26 and 27 regarding the performance of the various passages because of the complexities introduced by the transition process, that is, by variations in values of the critical friction factor and Nusselt number. This difficulty is not eliminated by the use of the similarity parameter Re_m which, as documented in the preceding sections, affords satisfactory treatment of the experimental data. In fact, it may be argued that the straightforward use of $(Nu_e/Nu_s)/(f_e/f_s)$ (or $(St_e/St_s)/(f_e/f_s)$) leads to conclusions that are not of general validity, regardless of the choice of the correlating parameter for the abscissa. These considerations favor the use of the corresponding states method to provide a generalized reference condition of a physical nature for performance evaluations.

Figures 28 and 29 are plots of $\epsilon_m = (Nu_m/Nu_s)/(f_m/f_s)$ versus Re_m at the same reduced conditions. It is quite apparent from comparison between Figs. 26 (or 27) and 28 (or 29) that each of the latter affords definite conclusions on the performance of related as well as unrelated enhanced passages. For instance, in sharp contrast to the behavior in Figs. 26 and 27, the same trend with increasing Re_m is clearly in evidence for

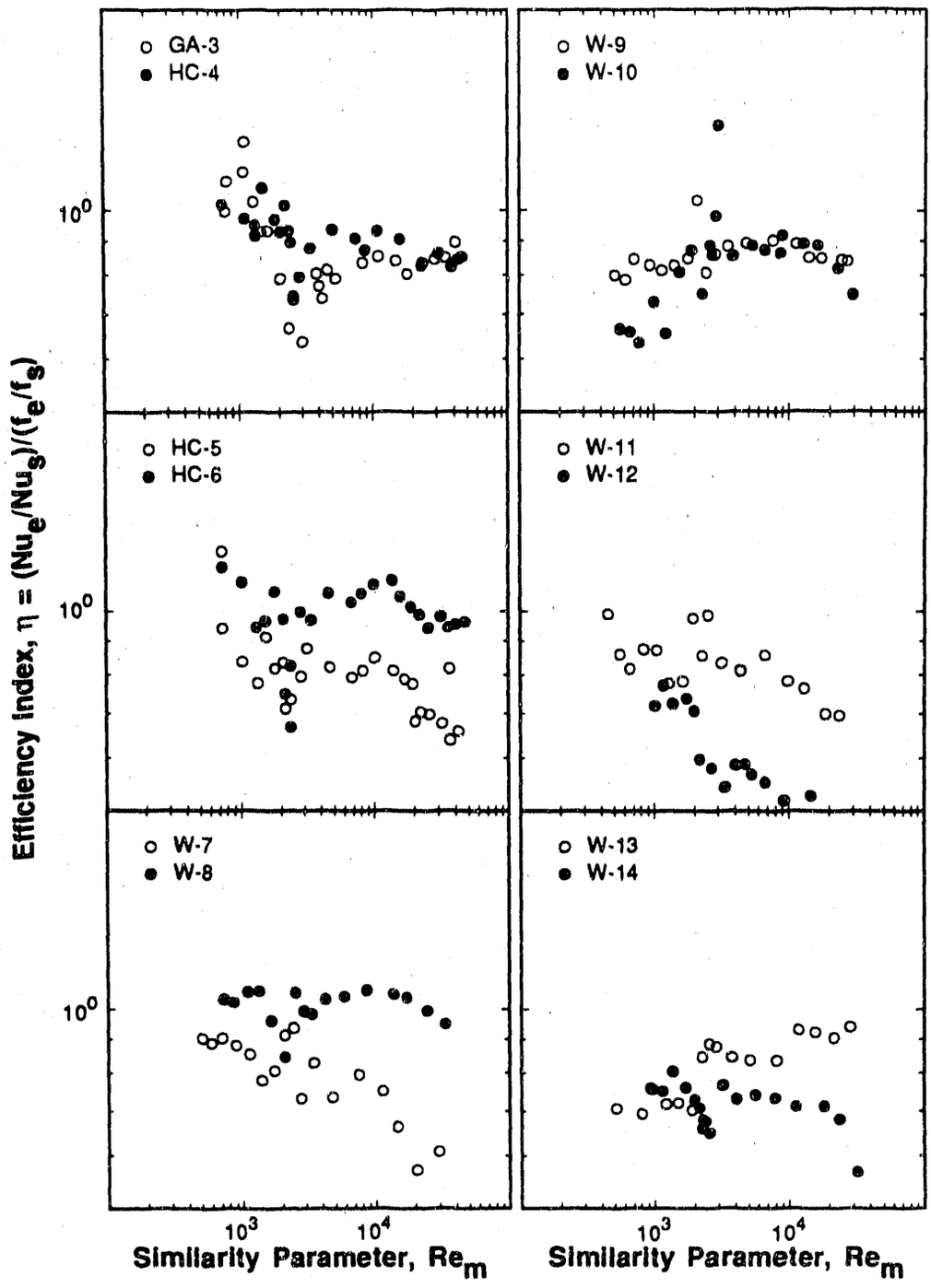

Fig. 26 Plot of efficiency index vs. *Re* for GA-3 - Y-14.

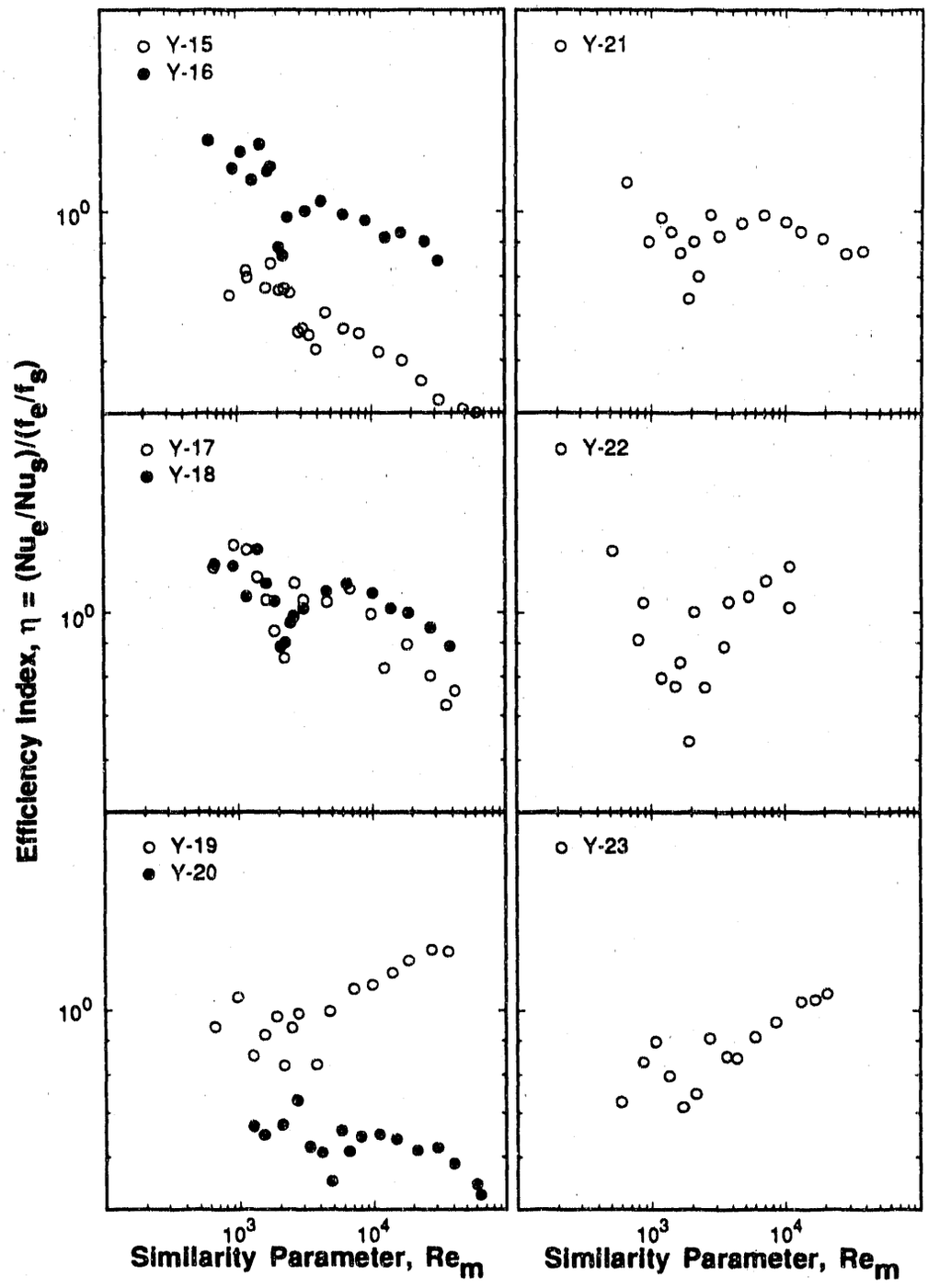

Fig. 27 Plot of efficiency index vs. *Re* for Y-15 - Y-23.

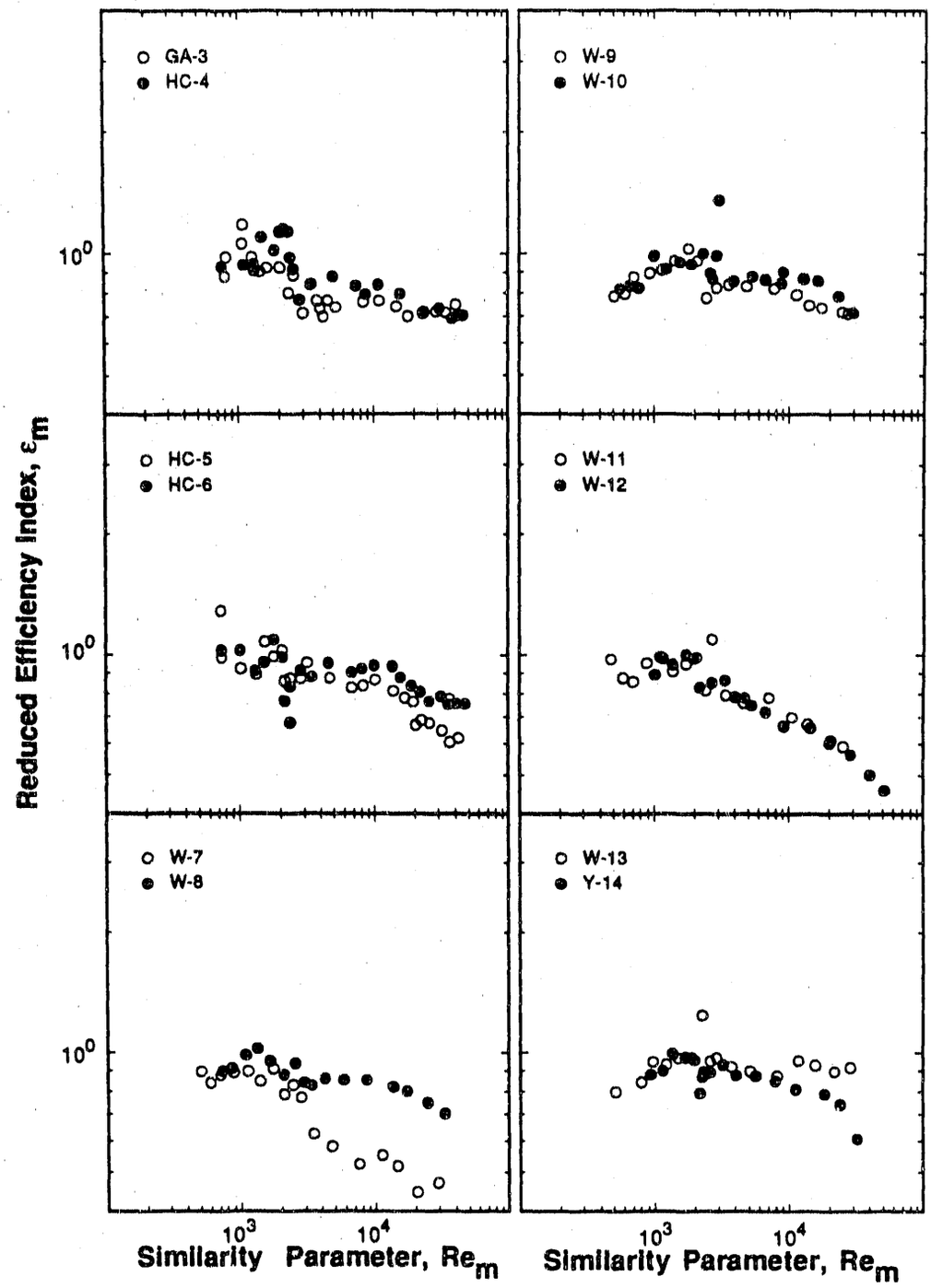

Fig. 28 Plot of reduced efficiency index vs. Re_m for GA-3 - Y-14.

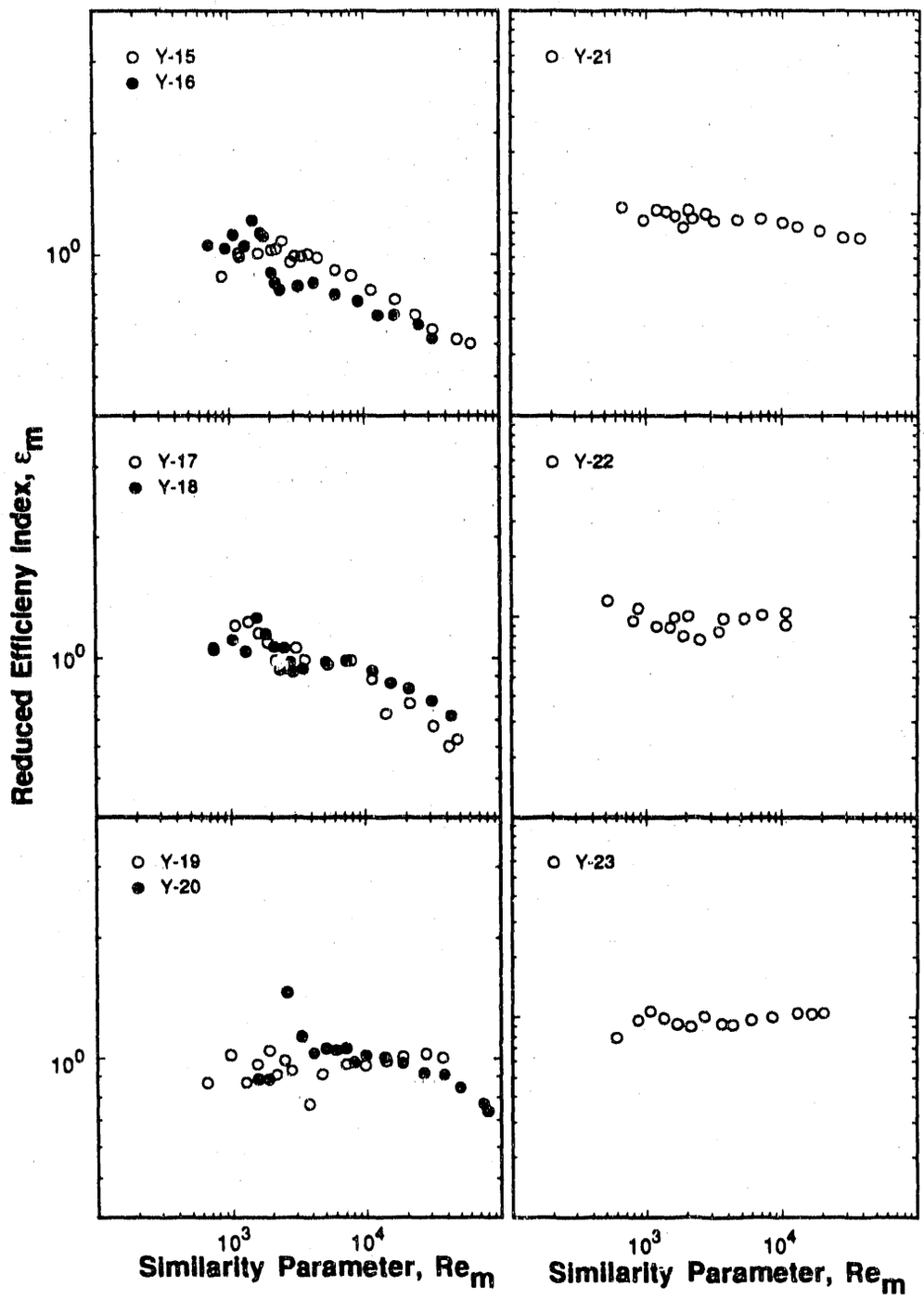

Fig. 29 Plot of reduced efficiency index vs. Re_m for Y-15 - Y-23.

passages of the spirally fluted type (GA-3, Y-22 and Y-23). Similarly, the performance of the enhanced passages from different suppliers, such as the spirally ribbed (W-7 through W-13) or indented (Y-14 through Y-21) passages, can be compared without regard to the differences in e/D_i, p/e, α and N_s.

In laminar flow, ϵ_m approaches unity for all passages. Note that this behavior is a consistent one and, in contradistinction to that depicted on Figs. 26 and 27, the deviations from unity are small. Clearly, this is an indication that the best performance is realized in laminar flow. This rather interesting observation is not surprising because $Nu_m/f_m \propto Re_m^n$, where $n = 1.5$ in laminar flow and decreases within the transition region to approach nearly 1 for turbulent flow.

For $Re_m \geq 2100$, ϵ_m decreases gradually with increasing Re_m; exceptions to this trend are observed for 6 passages (GA-3, W-8, W-13, Y-19, Y-22 and Y-23). For the latter, ϵ_m is essentially independent of Re_m; the trends as well as the magnitude of ϵ_m differ markedly from those on Figs. 26 and 27 for η. Note that the GA-3, Y-22 and Y-23 passages are of the spirally fluted type.

In summary, it is demonstrated that consideration of the effects of transition to turbulence on friction factor and heat transfer is central to a meaningful comparison of the performance of various types of enhanced surfaces. The selection of enhanced passages based on the conventional $(Nu_e/Nu_s)/(f_e/f_s)$ data is not recommended.

4.6 Comparisons with Published Data

It is stated at the outset that a 0.4 power dependence of the Nusselt number on the Prandtl number is assumed in order to effect comparisons of the present air data with those obtained with liquids. It would be unwise to infer from this presentation that Nu always varies as the 0.4 power of Pr for air. Also, it is noted that exact coincidence of the present smooth passage heat transfer data in turbulent with the air data of Ravigururajan and Bergles (1986) was obtained (Obot *et al.*, 1991b). And, further, agreement of the smooth tube turbulent heat transfer data with the Petukhov-Popov (1963) correlation is good, as documented in the paper cited above.

Figures 30 and 31 are comparisons of the present friction factor data with those of previous studies. For the GA-1 - GA-3 passages of the spirally fluted type, Fig. 6 established that the f versus Re data are practically the same. In Fig. 30, the present data for GA-3 are compared with those obtained with water as the working fluid (Ravigururajan and Bergles, 1986; Yampolsky *et al.*, 1984; Panchal and France, 1986). For the last two studies, the pressure drop and flowrate data were reduced using the hydraulic diameter D_h $(= 4A_x/P_w)$; the value of which is, for an enhanced passage, smaller than the maximum internal diameter, D_i. The results of these authors have been re-evaluated in terms of D_i using the values of D_h and D_i in the original publications. In Fig. 31, the data for the three-dimensional spiral ribs are compared with those of Takahashi *et al.* (1985).

Figure 30 shows that the differences between the present data and those of Panchal and France or Yampolsky *et al.* are small; the data of Ravigururajan and Bergles are about 30% lower than the present results. For the three-dimensional spiral ribs (Fig. 31), our data for $e_1/D_i = 0.028$ and $p_1/e_1 = 11.4$ are almost coincident with those of Takahashi *et al.* for $e_1/D_i = 0.022$ and $p_1/e_1 = 12.6$. Their results for the other test conditions lie above the present data, a reflection of the differences in the geometric details (height, pitch, helix, angle, etc.) of the enhanced surfaces. Note that only the primary values of relative height and pitch are given in Fig. 31.

Figures 32 and 33 show comparisons of the corresponding heat transfer results for which the friction factors are given in Figs. 30 and 31, respectively. As with Fig. 30, Fig. 32 shows that there are no significant differences between the scaled air data and those of the other investigators for the comparable GA-3 passage. Similarly, in Fig. 33, the deviations of the air data from those of Takahashi *et al.* for the comparable geometry are small.

In summary, it is evident from the results on Figs. 30-33 that the laminar and transition regions were not considered in the studies cited herein. A review of the literature revealed no systematic studies with comparable enhanced passages for the laminar, transition and turbulent regimes. As a result, the method developed in this study cannot be applied to these confirmable turbulent flow results.

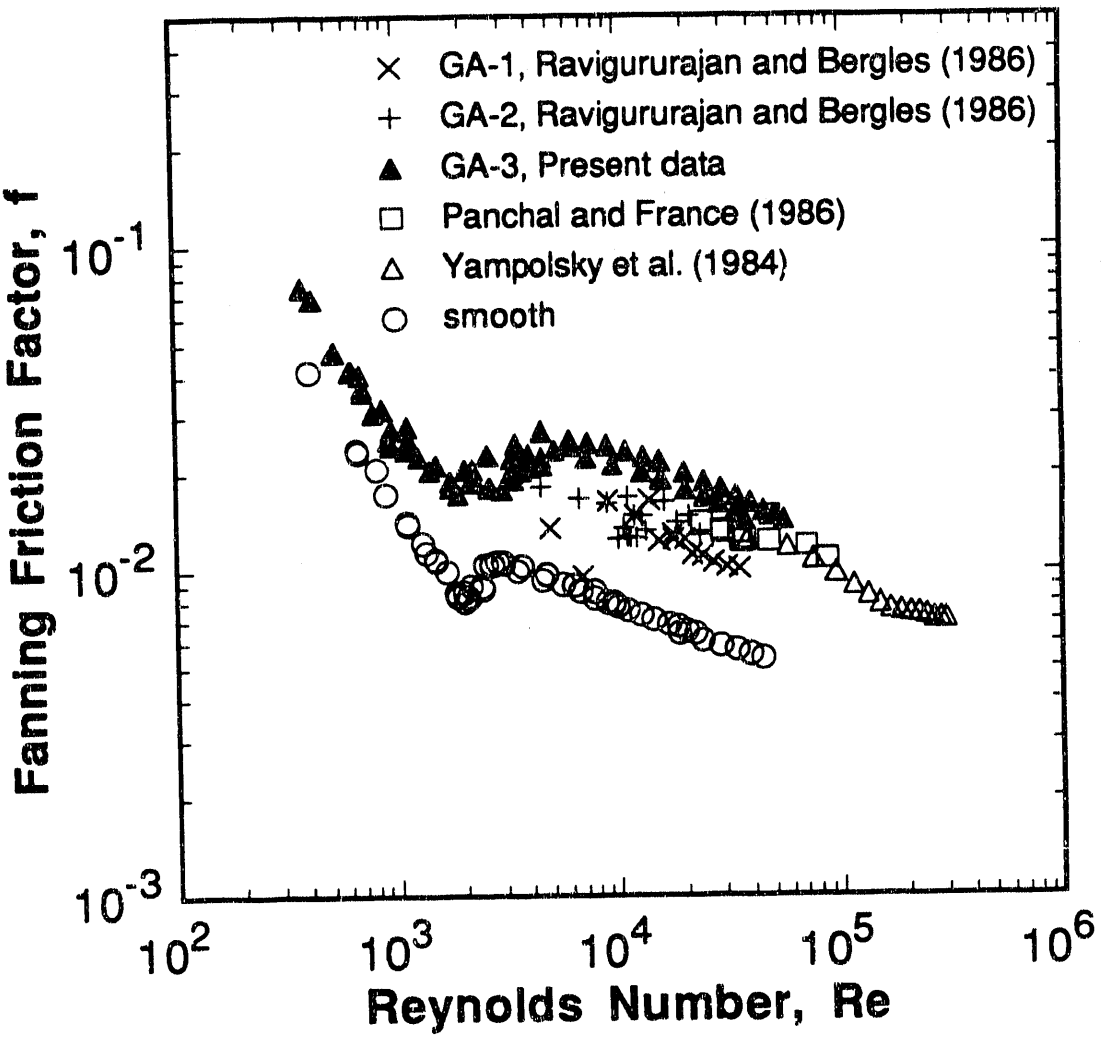

Fig. 30 Comparison of spirally fluted friction factor with published data.

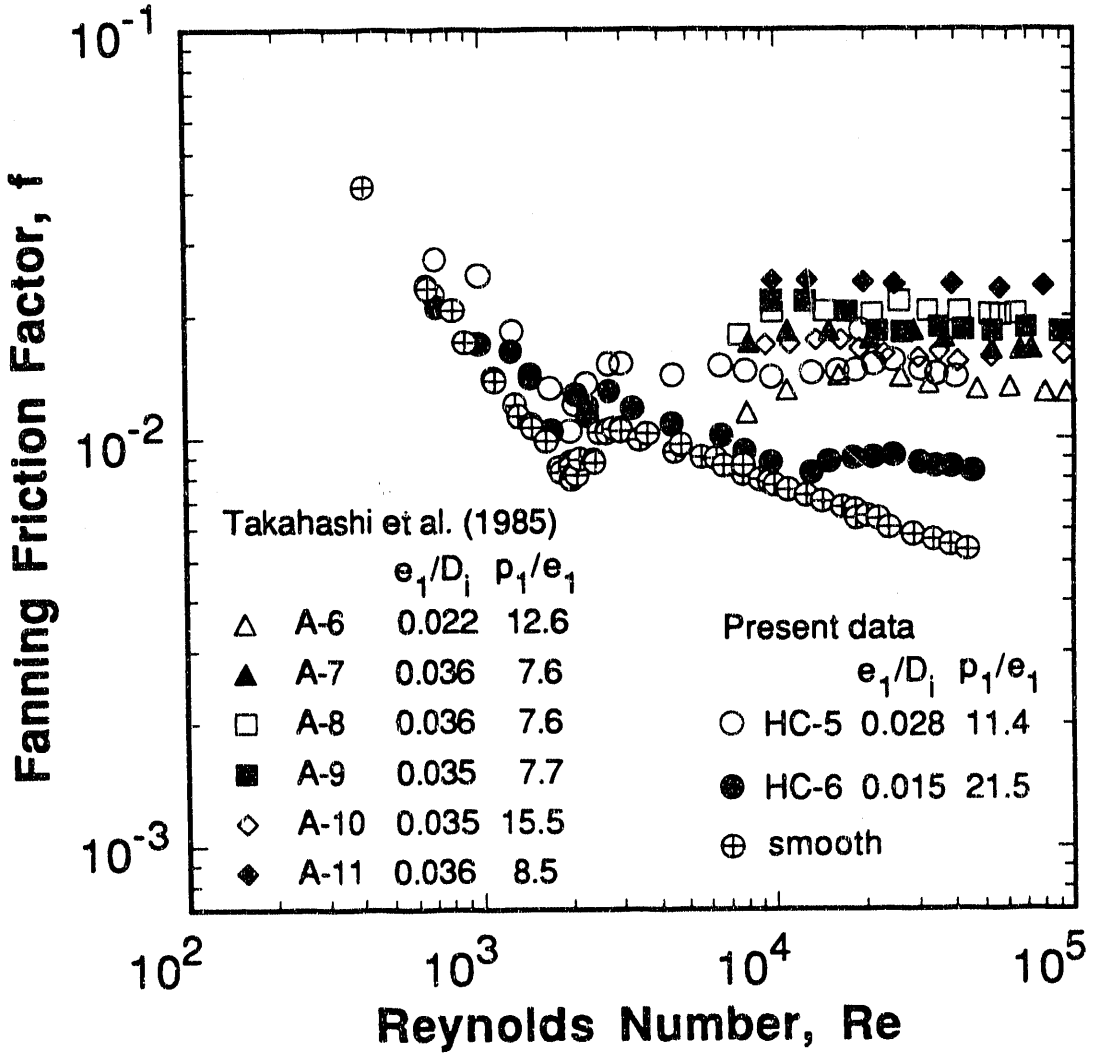

Fig. 31 Comparison of 3D friction factor with those of Takahashi *et al.*

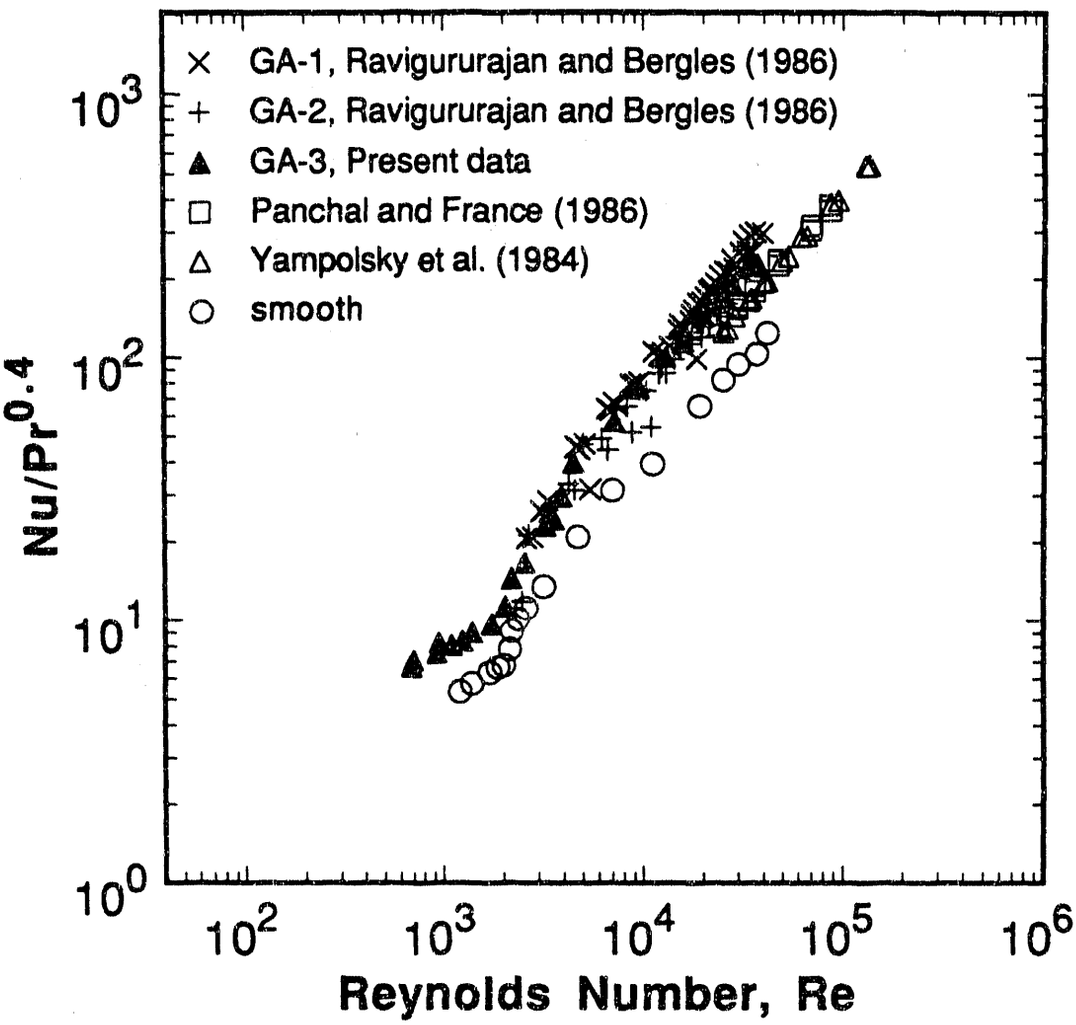

Fig. 32 Comparison of spirally fluted tube Nu data with published results.

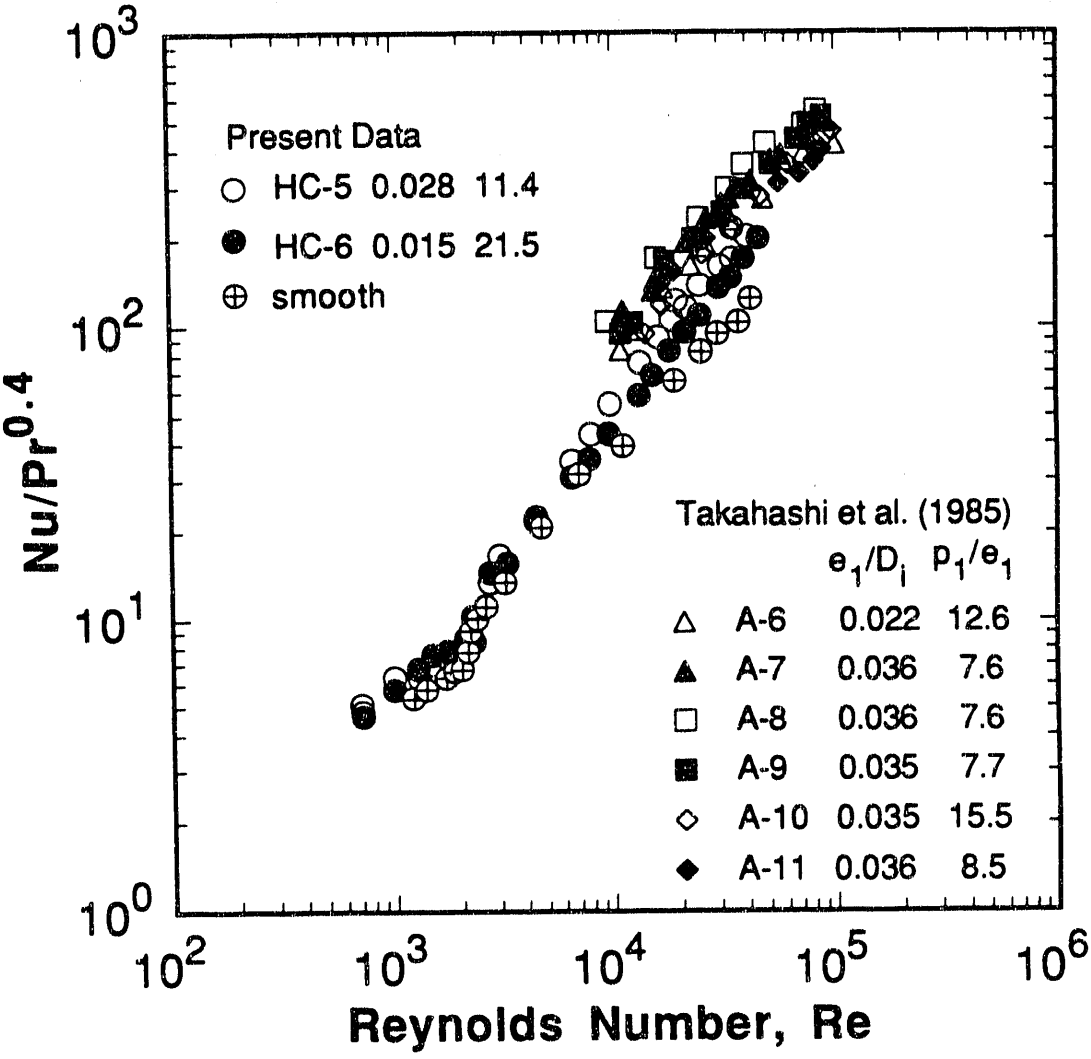

Fig. 33 Comparison of Nu data with those of Takahashi *et al.* for 3D geometries.

5. CONCLUSIONS AND RECOMMENDATIONS

5.1 Conclusions

An extensive experimental investigation was carried out to determine the pressure drop and heat transfer characteristics in laminar, transitional and turbulent flow of air through smooth and enhanced passages. A total of twenty-four (one smooth and twenty-three enhanced) passages were tested. The spirally shaped surface geometries were of the fluted, ribbed/finned and indented types. The Reynolds number based on the maximum internal diameter of a flow passage was varied between 400 and 50000. The most important findings can be summarized as follows:

1. The effect of heat transfer (wall cooling or fluid heating) on pressure drop is most significant within the transition region. The recorded pressure drop is much higher with than without heat transfer for a given Reynolds number. The magnitude of this effect depends to a marked extent on the average surface temperature and, to a lesser extent, on the geometric details of the enhanced passage. When the pressure drop data are reduced as values of friction factor, the results are about the same with and without heat transfer for turbulent flow, with moderate differences in the laminar and transition regions.

2. For any particular enhanced passage, the respective increases in friction factor and the nondimensional heat transfer coefficient are no more than 4.5 and 3.0 times the correponding values for the smooth passage.

3. In laminar flow, it is established that $Nu/Re^{1/2} = C_h$, where C_h is geometry dependent. The experimental results of previous investigators were re-analyzed, and they support the 1/2 power dependence of Nu on Re in laminar flow. This effect of Reynolds number on Nusselt number parallels that for laminar boundary layers.

4. An analogy between friction and heat transfer is developed for smooth and enhanced passages; explicit relationships between friction factor and the nondimensional heat transfer coefficient are established for laminar flow, as well as, for the transition and turbulent regime.

5. At the onset of transition to turbulent flow, the three critical parameters, f_c, Nu_c and Re_c, are related by the equation:

$$Nu_c/(Re_c^{3/2} f_c) = 0.0075$$

The error band on the constant is ±12%. The above relation affords direct calculation of the critical Nusselt number from known values of f_c and Re_c, and hence the calculation of heat transfer coefficient for arbitrary conditions from the friction factor-Reynolds number data.

6. The *frictional law of corresponding states* has been verified. It is demonstrated conclusively that heat transfer coefficients for both smooth and enhanced passages can be computed from a reference set of data if the critical parameters at the onset of transition to turbulent flow are known. This predictive method gives errors that are, for the most part, under ±10% for laminar flow, and under ±20% for both the transition and turbulent regimes.

7. For turbulent flow, the reduced friction factor-Nusselt number relation for smooth and enhanced passages is given by

$$Nu_m/Re_m^{3/2} f_m = 0.16 Re_m^{-0.43}$$

Since the Stanton number, $St = Nu/RePr$, an alternative form of the above relation for $Pr = 0.7$ is

$$St_m = \frac{1}{2} f_m$$

which is basically a statement of the well known Reynolds analogy.

8. At the same reduced conditions, the thermal performance defined as the increase in heat transfer coefficient over that for the frictional pressure coefficient (also referred to as the efficiency index) attains a value close to unity in laminar flow for all enhanced passages. The index is independent of Re_m or decreases with increasing Re_m depending on the geometric characteristics of the enhanced passage. It is demonstrated that, due to the inseparable effects of transition on friction and heat transfer, a meaningful evaluation of the thermal performance of enhanced passages cannot be made without corrections to account for the influence of transition.

9. Besides providing better understanding of the role of transition in determining friction and heat transfer in flow passages, this study has provided extensive data to fill gaps in the existing literature, at least insofar as the laminar and transition regions are concerned.

5.2 Recommendations

As discussed in Section 4.6, a search of the literature revealed very limited studies of friction and heat transfer with comparable enhanced passages for the laminar and transition regions. In general, while previous studies provided very valuable data for turbulent flow, such data cannot be reduced in accordance with the *frictional law of corresponding states*; the primary reason is the almost total neglect of laminar and transitional flow. Measurements of pressure drop and heat transfer for the entire range of flow conditions is recommended for all subsequent studies, especially since little additional instrumentation is required beyond what is needed for turbulent flow studies.

Although the laminar and transitional flow regions are often dismissed as being of little practical significance, the results of this study make it perfectly clear that these types of flow are propbably more important than turbulent flow, at least insofar as the application of the *frictional law of corresponding states* is concerned. There are other reasons in support of the emphasis on the laminar and transition regions: 1) such data provide the basis for verification of turbulent flow data; 2) they provide clearer insight into the origin of the differences between ones' test data and other confirmable data sets; and 3) laminar flow data are important in the design of compact heat exchangers.

There is the need for extensive studies of the effect of Prandtl number on pressure drop and heat transfer for smooth and enhanced passages, because this is undoubtedly one of the least understood aspects of the enhancement phenomena. Although a similar observation was made by Webb *et al.* (1971) more than two decades ago, the present state of knowledge is not entirely satisfactory.

The comparison of the the smooth tube air results of this study with those for higher Prandtl number fluids (Appendix 1) suggests that the effect of Prandtl number manifests itself through variations in C_f, C_h and the critical parameters at the onset of

transition. For enhanced passages, the application of the corresponding states method to the data of Watkinson *et al.* (1984) and Smith and Gowen (1965) does not modify the above observation. For these reasons, it is strongly recommended that the scope of any Prandtl number investigation cover the laminar, transitional and turbulent flow regimes.

Finally, the widely held view for nearly a century is that the Nusselt number (Nu) is constant for fully developed laminar flow in smooth passages. The experimental results of this study as well as several aspects of the data correlation indicate conclusively that Nu varies as the 1/2 power of the Reynolds number in laminar flow. Analytical studies with realistic, practical boundary conditions are needed to shed further light on this disagreement between theory and experiments.

ACKNOWLEDGMENTS

This work was funded by the U.S. Department of Energy, Office of Conservation and Renewable Energy, Division of Advanced Industrial Concepts, Marvin E. Gunn, Jr. and E. P. HuangFu, Program Managers, Contract No. DE-FG02-89CE90029. Technical Support was provided by Mr. A. Thomas, Manager, Experimental Systems Engineering, and by Dr. T. J. Rabas, Energy Systems Division, Argonne National Laboratory.

The authors thank two undergraduate assistants, Mr. K. H. Snell and Ms. P. D. Kelly, for their important contributions to this work.

REFERENCES

Carnavos, T. C., 1980, "Heat Transfer Performance of Internally Finned Tubes in Turbulent Flow," *Heat Transfer Eng.*, Vol. 1, pp. 32-37.

Gee, D. L. and Webb, R. L., 1980, "Forced Convection Heat Transfer in Helically Rib-Roughened Tubes," *Int. J. Heat Mass Transfer*, Vol. 23, pp. 1127-1136.

Kaupas, V. E., Poškas, P. S., and Vilemas, V. J., 1989, "Heat Transfer to a Transition-Range Gas Flow in a Pipe at High Heat Fluxes (2. Heat Transfer in Laminar to Turbulent Flow Transition)," *Heat Transfer - Soviet Research*, Vol. 21, pp. 340-351.

Koch, R., 1960, "Pressure Loss and Heat Transfer for Turbulent Flow," United States Atomic Energy Commission, AEC-tr-3875.

Lindgren, E. R., 1957, "The Transition Process and Other Phenomena in Viscous Flow," *Arkiv for Fysik*, Vol. 12, pp. 1-169.

Marner, W. J., and Bergles, A. E., 1978, "Augmentation of Tubeside Laminar Flow Heat Transfer by Means of Twisted-Tape, Static-Mixer Inserts, and Internally Finned Tubes," *Proc. 6th Int. Heat Transfer Conf.*, Vol. 2, pp. 583-588.

Measurement of Fluid Flow in Pipes Using Orifice, Nozzles, and Venturi, ASME STANDARD, ASME MFC-3M-1984, American Society of Mechanical Engineers, New York, NY.

Nikuradse, J., 1933, "Laws of Flow in Rough Pipes," NACA TM 1292

Nunner, W., 1956, "Heat Transfer and Pressure Drop in Rough Tubes," Atomic Energy Research Establishment (U. K.), Lib/Trans. 786.

Obot, N. T. and Esen, E. B., 1992a, "Smooth Tube Friction and Heat Transfer in

Laminar and Transitional Flow," *Int. Comm. Heat Mass Transfer*, Vol. 19, pp. 299-310.

Obot, N. T., Esen, E. B., Snell, K. H. and Rabas, T. J., 1992b, "Pressure Drop and Heat Transfer Characteristics for Air Flow Through Spirally Fluted Tubes," *Int. Comm. Heat Mass Transfer*, Vol. 19, pp. 41-50.

Obot, N. T. and Esen, E. B., 1991a, "Experimental Investigation of Pressure Drop and Heat Transfer for Air Flow Through Enhanced Tubes," Final Report, DOE/CE/90029-5, Fluid Mechanics, Heat and Mass Transfer Laboratory Report, FHMT Report No. 006, Dept. of Chemical Engineering, Clarkson University.

Obot, N. T., Esen, E. B., and Rabas, T. J., 1991b, "Pressure Drop and Heat Transfer for Spirally Fluted Tubes Including Validation of the Role of Transition," *Fouling and Enhancement Interactions*, HTD-Vol. 164, T. J. Rabas and J. M. Chenoweth, eds., American Society of Mechanical Engineers, NY, pp. 85-92.

Obot, N. T., Wambsganss, M. W. and Jendrzejczyk, J. A., 1991c, "Direct Determination of the Onset of Transition to Turbulence in Flow Passages," *Trans. ASME, J. Fluids Eng.*, Vol. 113, pp. 602-607.

Obot, N. T., Esen, E. B., and Rabas, T. J., 1990a, "Theoretical Studies on the Role of Transition in Determining Friction and Heat Transfer in Smooth and Rough Passages," Final Report, DOE/CE/90029-2, Fluid Mechanics, Heat and Mass Transfer Laboratory Report, FHMT Report No. 005, Department of Chemical Engineering, Clarkson University.

Obot, N. T., Esen, E. B., and Rabas, T. J., 1990b, "The Role of Transition in Determining Friction and Heat Transfer in Smooth and Rough Passages," *Int. J. Heat Mass*

Transfer, Vol. 33, pp. 2133-2143.

Obot, N. T., 1988, "Determination of Incompressible Flow Friction in Smooth Circular and Noncircular Passages: A Generalized Approach Including Validation of the Century Old Hydraulic Diameter Concept," *Trans. ASME J. Fluids Eng.*, Vol. 110, pp. 431-440.

Panchal, C. B., and France, D. M., 1986, "Performance Tests of the Spirally Fluted Tube Heat Exchanger for Industrial Cogeneration Applications,"Argonne National Laboratory Report ANL/CNSV-59.

Petukhov, B. S., and Popov, V. N., 1963, "Theoretical Calculation of Heat Exchange and Frictional Resistance in Turbulent Flow in Tubes of an Incompressible Fluid with Variable Physical Properties," *High Temperature*, Vol. 1, pp. 69-83.

Rabas, T. J., 1989, "Selection of the Energy-Efficient Enhancement Geometry For Single-Phase Turbulent Flow Inside Tubes," Heat Transfer Equipment Fundamentals, Design, Applications and Operating Problems, HTD-Vol. 108, R. K. Shah, ed., American Society of Mechanical Engineers, N.Y., pp 193-204.

Ravigururajan, T. S., and Bergles, A. E., 1986, "Study of Water-Side Enhancement for Ocean Thermal Conversion Heat Exchangers," HTL-44/ERI Project 1718, Iowa State University.

Reay, D. A., 1991, "Heat Transfer Enhancement - A Review of Techniques and Their Possible Impact on Energy Efficiency in the U.K.," *Heat Recovery Systems & CHP*, Vol. 11, pp. 1-40.

Smith, J. W. and Gowen, R. A., 1965, "Heat Transfer Efficiency in Rough Pipes at High Prandtl Number," *AIChE Journal*, Vol. 11, pp. 941-43.

Takahashi, K., Nakayama, W. and Kuwahara, H., 1985, "Enhancement of Forced Con-

vective Heat Transfer in Tubes Having Three-Dimensional Spiral Ribs," *Trans. JSME*, Vol. 51-461, pp. 350-355.

Watkinson, A. P., Miletti, D. L., and Kubanek, G. R., 1974, "Heat Transfer and Pressure Drop of Forge-Fin Tubes in Laminar Oil Flow," Noranda Research Center, Internal Report # 303.

Webb, R. L., 1987, "Enhancement of Single-Phase Heat Transfer," in *Handbook of Single-Phase Convective Heat Transfer*, S. Kakac, R. K. Shah, and W. Aung, Eds., John Wiley and Sons, New York, NY.

Webb, R. L., Eckert, E. R. G. and Goldstein, R. J., 1971, "Heat Transfer and Friction in Tubes with Repeated-Rib Roughness," *Int. J. Heat Mass Transfer*, Vol. 14, pp. 601-617.

Withers, J. G., 1980a, "Tube-Side Heat Transfer and Pressure Drop for Tubes Having Helical Internal Ridging with Turbulent/Transitional Flow of Single-Phase Fluid. Part 1. Single-Helix Ridging," *Heat Transfer Eng.*, Vol. 2, # 1, pp. 48-58.

Withers, J. G., 1980b, "Tube-Side Heat Transfer and Pressure Drop for Tubes Having Helical Internal Ridging with Turbulent/Transitional Flow of Single-Phase Fluid. Part 2. Multiple-Helix Ridging," *Heat Transfer Eng.*, Vol. 2, # 2, pp. 43-50.

Yampolsky, J. S., Libby, P. A., Launder, B. E., and LaRue, J. C., 1984, "Fluid Mechanics and Heat Transfer Spiral Fluted Tubing," GA Technologies Report GA-A17833.

APPENDIX 1: THE SMOOTH PASSAGE PAPER

Int. Comm. Heat Mass Transfer, Vol. 19, pp. 299-310 (1992)

INT. COMM. HEAT MASS TRANSFER
Vol. 19, pp. 299-310, 1992
Printed in the USA

0735-1933/92 $5.00 + .00

SMOOTH TUBE FRICTION AND HEAT TRANSFER IN LAMINAR AND TRANSITIONAL FLOW

N.T. Obot and E.B. Esen
Fluid Mechanics, Heat and Mass Transfer Laboratory
Department of Chemical Engineering
Clarkson University
Potsdam, New York 13699-5705

(Communicated by J.P. Hartnett and W.J. Minkowycz)

ABSTRACT

An experimental investigation of pressure drop and heat transfer for laminar and transitional flow of air was made. The effect of wall cooling or fluid heating on pressure drop is most significant within the transition region and depends, to a marked extent, on the magnitude of the heat input. For heat transfer, the Nusselt number is directly proportional to the square root of the Reynolds number. The experimental results of previous investigators support the 1/2 power dependence of the Nusselt number on the Reynolds number. Explicit relationships between laminar friction factor and heat transfer are established.

Introduction

Friction and heat transfer for laminar and transitional flow through smooth passages are important in many engineering applications, especially in connection with the design of compact heat exchangers. For example, the results of several studies [1,2] suggest that significant benefits may be realized from the laminar flow design strategy for compact exchangers if fouling can be kept within acceptable levels.

Although pressure drop and heat transfer in smooth tubes have been studied for nearly a century, the state of knowledge with regard to heat transfer in laminar flow has not been entirely satisfactory. Unlike the turbulent flow counterpart, the literature on experimental heat transfer in laminar flow is limited, probably because such studies were considered to be of little practical interest. Virtually all available results show a common trend with increasing Reynolds number; this trend is at variance with theoretical results.

The results of analytical studies, that are given in virtually all standard heat transfer texts, indicate that the average Nusselt number (Nu) is independent of the Reynolds number (Re) for the so-called fully developed laminar flow. The empirical correlation of Kern and Othmer [3] complement that of Sieder and Tate [4] in that Nu varies as the 1/3 power of Re. The other parameters in the correlations include, among other things, the Prandtl number, L_h/D, and the viscosity ratio. Watkinson *et al.* [5] reported good agreement betweeen their data and the correlations.

Cholette [6] reported a constant value of Nu for laminar flow, while Molloy [7] found Nu to be constant with a ±20% error band. In each study, the conclusion is at variance with the experimental data, the trend of which is one of increasing Nu with Re. The data of Marner and Bergles [8] indicate a monotonic increasing Nu with Re for wall cooling or heating with ethylene glycol as the working fluid. Similarly, the results of numerous air studies [9-16] indicate that Nu increases steadily with increasing Re in laminar flow. In particular, Obot *et al.* [15,16] established that $Nu \propto Re^{1/2}$, an indication that the effect of Re parallels the well known behavior for laminar boundary layers. Note that Nu varies as the 0.7 to 0.8 power of the Reynolds number in turbulent flow for a range of external boundary layer flows and duct flows.

This work grew out of the need for base-line data that would aid the determination of the thermal performance of various enhanced tubes in laminar, transitional and turbulent flow. The 600 to 50000 Re range was covered in this study. Since comparisons of our smooth tube results with published data were given elsewhere for $Re > 10^4$ [15,16], this presentation considers Re values up to 10^4.

Experiments

Tests were performed using the facility described in Obot *et al.* [15,16]; instrumentation for pressure drop and surface temperature measurements were the same as given in the papers. The internal diameter of the tube was 13.4 mm. The heated section was 34.2 diameters long and was preceded by an unheated entry length of 147 diameters.

Experiments were carried out for two conditions, one of which involved maintaining a fixed average surface temperature for all Reynolds numbers tested. Naturally, the total electrical power input (Q_T) varied with Re. For the other condition, Q_T was held fixed for all Re and the average surface temperature decreased with increasing Re from laminar flow. Three values of Q_T were tested: Q_T = 14.9, 32.8 and 48.3 W which correspond to q_T = 773, 1708 and 2509 W/m^2, respectively. The largest value of Re tested for each Q_T was dictated by the requirement that the air temperature rise be greater than 5°C. For Q_T = 14.9 W,

TABLE 1
Summary of Typical Test Data

Re	Q_T, W	Q_c, W	Q_m, W	T_i, °C	T_o, °C	T_w, °C	T_b, °C
1214	48.3	17.7	16.0	23.4	77.6	158.0	50.5
1387	48.2	18.3	15.6	25.7	73.5	155.3	49.6
1707	48.2	19.4	18.3	26.0	72.6	150.3	49.3
1867	48.2	20.1	18.2	26.3	68.7	147.3	47.5
2014	48.2	20.2	20.7	25.9	69.5	146.4	47.7
2150	48.2	21.6	20.2	27.5	68.5	140.0	48.0
2207	48.2	23.1	22.5	27.8	75.0	133.3	51.4
2371	48.3	24.4	23.0	27.0	71.7	127.1	49.4
2607	48.2	24.1	24.8	26.6	69.9	118.0	48.3
3185	48.3	27.7	25.5	27.1	66.2	112.5	46.7
4708	48.4	32.4	31.8	27.5	59.6	93.9	43.6
7029	48.5	36.1	35.8	28.5	53.7	78.5	41.1
11187	48.5	40.1	43.1	25.0	44.4	68.0	34.7

T_w decreased monotonically with Re from 75.3°C at $Re = 736$ to 41.7°C at $Re = 9249$, and from 131.3°C at $Re = 709$ to 41.2°C at $Re = 26896$. Table 1 gives the relevant information for $Q_T = 48.3$ W.

The Nusselt number results were calculated from the relation

$$Nu = D_i(Q_T - Q_L)/(Ak_b)(T_w - T_b) \tag{1}$$

where Q_T and Q_L, respectively, are the total electrical power input with and without air flow at the average surface temperature of a trial. The values of the convective heat transfer rate (Q_c), determined as the difference between Q_T and Q_L, are compared to those calculated from the relation $Q_m = \dot{m}C_p(T_o - T_i)$ in Table 1 for the highest Q_T value tested. Expressed as percentages, the convective contributions for the other smooth tube trials were about the same as those inferred from Table 1.

Table 1 shows good agreement between values of Q_c and Q_m. The differences are, on an average basis, about 6%; the largest is calculated for $Re = 1387$. At the lowest Re, Q_c is about 37% of Q_T, it increases with increasing Re to almost 83% of Q_T at $Re = 11187$. For $Re > 11187$, values of Q_c were in the 90% to 95% range. The fact that Q_c values in laminar flow through the smooth tube are no more than 50% of Q_T is not the result of poor/inadequate insulation or other peculiarities of the present experimental design; it is simply a reflection of the fact that the convective ability in laminar flow is limited for a given set of conditions. It should perhaps also be mentioned that values of the ratio Q_c/Q_T with enhanced tubes in laminar flow can be significantly higher than those for the smooth tube at

comparable average surface temperature and Re, depending on the geometric characteristics of the surface protrusions.

A study of the temperature data in Table 1 reveals an interesting behavior in the narrow $2014 \leq Re < 3000$ range within the transition region. Note that the onset of transition to turbulent flow based on these data occurs at $Re = 2014$. A sharp rise in exit temperature (T_o) is observed for $Re = 2207$, followed by a decreasing trend with increasing Re. The magnitude of the rise, which was found to depend on the level of heat input and roughness, is significant; it is about 7°C higher than the T_o value for $Re = 2150$. This behavior, which cannot be explained by the small differences in the inlet temperature (T_i), is a manifestation of the dominant effect of transition to turbulence on the heat transfer process. As shown subsequently, the influence of heat transfer on pressure drop is most pronounced over this narrow Re range.

Results and Discussion

It is noted at the outset that the air density ρ_w in the friction factor equation ($f = \Delta p \rho_w A^2 D_i / 2 L_p \dot{m}^2$) was evaluated at the average surface temperature of a trial. The reasons will be evident from the subsequent discussion of the results. The physical properties in the Nusselt and Reynolds numbers were based on the bulk mean temperature (T_b) with D_i as the characteristic dimension.

Pressure Drop

Fig. 1 is a plot of $f \times Re$ ($= C_f$) versus Re. This compact presentation gives results obtained with the 3 values of q_T along with those for the fixed average surface temperature. The C_f values in laminar flow are 15.9, 17.7 and 19.5 for $q_T = 773$, 1708 and 2509 W/m^2, respectively; the $T_w = 52.7$°C value is 14.1. In each case, the error band on C_f is under 7%.

Fig. 2 is a plot of $\Delta p_{w,h} / \Delta p_w$ versus Re for the three values of q_T. Here, $\Delta p_{w,h}$ is the steady state pressure drop with wall cooling (or fluid heating) at the average surface temperature of a test trial; the corresponding value recorded at the same Reynolds number just before the onset of heating of the test section is denoted by Δp_w. The Δp_w data were not recorded prior to heating for tests with $T_w = 52.7$°C, hence the ratios are not shown on Fig. 2.

One of the striking features of Fig. 2 is the marked effect of heat transfer on pressure drop. In general, the largest values of the pressure drop ratio are observed in the vicinity of the Reynolds number at which transition to turbulent flow begins, an indication that the behavior depicted by the data may be used to determine the onset of transition to turbulence. A marked drop in the values is also observed around the onset of fully turbulent

flow, implying that the upper critical Reynolds number at the end of transitional flow can also be determined from the $\Delta p_{wh}/\Delta p_w$ trend.

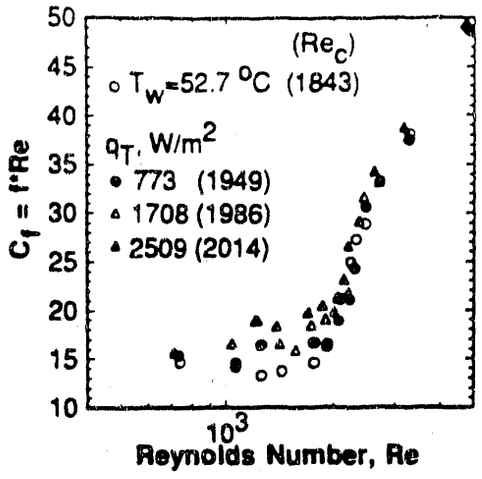

FIG. 1
$f \times Re$ vs. Re for smooth tube.

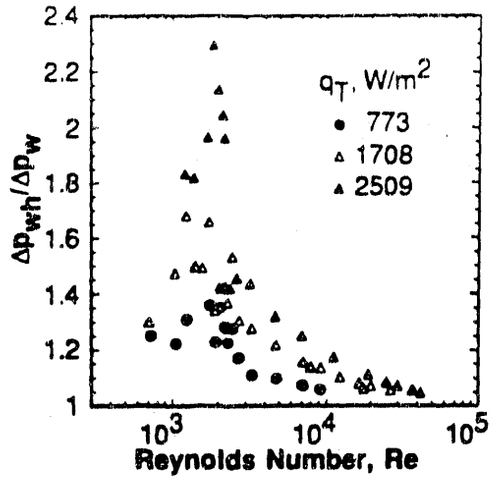

FIG. 2
$\Delta p_{wh}/\Delta p_w$ vs. Re for smooth tube.

Heat Transfer

To provide a clearer insight into the Reynolds number effect in laminar flow and the connection between friction and heat transfer, the present results are presented on Fig. 3 as $Nu/Re^{1/2}$ ($= C_A$) versus Re. This figure shows that, consistent with the friction factor trend of Fig. 1, Nu values vary with q_T in the laminar and transition region; the residual effects of q_T were still in evidence up to $Re = 15000$. It is noted that the use of the physical properties evaluated at the film temperature in the calculations of Nu and Re, instead of the present use of those based on the bulk mean temperature, does not modify the trend on Fig. 3. The C_A values in laminar flow are 0.096, 0.106 and 0.116 for q_T = 773, 1708 and 2509 W/m^2; the value for $T_w = 52.7$°C is 0.088. For each data set, the uncertainty on C_A is no more than ±5%.

It is evident from a comparison between Figs. 1 and 3 that the lower critical Reynolds number, which corresponds to the onset of transition to turbulent flow, can be determined from the friction factor or heat transfer data; the differences between the two sets of Re_c values are no more than 5%. Both figures show that the curves, which are basically horizontal lines in laminar flow, rise steeply around the onset of transition to turbulence. Also, Fig. 3 shows that a change in direction occurs at the onset of fully turbulent flow. The intersection of the transitional and turbulent flow curve segments can be determined easily, thus yielding the value for the upper critical Reynolds number.

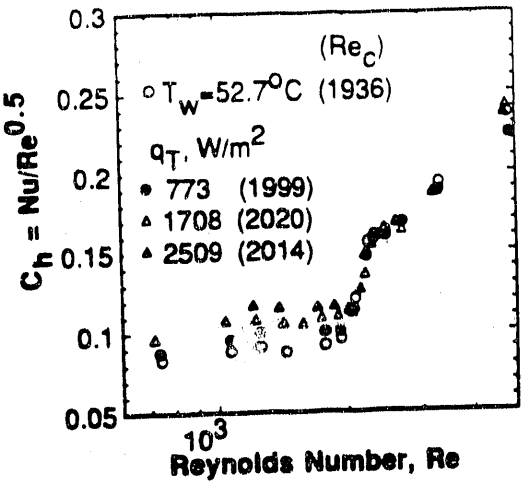

FIG. 3
Plot of $Nu/Re^{1/2}$ vs. Re for smooth tube.

Since C_f and C_h are constants and independent of Re in laminar flow f q_T or T_w, it follows that the ratio C_h/C_f must also be constant. A plot of (is given on Fig. 4. A close approximation to the four sets of laminar flow d data points) is given by

$$Nu/(Re^{3/2}f) = C_h/C_f = 0.0061$$

The error band associated with the constant is ±6%.

In equation (2), the physical properties in Nu and Re are based or temperature, T_b. When friction factor was calculated using the air density ρ on the mean value of the constant in (2) was about ±12%. Allowing for th of transition and Prandtl number gave deviations about the mean value t order of ±10%. For these reasons, values of friction factor in (2) were con air density based on the average wall temperature. The ranges of validity are $41 \leq T_w \leq 158$°C and $29 \leq T_b \leq 51$°C.

Equation (2) is a statement of the relationship between friction factor coefficient in laminar flow, and it can afford direct calculation of the heat tr from the friction factor-Reynolds number data. Also, since the limiting poin Re on the horizontal line given by equation (4) corresponds to the the onse turbulent flow, the critical value of the Nusselt number at transition for s be calculated from known critical values of Re and f using the relation

$$Nu_c/(Re_c^{3/2}f_c) = C_{h,c}/C_{f,c} = 0.0061$$

Conversely, the critical friction factor can be evaluated from those for Nu and Re.

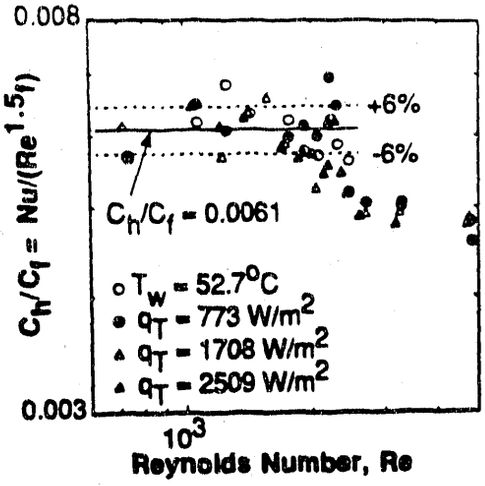

FIG. 4
Plot of $Nu/(Re^{3/2}f)$ vs. Re.

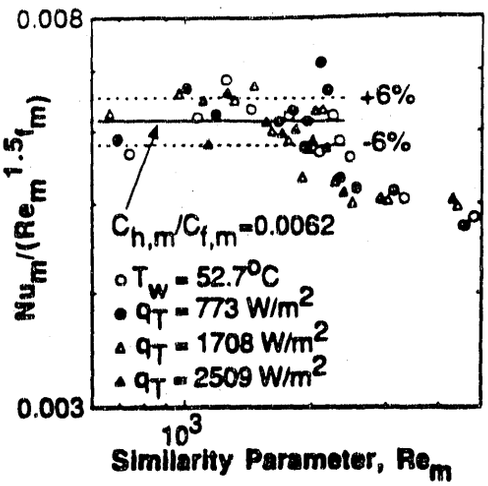

FIG. 5
Plot of $Nu_m/(Re_m^{3/2}f_m)$ vs. Re_m.

The significance of the preceding observation must not be overlooked. In previous studies [16,17], it was demonstrated that the Nusselt numbers for enhanced tubes can be obtained from a smooth tube data if the appropriate critical parameters are known. Given the remarkable consistency in values of the critical Re deduced from friction factor and heat transfer data (Figs. 1 and 3), it is readily appreciated that equation (2) is what may be needed to effect the calculation of critical Nu from the friction factor data. This, in turn, should permit the calculation of the Nusselt number at any Reynolds number from a reference set of data via the corresponding states relations [16,17]. It is worthy of note that the laminar heat transfer trend with increasing Re is the same for smooth and enhanced passages.

Since friction factor and Nusselt number in the laminar and transition region depend on several factors (passage geometry, roughness, fluid properties, level of heat input, etc), the results on Fig. 4 must be presented at the same reduced conditions that should be independent of these factors. Accordingly, the reduced data are given in Fig. 5, where $Nu_m/Re_m^{3/2}f_m$ is plotted against Re_m. Values of Nu_m, Re_m and f_m were computed from the relations $Nu_m = (Nu_{c,r}/Nu_{c,a})Nu_a$, $Re_m = (Re_{c,r}/Re_{c,a})Re_a$ and $f_m = (f_{c,r}/f_{c,a})f_a$; the reference values for $Nu_{c,r}$ (= 4.0), $Re_{c,r}$ (= 1843) and $f_{c,r}$ (= 0.0077) are those for the present study with T_w = 52.7°C. The results are closely approximated by

$$Nu_m/Re_m^{3/2}f_m = C_{h,m}/C_{f,m} = 0.0062 \tag{4}$$

with about a ±6% error band. Equation (4) is a general expression that should be valid for

other passage geometries (smooth or rough) and flow conditions. This wil the subsequent comparison of the present data with published results.

The fact that the constant in equation (2) or (3) is essentially the the reduced equation (4) implies several things. First, it suggests that the universal. Second, it supports the proposition that equation (3) can be used parameter information for arbitrary conditions which, in turn, can permit c corresponding Nusselt number.

Fig. 6 is a comparison of the present results with those of several in friction factor data were not provided by some of the investigators [13,14] here is that of C_A versus Re. The results of Watkinson *et al.* [5] and Marn were obtained with SAE 10W30 motor oil and ethylene glycol, respectivel data are for air studies. For ethylene glycol and the motor oil, the Prandtl n 120 and 280 respectively, while the value for air is about 0.71. Kaupas *et* local average Nu data for three values of heat flux at each of three heat Eight of the nine sets of data are shown in Fig. 6 using a common symbol; because the critical values of Nu and Re could not be determined. The the heated section (L_A/D_i) is given in the figure where such information is

Clearly, the results on Fig. 6 fall into two groups, the higher and th are for studies with liquids and air, respectively. The data of Watkinson e and Bergles give 0.61±0.09 and 0.83±0.10 for C_A, respectively. By contrast sets of air data give C_A values ranging from 0.073 to 0.13 depending, of cou length and the level of heat input. For each of the 13 sets of air data, t C_A is no more than 8%. The error bands associated with the data sets part, well within the experimental uncertainties provided in the original considerably smaller than the values that would result by assuming that N of Re or varies as the 1/3 power of Re. These results clearly support the co is directly proportional to the square root of the Reynolds number, in line w for other laminar boundary layer flows.

Another striking feature of Fig. 6 is the differences in the critical or tra number among the various results. The critical Re varies from about 1215 Watkinson *et al.* to the rather high value of 5030 for one of the test cond *et al.*. Even for the air studies, the critical Re values differ by more th Differences of these magnitude introduce difficulties in the comparison of This is one of the considerations that prompted the formulation of the corr criteria to effect data analysis at the same reduced conditions for transitio

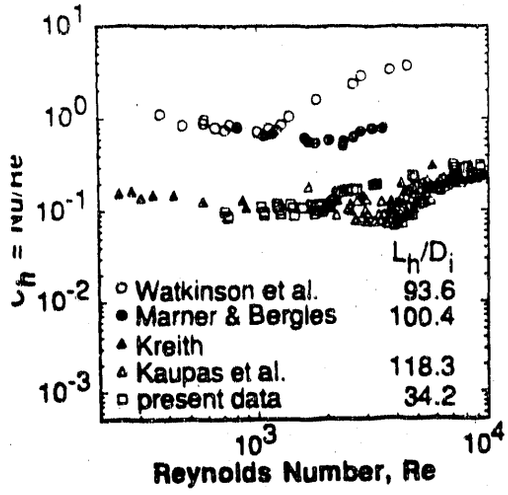

FIG. 6
Plot of $Nu/Re^{1/2}$ vs. Re.

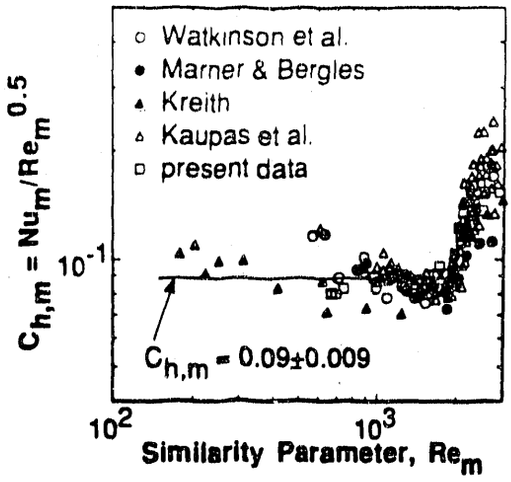

FIG. 7
Plot of $Nu_m/Re_m^{1/2}$ vs. Re_m.

Fig. 7 is a plot of $Nu_m/Re_m^{1/2}$ versus Re_m at the same reduced conditions, that account for the variability of the critical values of Nu and Re at the onset of transition to turbulent flow. Interestingly, the trends on Fig. 7 do not reflect a dependence on Prandtl number. It is evident that, despite the marked differences in values of C_h (Fig. 6), the reduced data in laminar flow are closely approximated by a single constant with errors that are, for the most part, under 10%. Similarly, in the transition region, the data can be approximated by a single relation with a $\pm 15\%$ error band.

To calculate the Nusselt number in laminar flow through smooth tubes from the friction factor-Reynolds number data for an arbitrary condition, the steps are as follows:

- Determine the critical parameters, $f_{c,a}$ and $Re_{c,a}$, from the data, and compute $Nu_{c,a}$ from equation (3).
- Calculate f_m and Re_m using $f_m = (f_{c,r}/f_{c,a})f_a$ and $Re_m = (Re_{c,r}/Re_{c,a})Re_a$, where $f_{c,r} = 0.0077$ and $Re_{c,r} = 1843$.
- Compute Nu_m from equation (4) and the desired Nusselt number (Nu_a) from the relation $Nu_a = Nu_m(Nu_{c,a}/Nu_{c,r})$, where $Nu_{c,r} = 4.0$.

Alternatively, estimates of the Nusselt number can be obtained from the relation $C_{h,m} = 0.09$ (Figure 7), but this equation is subject to further refinement when more data are available because the uncertainty on $C_{h,m}$ is 10%. The predictive equation for the transition region will be given in a later paper because of the limited data base considered here.

The final remarks are on the disagreement between theory and exper that Nu increases with Re in laminar flow, in contradistinction to the co tained analytically with a constant heat flux and constant wall tempera tributed to the use of insufficiently long heated sections. However, it discrepancy may be the result of the differences in the thermal boundary cc experiment and theory. Neither this study nor any of the studies cited main convective heat flux with increasing Re. With a fixed electrical power inpu and given the trends in Table 1 for the pertinent parameters, it is unlikel Nu for all Re would result even for a sufficiently long heated section. Tl case when T_w is fixed with increasing Re because, although Q_T varies wit and temperature trends parallel those in Table 1.

Concluding Remarks

The pressure drop data in laminar and transitional flow are signific than without heat transfer, and the magnitudes of the differences betwee data depend, to a marked extent, on the applied heat flux. The heat trans study and those of previous investigators support the conclusion that the is directly proportional to the square root of the Reynolds number. Th constant depends on the heat flux, surface roughness and could well be with the passage geometry (rectangular, triangular, etc.), paralleling the be factor.

Acknowledgements

The work was supported by the U. S. Department of Energy, Offic and Renewable Energy, Division of Advanced Industrial Concepts, Marvin E.P. Huang-Fu, Program Managers, Contract No. DE-FG02-89CE90029. grateful to Dr. T. J. Rabas of Argonne National Laboratory for providing t

Nomenclature

A_h	heat transfer area
C_f	$f \times Re$
C_h	$Nu/Re^{1/3}$
C_p	specific heat
D_i	internal tube diameter
f	Fanning friction factor

k_b fluid thermal conductivity at T_b
L_h heated length
L_p distance between pressure taps
$\dot{m}$ mass flowrate
Nu Nusselt number
Δp pressure drop
Δp_ω pressure drop without heat transfer
$\Delta p_{\omega h}$ pressure drop with heat transfer
Q_c convective transfer rate, $Q_T - Q_L$
Q_L total electrical power without flow
Q_m $\dot{m}C_p(T_o - T_i)$
Q_T total electrical power with flow
q_T heat flux, Q_T/A_h
Re Reynolds number
T_b bulk mean temperature, $(T_i + T_o)/2$
T_i inlet temperature
T_o exit temperature
T_w average surface temperature

Additional Subscripts

a value for arbitrary condition
c critical value
c,a critical value for arbitrary condition
c,r reference critical value
m value at reduced condition

References

1. W.T. Cross and C. Ramshaw, *Chem. Eng. Res. Des.* 64, 293(1986).
2. D.A. Reay, *J. Heat Recovery Systems & CHP* 8, 309(1988).
3. D.Q. Kern and D.F. Othmer, *Trans. AIChE* 39, 517(1943).
4. E.N. Sieder and G.E. Tate, *Ind. Eng. Chem.* 28, 1429(1936).

5. A.P. Watkinson, D.L. Miletti and G.R. Kubanek, Heat Transfer at of Forge-Fin Tubes in Laminar Oil Flow, Noranda Research Cent Quebec, Internal Report No. 303(1974).

6. A. Cholette, *Chem. Eng. Prog.* 44, 81(1948).

7. J. Molloy, Rough Tube Friction Factors and Heat Transfer Coefficient Transitional Flow, Atomic Energy Research Establishment, AERE-R

8. W.J. Marner and A.E. Bergles, *Proc. 6th Int. Heat Transfer Conf.* 2

9. W. Nunner, Heat Transfer and Pressure Drop in Rough Tubes, A 786(1956).

10. R. Koch, Pressure Loss and Heat Transfer for Turbulent Flow, AEC-

11. R. Koch and K. Feind, *Chemie-Ingr-Tech.* 30, 577(1958).

12. L.V. Humble, W.H. Lowdermilk and L.G. Desmon, Measurements Transfer and Friction Coefficients for Subsonic Flow of Air in Smoot Surface and Fluid Temperatures, NACA Report 1020(1951).

13. F. Kreith and M.S. Bohn, Principles of Heat Transfer, 4th Ed., p. 289 New York(1986).

14. V.E. Kaupas, P.S. Poškas, and V.J. Vilemas, *Heat Transfer - So* 340(1989).

15. N.T. Obot, E.B. Esen, K.H. Snell and T.J. Rabas, *Int. Comm. He* 19, 41(1992).

16. N.T. Obot, E.B. Esen, K.H. Snell and T.J. Rabas, Fouling and Enhanc HTD-Vol. 164, p. 85, American Society of Mechanical Engineers, N.

17. N.T. Obot, E.B. Esen and T.J. Rabas, *Int. J. Heat Mass Transfer* 3

APPENDIX 2

TABULATION OF EXPERIMENTAL DATA

This appendix gives a complete tabulation of the experimental data for all flow passages. There are a total of thirty-four tables, 2.1 through 2.34, each of which gives data for specific test conditions. The following comments will be helpful to the the user:

- Friction factor data for tests without heat transfer are given in Table 2.1 for the smooth passage, and in Tables 2.6 through 2.13 for the GA-1 - GA-3 passages of the spirally fluted type. For these tables, only the Reynolds number (Re) and the friction factor are given.

- With the exception of Table 2.5 which gives Re, f, Nu and $\Delta p_{wh}/\Delta p_w$ data for the smooth passage with $q_T = 2509$ W/m^2, the remaining tables also give Re_m, f_m and Nu_m at reduced conditions. The reference critical parameters used in the calculation of Re_m, f_m and Nu_m are those for the smooth passage with $q_T = 2509$ W/m^2, hence $Re = Re_m$, $f = f_m$ and $Nu = Nu_m$ for the reference.

- The critical parameters for all passages are given in Table 3.

TABLE 2.1 Data summary for the smooth tube (without heating).

Re	f	Re	f
409	0.0412	3462	0.0100
662	0.0236	3647	0.0103
665	0.0232	3664	0.0103
815	0.0206	4530	0.0093
893	0.0173	4728	0.0097
1105	0.0141	4745	0.0097
1110	0.0139	5601	0.0090
1303	0.0122	6278	0.0090
1342	0.0114	6293	0.0090
1489	0.0109	6681	0.0086
1497	0.0107	7758	0.0082
1666	0.0099	7772	0.0086
1847	0.0085	8849	0.0080
1870	0.0831	9540	0.0079
2004	0.0086	9541	0.0079
2014	0.0080	9944	0.0077
2086	0.0083	11050	0.0075
2095	0.0082	12732	0.0073
2142	0.0089	14439	0.0071
2399	0.0089	16755	0.0068
2419	0.0088	18518	0.0067
2500	0.0104	18679	0.0064
2652	0.0105	20312	0.0065
2664	0.0104	22131	0.0064
2664	0.0104	23983	0.0061
2816	0.0106	28847	0.0058
2981	0.0106	33901	0.0057
2995	0.0105	38841	0.0055
		43996	0.0054

TABLE 2.2 Data summary for the smooth tube (T_w = 52.7°C).

Re	f	Nu	Re_m	f_m	Nu_m
740	0.0198	3.20	838	0.0219	3.54
1074	0.0133	4.09	1216	0.0147	4.52
1261	0.0105	4.68	1428	0.0117	5.18
1438	0.0096	4.89	1629	0.0106	5.41
1774	0.0082	5.59	2009	0.0091	6.19
1935	0.0085	5.96	2192	0.0095	6.60
2093	0.0101	7.46	2371	0.0112	8.26
2247	0.0111	9.57	2545	0.0123	10.59
2328	0.0117	9.85	2636	0.0130	10.90
2468	0.0117	10.35	2795	0.0130	11.46
3300	0.0116	13.79	3738	0.0128	15.26
4809	0.0102	20.08	5447	0.0113	22.23
7107	0.0093	28.88	8049	0.0103	31.96
9200	0.0084	34.89	10420	0.0093	38.62
8190	0.0085	31.60	9275	0.0095	34.97
12240	0.0077	43.81	13862	0.0086	48.48
16523	0.0072	55.70	18713	0.0080	61.63
18004	0.0066	56.51	20391	0.0073	62.53
19344	0.0070	63.63	21909	0.0078	70.41
25818	0.0061	77.08	29241	0.0068	85.30
30513	0.0059	86.85	34558	0.0065	96.11
35620	0.0057	94.69	40342	0.0063	104.79
35752	0.0058	93.61	40492	0.0064	103.60
40879	0.0056	104.31	46299	0.0062	115.43
44891	0.0054	107.50	50843	0.0060	118.97

TABLE 2.3 Data summary for the smooth tube (q_T = 773 W/m^2).

Re	f	Nu	$\Delta p_{wh}/\Delta p_w$	Re_m	f_m	Nu_m
732	0.0209	3.15	1.25	777	0.0241	3.33
1070	0.0136	4.28	1.22	1137	0.0157	4.52
1261	0.0130	4.77	1.31	1340	0.0150	5.05
1773	0.0094	5.49	1.36	1883	0.0109	5.81
1927	0.0084	5.71	1.23	2047	0.0097	6.04
2077	0.0091	6.79	1.35	2207	0.0105	7.18
2231	0.0095	8.94	1.28	2370	0.0109	9.45
2315	0.0105	9.61	1.23	2459	0.0121	10.17
2478	0.0124	9.90	1.28	2633	0.0143	10.47
2715	0.0123	10.87	1.17	2885	0.0142	11.50
3305	0.0114	13.19	1.11	3511	0.0131	13.95
4842	0.0101	19.21	1.10	5144	0.0116	20.32
7159	0.0091	28.42	1.07	7606	0.0105	30.06
9244	0.0082	35.22	1.06	9821	0.0095	37.25

TABLE 2.4 Data summary for the smooth tube (q_T = 1708 W/m^2).

Re	f	Nu	$\Delta p_{wh}/\Delta p_w$	Re_m	f_m	Nu_m
709	0.0220	3.10	1.30	721	0.0236	3.28
1039	0.0160	4.16	1.48	1055	0.0171	4.39
1227	0.0154	4.48	1.68	1247	0.0166	4.74
1409	0.0117	4.57	1.50	1432	0.0126	4.84
1573	0.0101	4.95	1.49	1598	0.0109	5.23
1737	0.0106	5.27	1.66	1765	0.0114	5.58
1899	0.0100	5.51	1.34	1930	0.0108	5.83
2050	0.0104	5.89	1.42	2083	0.0111	6.23
2202	0.0099	7.36	1.43	2237	0.0106	7.79
2289	0.0108	8.39	1.37	2325	0.0116	8.87
2442	0.0130	9.19	1.53	2481	0.0139	9.72
2691	0.0123	9.58	1.30	2734	0.0132	10.14
3259	0.0116	12.00	1.28	3311	0.0124	12.70
4755	0.0104	18.66	1.22	4832	0.0112	19.73
7134	0.0093	27.44	1.16	7248	0.0100	29.02
9223	0.0084	34.29	1.14	9371	0.0090	36.26
7928	0.0085	29.58	1.14	8055	0.0091	31.28
12352	0.0077	44.31	1.10	12549	0.0082	46.86
16684	0.0072	56.12	1.08	16951	0.0077	59.36
19910	0.0069	65.41	1.07	20229	0.0074	69.19
17809	0.0070	58.05	1.06	18095	0.0075	61.40
26899	0.0064	76.29	1.06	27330	0.0068	80.70

TABLE 2.5 Data summary for the smooth tube (q_T = 2509 W/m^2).

Re	f	Nu	$\Delta p_{wh}/\Delta p_w$
1207	0.0157	4.67	1.83
1382	0.0133	5.00	2.11
1702	0.0116	5.52	2.24
1862	0.0110	5.78	2.06
2006	0.0099	5.88	1.93
2146	0.0108	6.76	2.05
2205	0.0121	7.97	1.96
2368	0.0124	8.80	1.42
2603	0.0132	9.69	1.46
3186	0.0122	11.72	1.44
4705	0.0105	18.13	1.32
7028	0.0095	27.36	1.25
11142	0.0067	34.32	1.17
19152	0.0063	56.84	1.11
25173	0.0061	71.38	1.09
29892	0.0061	82.37	1.07
37063	0.0059	89.89	1.06
41990	0.0058	108.18	1.05

TABLE 2.6 Data summary for the GA-1 passage (Test# 1).
(L_p/D_i = 72.0)

Re	*f*	*Re*	*f*	*Re*	*f*
257	0.0775	1463	0.0223	3828	0.0227
257	0.1033	1466	0.0231	3942	0.0238
338	0.0597	1498	0.0213	4168	0.0235
416	0.0493	1568	0.0215	4412	0.0247
490	0.0427	1668	0.0202	4841	0.0239
508	0.0463	1670	0.0208	4874	0.0252
561	0.0326	1773	0.0201	5327	0.0251
561	0.0434	1829	0.0189	5521	0.0241
640	0.0376	1873	0.0190	5990	0.0242
695	0.0318	1875	0.0194	5991	0.0243
695	0.0353	1978	0.0188	6197	0.0239
819	0.0331	2030	0.0187	6893	0.0239
820	0.0356	2085	0.0192	8280	0.0230
837	0.0341	2087	0.0196	8464	0.0218
936	0.0312	2138	0.0190	9710	0.0222
1047	0.0280	2161	0.0179	11149	0.0215
1049	0.0279	2189	0.0194	11744	0.0206
1155	0.0256	2291	0.0199	12639	0.0210
1156	0.0268	2293	0.0205	14052	0.0206
1167	0.0238	2492	0.0217	14870	0.0197
1259	0.0237	2828	0.0203	15136	0.0203
1261	0.0247	2969	0.0219	17807	0.0191
1362	0.0239	3160	0.0214	20483	0.0190
1364	0.0230	3462	0.0227	23969	0.0177
				26971	0.0172

TABLE 2.7 Data summary for the GA-1 passage (Test#2).
(L_e/D_i = 62.9, L_p/D_i = 11.8)

Re	*f*	*Re*	*f*
257	0.0899	3455	0.0187
416	0.0515	3934	0.0206
561	0.0377	3957	0.0203
694	0.0332	4152	0.0213
819	0.0283	4405	0.0224
935	0.0251	4866	0.0230
1047	0.0226	5302	0.0220
1154	0.0204	5316	0.0234
1258	0.0195	5501	0.0229
1361	0.0178	5977	0.0228
1463	0.0169	6858	0.0231
1496	0.0177	8264	0.0218
1564	0.0162	9650	0.0216
1667	0.0157	11616	0.0203
1769	0.0150	12538	0.0204
1874	0.0144	15047	0.0191
2083	0.0135	16950	0.0188
2290	0.0130	17831	0.0185
2467	0.0142	20477	0.0180
2602	0.0140	23391	0.0175
2822	0.0153	26421	0.0170
2966	0.0167	29450	0.0165
		30543	0.0164

TABLE 2.8 Data summary for the GA-1 passage (Test #3).
(L_e/D_i = 47.2, L_p/D_i = 42.8)

Re	f	Re	f
255	0.0893	3710	0.0228
413	0.0512	3906	0.0223
557	0.0375	4130	0.0234
690	0.0306	4372	0.0240
813	0.0308	4829	0.0249
930	0.0269	5197	0.0247
1040	0.0242	5276	0.0252
1147	0.0221	5470	0.0248
1251	0.0204	5932	0.0244
1353	0.0191	6822	0.0245
1454	0.0179	9585	0.0231
1555	0.0168	11625	0.0215
1657	0.0159	12449	0.0218
1759	0.0150	16583	0.0204
1862	0.0151	17745	0.0194
2070	0.0136	23486	0.0181
2277	0.0135	29722	0.0170
2452	0.0145	35959	0.0162
2476	0.0142	42579	0.0155
2804	0.0175	49400	0.0149
2946	0.0171	56031	0.0146
3430	0.0210	63121	0.0142

TABLE 2.9 Data summary for the GA-2 passage (Test# 1).
($L_p/D_i = 66.3$)

Re	*f*	*Re*	*f*
230	0.0895	2226	0.0200
230	0.0892	2318	0.0219
371	0.0513	2532	0.0198
372	0.0511	2652	0.0204
455	0.0683	3091	0.0210
501	0.0376	3451	0.0224
502	0.0374	3520	0.0219
620	0.0490	3733	0.0218
622	0.0366	3940	0.0235
732	0.0396	4352	0.0245
733	0.0351	4758	0.0249
749	0.0419	4773	0.0241
836	0.0337	4938	0.0241
838	0.0336	5352	0.0243
936	0.0323	6156	0.0245
1032	0.0310	7418	0.0244
1125	0.0279	8667	0.0238
1217	0.0255	10295	0.0227
1308	0.0248	10610	0.0229
1341	0.0234	13131	0.0215
1399	0.0241	14059	0.0213
1490	0.0233	15797	0.0205
1582	0.0217	18453	0.0197
1674	0.0210	21114	0.0189
1860	0.0198	23889	0.0182
2046	0.0186	29700	0.0168
		32460	0.0163

TABLE 2.10 Data summary for the GA-2 passage (Test#2).
($L_e/D_i = 10.6$, $L_p/D_i = 56.1$)

Re	*f*	*Re*	*f*
228	0.1067	3464	0.0183
370	0.0611	3498	0.0191
452	0.0544	3711	0.0192
499	0.0448	3916	0.0212
617	0.0365	4324	0.0226
728	0.0315	4726	0.0237
745	0.0300	4754	0.0216
832	0.0282	4907	0.0230
931	0.0257	5314	0.0232
1026	0.0238	6117	0.0237
1119	0.0222	7346	0.0238
1210	0.0209	7428	0.0229
1300	0.0198	8595	0.0234
1334	0.0188	10261	0.0220
1390	0.0187	10507	0.0222
1481	0.0178	12789	0.0211
1573	0.0169	15231	0.0206
1665	0.0171	15742	0.0200
1851	0.0154	18267	0.0194
2036	0.0154	20909	0.0187
2193	0.0150	23562	0.0181
2518	0.0145	26212	0.0176
2637	0.0156	28939	0.0177
3071	0.0180	31737	0.0165
		34506	0.0161

TABLE 2.11 Data summary for the GA-3 passage (Test# 1).
(L_e/D_i = 8.9, L_p/D_i = 97.3)

Re	*f*	*Re*	*f*
381	0.0781	4136	0.0210
614	0.0421	4477	0.0220
627	0.0460	5156	0.0232
701	0.0368	6193	0.0239
784	0.0331	6290	0.0237
865	0.0303	7250	0.0242
943	0.0280	8771	0.0231
1020	0.0261	8860	0.0237
1096	0.0245	10997	0.0225
1122	0.0252	13013	0.0217
1172	0.0231	13286	0.0214
1249	0.0218	15437	0.0207
1326	0.0206	17630	0.0201
1403	0.0195	19926	0.0195
1560	0.0186	22114	0.0190
1716	0.0177	24531	0.0183
1848	0.0179	24595	0.0182
1866	0.0176	26830	0.0178
2118	0.0171	29203	0.0174
2222	0.0188	29255	0.0172
2588	0.0196	31727	0.0169
2858	0.0201	34144	0.0163
2947	0.0195	36639	0.0160
3122	0.0190	39204	0.0156
3299	0.0202	42069	0.0152
3644	0.0211	44605	0.0150
3950	0.0209	47275	0.0147
3981	0.0220	50055	0.0145
		52749	0.0142

TABLE 2.12 Data summary for the GA-3 passage (Test# 2).
(L_e/D_i = 38.2, L_p/D_i = 32.3)

Re	*f*	*Re*	*f*
382	0.0748	3664	0.0203
422	0.0689	4002	0.0208
522	0.0474	4145	0.0213
616	0.0413	4499	0.0222
629	0.0413	4521	0.0211
704	0.0358	5172	0.0234
788	0.0308	6045	0.0252
868	0.0314	6213	0.0243
946	0.0272	7269	0.0247
1107	0.0278	8891	0.0244
1126	0.0253	10886	0.0233
1499	0.0212	13118	0.0224
1735	0.0181	15410	0.0217
1886	0.0172	19786	0.0200
2125	0.0187	24340	0.0188
2237	0.0191	29137	0.0179
2605	0.0181	34035	0.0169
2616	0.0181	39125	0.0162
2965	0.0178	44656	0.0153
3132	0.0191	49950	0.0149
3318	0.0198	55105	0.0143
3333	0.0191		

TABLE 2.13 Data summary for the GA-3 passage (Test# 3).
($L_{e,r}/D_i = 1.3$, $L_p/D_i = 29.4$)

Re	f	Re	f
783	0.0403	3304	0.0198
942	0.0304	3370	0.0178
1096	0.0256	3621	0.0177
1249	0.0226	3644	0.0201
1404	0.0198	3649	0.0207
1561	0.0206	3982	0.0206
1568	0.0204	3986	0.0206
1717	0.0178	4128	0.0189
1724	0.0182	4478	0.0213
1850	0.0186	4481	0.0211
1868	0.0183	5154	0.0217
1874	0.0169	6150	0.0234
1926	0.0162	6193	0.0229
2038	0.0186	7249	0.0232
2125	0.0166	8322	0.0230
2224	0.0177	9415	0.0227
2224	0.0164	11175	0.0219
2373	0.0160	12834	0.0214
2590	0.0169	15385	0.0203
2592	0.0177	19837	0.0190
2621	0.0164	24307	0.0179
2870	0.0173	29082	0.0169
2949	0.0182	34051	0.0159
2951	0.0188	39120	0.0152
3122	0.0177	44316	0.0145
3300	0.0188	49899	0.0139
		54784	0.0135

TABLE 2.14 Data summary for the GA-3 passage (T_w = 45.5°C).

Re	f	Nu	$\Delta p_{wh}/\Delta p_w$	Re_m	f_m	Nu_m
701	0.0347	6.12	1.00	821	0.0227	4.09
683	0.0380	5.82	1.02	800	0.0249	3.89
924	0.0240	6.56	1.16	1082	0.0157	4.38
941	0.0231	7.19	1.13	1103	0.0151	4.81
1095	0.0221	7.00	1.17	1284	0.0145	4.68
1245	0.0211	7.26	1.15	1459	0.0138	4.85
1395	0.0192	7.84	1.10	1635	0.0126	5.24
1738	0.0177	8.46	1.17	2037	0.0116	5.65
2021	0.0192	9.88	1.11	2368	0.0126	6.60
2195	0.0194	12.64	1.07	2572	0.0127	8.45
2567	0.0216	14.47	1.09	3008	0.0141	9.67
3254	0.0212	20.07	1.05	3813	0.0139	13.42
3601	0.0218	21.12	1.07	4220	0.0142	14.12
3916	0.0220	25.80	1.02	4590	0.0144	17.24
3415	0.0237	22.63	1.04	4002	0.0155	15.13
4498	0.0262	34.80	1.05	5271	0.0172	23.25
7223	0.0211	49.98	1.04	8464	0.0138	33.40
9447	0.0206	66.74	1.05	11071	0.0135	44.60
12700	0.0198	87.61	1.06	14883	0.0129	58.55
15391	0.0191	99.57	1.07	18037	0.0125	66.54
20285	0.0170	124.97	1.08	23772	0.0111	83.52
24996	0.0156	147.14	1.08	29293	0.0102	98.33
29283	0.0147	165.14	1.07	34317	0.0096	110.37
34833	0.0137	196.84	1.06	40821	0.0090	131.55
38886	0.0129	199.18	1.04	45570	0.0085	133.11

TABLE 2.15 Data summary for the HC-4 passage.

Re	f	Nu	$\Delta p_{wh}/\Delta p_w$	Re_m	f_m	Nu_m
711	0.0250	4.16	1.06	758	0.0260	4.00
1039	0.0178	4.92	1.11	1107	0.0186	4.73
1249	0.0148	5.03	1.13	1330	0.0154	4.83
1242	0.0132	4.62	1.06	1322	0.0137	4.44
1416	0.0114	5.50	1.13	1508	0.0119	5.29
1752	0.0102	6.03	1.21	1866	0.0106	5.80
1915	0.0092	5.97	1.15	2040	0.0096	5.73
2068	0.0095	6.94	1.05	220	0.0098	6.67
2215	0.0112	8.96	1.20	2360	0.0117	8.61
2282	0.0109	8.81	1.07	2431	0.0114	8.47
2412	0.0129	9.61	1.14	2569	0.0134	9.23
2673	0.0131	9.86	1.08	2847	0.0136	9.47
3226	0.0123	12.57	1.09	3436	0.0128	12.08
4721	0.0114	18.97	1.11	5028	0.0119	18.22
7015	0.0108	26.94	1.10	7472	0.0113	25.88
8266	0.0089	25.44	1.08	8804	0.0092	24.44
10259	0.0093	36.03	1.08	10928	0.0097	34.61
14920	0.0091	51.63	1.08	15892	0.0094	49.59
21814	0.0086	67.89	1.07	23235	0.0089	65.22
29163	0.0083	94.00	1.06	31063	0.0086	90.29
35926	0.0081	110.94	1.05	38266	0.0085	106.57
40190	0.0080	126.05	1.04	42808	0.0083	121.08
43392	0.0079	137.64	1.02	46218	0.0082	132.22

TABLE 2.16 Data summary for the HC-5 passage.

Re	f	Nu	$\Delta p_{wh}/\Delta p_w$	Re_m	f_m	Nu_m
709	0.0274	4.18	1.30	743	0.0234	3.65
703	0.0224	4.43	1.17	737	0.0191	3.87
989	0.0250	5.53	1.28	1036	0.0214	4.82
1277	0.0184	5.48	1.33	1338	0.0157	4.78
1479	0.0141	6.14	1.26	1550	0.0121	5.36
1724	0.0133	6.48	1.28	1807	0.0113	5.66
1997	0.0105	6.47	1.18	2093	0.0089	5.65
2066	0.0122	6.61	1.40	2166	0.0104	5.77
2267	0.0137	8.94	1.23	2376	0.0116	7.80
2713	0.0153	11.68	1.19	2844	0.0130	10.19
3017	0.0153	14.50	1.10	3162	0.0130	12.65
4460	0.0144	19.64	1.11	4674	0.0123	17.13
6535	0.0151	30.39	1.08	6849	0.0129	26.51
7956	0.0147	37.59	1.04	8338	0.0125	32.79
9745	0.0142	47.51	1.05	10214	0.0121	41.45
13318	0.0145	65.37	1.05	13958	0.0124	57.02
16199	0.0147	79.94	1.05	16978	0.0125	69.73
18635	0.0147	92.10	1.05	19531	0.0126	80.34
19528	0.0184	106.22	1.05	20466	0.0157	92.66
21518	0.0152	101.12	1.05	22553	0.0130	88.21
24835	0.0156	120.17	1.05	26029	0.0133	104.83
30648	0.0148	139.20	1.05	32121	0.0126	121.43
34747	0.0144	188.63	1.04	36418	0.0123	164.55
34876	0.0144	147.51	1.04	36553	0.0123	128.68
40480	0.0142	176.51	1.03	42425	0.0121	153.98

TABLE 2.17 Data summary for the HC-6 passage.

Re	f	Nu	$\Delta p_{wh}/\Delta p_w$	Re_m	f_m	Nu_m
717	0.0210	4.05	1.05	745	0.0214	3.49
991	0.0171	5.01	1.10	1028	0.0174	4.32
1271	0.0164	5.90	1.04	1319	0.0167	5.08
1480	0.0144	6.61	1.03	1535	0.0146	5.70
1740	0.0105	6.79	1.00	1806	0.0107	5.85
2017	0.0088	6.30	1.09	2093	0.0090	5.43
2090	0.0129	7.52	1.22	2169	0.0131	6.48
2296	0.0120	7.33	1.41	2382	0.0122	6.32
2291	0.0114	8.60	1.20	2377	0.0116	7.41
2731	0.0131	12.69	1.13	2834	0.0133	10.94
3276	0.0119	13.63	1.04	3399	0.0121	11.75
4423	0.0109	19.14	1.08	4589	0.0111	16.49
6573	0.0102	26.89	1.06	6821	0.0104	23.18
7856	0.0094	30.93	1.07	8152	0.0095	26.66
9658	0.0088	37.64	1.08	10022	0.0089	32.45
13243	0.0083	50.85	1.08	13742	0.0084	43.83
15173	0.0088	59.40	1.04	15744	0.0089	51.20
18307	0.0090	72.00	1.03	18997	0.0091	62.06
21290	0.0090	83.08	1.06	22092	0.0092	71.61
24847	0.0091	94.90	1.06	25783	0.0093	81.80
30390	0.0087	118.33	1.06	31535	0.0089	101.99
34338	0.0086	127.85	1.05	35632	0.0087	110.20
39093	0.0085	148.35	1.04	40566	0.0087	127.87
45678	0.0083	173.63	1.03	47400	0.0085	149.66

TABLE 2.18 Data summary for the W-7 passage.

Re	f	Nu	$\Delta p_{wh}/\Delta p_w$	Re_m	f_m	Nu_m
717	0.0279	4.15	1.12	506	0.0342	2.95
844	0.0266	4.94	1.14	596	0.0325	3.51
1006	0.0210	5.13	1.10	710	0.0257	3.65
1268	0.0169	5.64	1.08	896	0.0206	4.01
1605	0.0135	6.20	1.13	1134	0.0165	4.41
1985	0.0118	6.75	1.09	1402	0.0145	4.80
2470	0.0097	7.90	1.18	1745	0.0119	5.62
2963	0.0086	8.31	1.18	2093	0.0105	5.91
3445	0.0078	9.16	1.12	2434	0.0096	6.52
3923	0.0095	10.06	1.16	2771	0.0116	7.16
4871	0.0173	22.49	1.05	3441	0.0212	16.00
6717	0.0181	34.01	1.05	4745	0.0222	24.19
10723	0.0151	48.12	1.03	7574	0.0184	34.22
15906	0.0156	74.80	1.05	11236	0.0191	53.19
20768	0.0159	95.49	1.03	14670	0.0195	67.91
29138	0.0182	136.02	1.01	20582	0.0223	96.74
41707	0.0162	187.81	1.00	29461	0.0198	133.56

TABLE 2.19 Data summary for the W-8 passage.

Re	f	Nu	$\Delta p_{wh}/\Delta p_w$	Re_m	f_m	Nu_m
695	0.0314	3.68	1.21	598	0.0410	3.05
856	0.0203	4.49	1.13	736	0.0265	3.73
1006	0.0173	4.78	1.26	865	0.0225	3.97
1279	0.0140	5.73	1.10	1100	0.0183	4.76
1561	0.0114	6.27	1.11	1343	0.0149	5.21
1916	0.0097	6.45	1.13	1648	0.0126	5.36
2434	0.0078	6.65	1.18	2093	0.0102	5.53
2937	0.0100	11.08	1.10	2525	0.0130	9.21
3412	0.0123	15.15	1.08	2934	0.0161	12.59
3900	0.0121	17.07	1.08	3353	0.0158	14.19
4900	0.0112	21.37	1.08	4213	0.0146	17.76
6833	0.0106	29.44	1.09	5876	0.0138	24.47
10096	0.0091	39.85	1.07	8681	0.0119	33.12
15856	0.0084	59.87	1.05	13635	0.0110	49.76
20148	0.0083	75.64	1.05	17325	0.0108	62.87
28792	0.0085	109.86	1.04	24759	0.0111	91.31
38616	0.0083	141.38	1.03	33206	0.0108	117.51

TABLE 2.20 Data summary for the W-9 passage.

Re	f	Nu	$\Delta p_{wh}/\Delta p_w$	Re_m	f_m	Nu_m
698	0.0323	4.08	1.03	509	0.0366	2.78
842	0.0286	4.68	1.07	613	0.0325	3.20
976	0.0232	5.07	1.04	711	0.0264	3.46
1282	0.0177	5.63	1.02	934	0.0201	3.84
1572	0.0147	6.18	1.17	1145	0.0166	4.22
1947	0.0118	6.91	1.10	1418	0.0134	4.71
2454	0.0100	8.47	1.14	1788	0.0113	5.78
2873	0.0088	9.29	1.06	2093	0.0100	6.34
3364	0.0108	10.58	1.02	2450	0.0122	7.22
3964	0.0149	18.72	1.08	2888	0.0170	12.77
4903	0.0146	23.77	1.05	3572	0.0165	16.21
6671	0.0163	37.67	1.03	4860	0.0185	25.69
10526	0.0153	58.93	1.04	7668	0.0173	40.20
15552	0.0150	87.83	1.05	11330	0.0170	59.91
19195	0.0155	109.27	1.06	13984	0.0176	74.54
23776	0.0148	132.08	1.05	17321	0.0168	90.10
33648	0.0132	171.43	1.03	24513	0.0150	116.94
37260	0.0126	182.69	1.02	27144	0.0143	124.62

TABLE 2.21 Data summary for the W-10 passage.

Re	f	Nu	$\Delta p_{wh}/\Delta p_w$	Re_m	f_m	Nu_m
699	0.0309	3.69	1.18	559	0.0326	2.92
832	0.0272	4.15	1.11	666	0.0287	3.28
975	0.0248	4.61	1.17	781	0.0262	3.64
1260	0.0176	5.47	1.07	1009	0.0186	4.33
1540	0.0143	5.36	1.16	1233	0.0151	4.24
1933	0.0123	6.42	1.19	1548	0.0130	5.08
2362	0.0103	6.95	1.18	1891	0.0109	5.49
2866	0.0090	8.44	1.07	2295	0.0095	6.68
3279	0.0092	9.02	1.06	2625	0.0097	7.13
3384	0.0098	9.64	1.02	2709	0.0104	7.63
3626	0.0120	14.63	1.12	2904	0.0127	11.57
3796	0.0138	24.15	1.03	3040	0.0145	19.09
4875	0.0184	27.26	1.04	3904	0.0194	21.56
6700	0.0197	43.20	1.05	5364	0.0208	34.17
8285	0.0185	51.01	1.06	6634	0.0196	40.34
10878	0.0177	65.68	1.06	8710	0.0187	51.94
11271	0.0145	59.66	1.06	9024	0.0153	47.18
15851	0.0149	87.48	1.08	12692	0.0157	69.18
20180	0.0142	108.73	1.06	16158	0.0149	85.98
28888	0.0139	147.96	1.05	23130	0.0146	117.01
37272	0.0130	169.92	1.02	29844	0.0137	134.38

TABLE 2.22 Data summary for the W-11 passage.

Re	f	Nu	$\Delta p_{wh}/\Delta p_w$	Re_m	f_m	Nu_m
686	0.0313	4.78	1.14	483	0.0359	3.17
841	0.0270	4.82	1.23	593	0.0309	3.20
1003	0.0234	5.14	1.22	707	0.0268	3.42
1268	0.0186	6.17	1.17	894	0.0213	4.09
1595	0.0151	7.01	1.13	1125	0.0173	4.65
1958	0.0129	7.18	1.25	1381	0.0147	4.77
2477	0.0105	8.28	1.17	1747	0.0120	5.50
2951	0.0087	8.94	1.13	2081	0.0100	5.94
3459	0.0110	11.85	1.14	2439	0.0126	7.87
3858	0.0143	19.97	1.09	2720	0.0163	13.26
4906	0.0168	25.88	1.06	3459	0.0192	17.19
6693	0.0178	37.72	1.06	4720	0.0204	25.05
6679	0.0179	37.72	1.06	4710	0.0205	25.05
10194	0.0144	51.03	1.05	7188	0.0165	33.89
14993	0.0140	69.65	1.04	10573	0.0161	46.26
19558	0.0135	87.48	1.03	13792	0.0155	58.10
28356	0.0128	114.17	1.03	19996	0.0146	75.82
36036	0.0122	140.65	1.01	25412	0.0139	93.41

TABLE 2.23 Data summary for the W-12 passage.

Re	f	Nu	$\Delta p_{wh}/\Delta p_w$	Re_m	f_m	Nu_m
736	0.0261	3.21	1.14	1024	0.0182	3.92
848	0.0237	3.84	1.14	1180	0.0165	4.68
995	0.0215	4.15	1.17	1384	0.0150	5.06
1259	0.0166	4.60	1.08	1752	0.0116	5.61
1424	0.0158	5.01	1.15	1981	0.0110	6.12
1584	0.0171	5.36	1.14	2204	0.0119	6.54
1955	0.0179	7.42	1.04	2720	0.0125	9.05
2443	0.0185	10.11	1.02	3400	0.0129	12.33
2925	0.0207	12.66	1.01	4070	0.0144	15.45
3425	0.0221	16.17	1.03	4766	0.0154	19.72
3829	0.0226	18.03	1.03	5328	0.0158	22.00
4852	0.0216	21.76	1.03	6752	0.0151	26.55
6675	0.0213	28.64	1.04	9289	0.0148	34.94
10456	0.0173	38.69	1.04	14551	0.0120	47.20
14801	0.0164	50.90	1.03	20597	0.0114	62.09
20782	0.0154	65.27	1.04	28921	0.0107	79.63
29232	0.0145	81.35	1.02	40680	0.0101	99.25
37112	0.0137	92.71	1.00	51645	0.0096	113.11

TABLE 2.24 Data summary for the W-13 passage.

Re	f	Nu	$\Delta p_{wh}/\Delta p_w$	Re_m	f_m	Nu_m
674	0.0330	3.50	1.17	518	0.0327	2.58
1054	0.0231	4.64	1.20	810	0.0229	3.43
1267	0.0199	5.71	1.25	973	0.0197	4.21
1592	0.0160	6.06	1.10	1223	0.0158	4.47
1950	0.0130	6.66	1.21	1499	0.0128	4.91
2471	0.0112	7.83	1.13	1899	0.0111	5.78
2978	0.0098	8.73	1.13	2288	0.0097	6.44
3396	0.0096	10.39	1.08	2610	0.0096	7.67
3811	0.0145	17.53	1.13	2928	0.0144	12.94
4913	0.0173	26.74	1.06	3775	0.0172	19.74
6718	0.0180	38.76	1.07	5162	0.0178	28.61
10629	0.0164	58.58	1.06	8167	0.0162	43.24
15332	0.0148	87.98	1.05	11780	0.0146	64.94
20422	0.0139	112.90	1.05	15692	0.0138	83.33
28339	0.0132	150.40	1.03	21774	0.0131	111.01
37432	0.0124	200.14	1.02	28761	0.0123	147.72

TABLE 2.25 Data summary for the Y-14 passage.

Re	f	Nu	$\Delta p_{wh}/\Delta p_w$	Re_m	f_m	Nu_m
789	0.0291	4.19	1.20	942	0.0202	3.84
964	0.0235	4.48	1.13	1151	0.0163	4.10
1149	0.0206	5.43	1.16	1372	0.0142	4.98
1431	0.0175	6.02	1.23	1708	0.0121	5.51
1671	0.0156	6.44	1.19	1995	0.0108	5.90
1836	0.0149	6.87	1.05	2192	0.0103	6.30
1911	0.0164	7.49	1.10	2281	0.0113	6.86
1955	0.0179	8.72	1.06	2334	0.0124	7.99
2043	0.0202	10.25	1.14	2439	0.0140	9.40
2198	0.0224	12.38	1.06	2625	0.0155	11.34
2732	0.0236	17.51	1.05	3262	0.0163	16.05
3420	0.0244	22.07	1.07	4083	0.0168	20.22
4757	0.0245	32.44	1.06	5679	0.0170	29.72
6686	0.0241	45.94	1.06	7983	0.0167	42.09
9411	0.0235	63.28	1.05	11236	0.0162	57.98
15400	0.0206	95.55	1.06	18387	0.0142	87.55
20119	0.0209	124.57	1.04	24022	0.0145	114.14
27164	0.0232	160.58	1.01	32433	0.0161	147.13

TABLE 2.26 Data summary for the Y-15 passage.

Re	f	Nu	$\Delta p_{wh}/\Delta p_w$	Re_m	f_m	Nu_m
526	0.0580	4.56	1.06	897	0.0204	3.66
711	0.0412	5.36	1.05	1213	0.0145	4.29
699	0.0423	5.48	1.02	1192	0.0148	4.40
981	0.0358	7.18	1.02	1672	0.0126	5.76
1070	0.0315	7.80	1.06	1824	0.0111	6.25
1228	0.0293	8.11	1.07	2093	0.0103	6.50
1340	0.0306	9.66	1.05	2285	0.0107	7.75
1474	0.0293	10.50	1.02	2513	0.0103	8.42
1707	0.0315	12.21	1.01	2909	0.0111	9.79
1826	0.0312	13.54	1.03	3113	0.0110	10.85
2048	0.0325	16.06	1.02	3491	0.0114	12.88
2298	0.0314	17.91	1.03	3916	0.0110	14.36
2704	0.0321	21.75	1.02	4609	0.0113	17.44
3678	0.0324	29.12	1.04	6269	0.0114	23.35
4821	0.0321	38.33	1.05	8217	0.0113	30.73
6714	0.0312	50.25	1.05	11443	0.0110	40.29
10104	0.0290	71.06	1.04	17222	0.0102	56.98
14117	0.0280	92.60	1.03	24060	0.0098	74.25
18909	0.0265	113.17	1.03	32228	0.0093	90.75
28819	0.0234	154.39	1.02	49119	0.0082	123.80
36301	0.0227	190.50	1.01	61871	0.0080	152.76

TABLE 2.27 Data summary for the Y-16 passage.

Re	f	Nu	$\Delta p_{wh}/\Delta p_w$	Re_m	f_m	Nu_m
702	0.0279	5.67	1.20	711	0.0261	4.13
1061	0.0203	6.90	1.11	1075	0.0190	5.03
1211	0.0166	7.23	1.10	1228	0.0155	5.26
1470	0.0139	7.28	1.16	1490	0.0130	5.30
1688	0.0108	7.90	1.14	1711	0.0102	5.75
1921	0.0104	8.29	1.24	1947	0.0097	6.04
2033	0.0099	8.39	1.08	2061	0.0092	6.11
2319	0.0116	9.52	1.13	2351	0.0108	6.94
2478	0.0142	12.18	1.14	2511	0.0133	8.87
2679	0.0170	15.65	1.12	2715	0.0160	11.40
3644	0.0154	20.22	1.15	3694	0.0144	14.72
4766	0.0150	27.40	1.04	4830	0.0140	19.96
6967	0.0142	37.75	1.08	7061	0.0133	27.50
10106	0.0140	55.04	1.06	10243	0.0131	40.09
14245	0.0144	78.09	1.04	14438	0.0135	56.88
18808	0.0133	99.38	1.03	19063	0.0125	72.39
28164	0.0125	141.82	1.02	28546	0.0117	103.30
35539	0.0125	170.66	1.02	36021	0.0117	124.31

TABLE 2.28 Data summary for the Y-17 passage.

Re	f	Nu	$\Delta p_{wh}/\Delta p_w$	Re_m	f_m	Nu_m
682	0.0303	5.40	1.15	765	0.0255	4.40
977	0.0211	6.91	1.13	1094	0.0178	5.62
1224	0.0165	7.36	1.15	1371	0.0139	6.00
1456	0.0140	7.35	1.17	1631	0.0118	5.99
1706	0.0121	7.39	1.13	1912	0.0102	6.02
1952	0.0112	7.53	1.16	2187	0.0095	6.13
2303	0.0123	9.69	1.15	2581	0.0104	7.89
2767	0.0132	14.39	1.01	3100	0.0111	11.71
3207	0.0137	16.59	1.02	3594	0.0116	13.50
4801	0.0141	26.39	1.05	5379	0.0119	21.48
7118	0.0126	38.20	1.02	7975	0.0107	31.10
10158	0.0137	56.33	1.05	11382	0.0116	45.86
12876	0.0169	74.87	1.02	14427	0.0143	60.95
19166	0.0140	104.15	1.03	21475	0.0118	84.79
28656	0.0146	152.00	1.02	32108	0.0123	123.74
37464	0.0149	187.94	1.02	41976	0.0125	153.00
43428	0.0153	239.14	1.02	48659	0.0129	194.68

TABLE 2.29 Data summary for the Y-18 passage.

Re	f	Nu	$\Delta p_{wh}/\Delta p_w$	Re_m	f_m	Nu_m
720	0.0304	5.96	1.20	760	0.0269	4.64
993	0.0207	6.46	1.19	1049	0.0183	5.04
1248	0.0166	6.48	1.22	1317	0.0146	5.05
1512	0.0123	7.54	1.13	1596	0.0109	5.88
1755	0.0117	7.88	1.23	1853	0.0103	6.14
2024	0.0102	7.81	1.17	2136	0.0090	6.09
2224	0.0104	7.98	1.02	2347	0.0092	6.22
2411	0.0103	9.35	1.02	2545	0.0091	7.29
2636	0.0129	12.52	1.05	2783	0.0114	9.76
2787	0.0140	13.65	1.03	2941	0.0123	10.64
3299	0.0129	15.63	1.04	3482	0.0114	12.19
4930	0.0117	23.38	1.07	5204	0.0103	18.23
6965	0.0108	32.41	1.05	7352	0.0095	25.27
10822	0.0103	48.54	1.06	11422	0.0091	37.84
14815	0.0102	64.73	1.07	15636	0.0090	50.47
20077	0.0097	84.58	1.04	21191	0.0086	65.95
29669	0.0095	121.74	1.04	31314	0.0084	94.91
41263	0.0099	170.14	1.03	43551	0.0087	132.65

TABLE 2.30 Data summary for the Y-19 passage.

Re	f	Nu	$\Delta p_{wh}/\Delta p_w$	Re_m	f_m	Nu_m
693	0.0406	6.00	1.18	659	0.0290	3.48
1030	0.0260	7.62	1.23	980	0.0190	4.39
1345	0.0227	8.04	1.16	1279	0.0166	4.62
1636	0.0168	8.52	1.25	1557	0.0122	4.90
2006	0.0135	9.68	1.13	1908	0.0099	5.57
2264	0.0145	10.67	1.04	2154	0.0105	6.14
2601	0.0170	16.15	1.08	2474	0.0124	9.29
2914	0.0172	17.65	1.09	2772	0.0125	10.16
3964	0.0166	20.06	1.10	3771	0.0121	11.54
4991	0.0152	28.54	1.10	4748	0.0111	16.42
7527	0.0124	39.60	1.12	7161	0.0090	22.79
10408	0.0114	52.81	1.13	9902	0.0083	30.39
14844	0.0096	68.26	1.11	14122	0.0070	39.28
19668	0.0084	85.00	1.11	18711	0.0061	48.91
29202	0.0069	112.96	1.06	27782	0.0050	64.99
38914	0.0065	143.61	1.07	37021	0.0047	82.63

TABLE 2.31 Data summary for the Y-20 passage.

Re	f	Nu	$\Delta p_{wh}/\Delta p_w$	Re_m	f_m	Nu_m
624	0.0396	3.55	1.09	1584	0.0116	4.35
749	0.0370	4.20	1.10	1899	0.0108	5.15
1021	0.0313	5.80	1.08	2590	0.0092	7.11
1315	0.0287	8.41	1.07	3337	0.0084	10.30
1629	0.0320	10.90	1.05	4133	0.0093	13.35
2013	0.0306	13.68	1.08	5107	0.0089	16.75
2385	0.0310	16.68	1.08	6052	0.0091	20.42
2820	0.0308	20.34	1.05	7153	0.0090	24.91
3215	0.0312	22.15	1.09	8156	0.0091	27.13
3931	0.0295	27.48	1.07	9974	0.0086	33.66
5441	0.0279	37.58	1.07	13804	0.0082	46.03
7330	0.0265	48.68	1.06	18596	0.0077	59.62
10503	0.0242	63.47	1.06	26646	0.0071	77.74
14908	0.0222	86.64	1.04	37820	0.0065	106.11
19814	0.0210	106.07	1.04	50267	0.0061	129.90
29516	0.0218	158.88	1.03	74880	0.0064	194.59
31509	0.0219	165.24	1.02	79938	0.0064	202.37

TABLE 2.32 Data summary for the Y-21 passage.

Re	f	Nu	$\Delta p_{wh}/\Delta p_w$	Re_m	f_m	Nu_m
696	0.0357	6.21	1.08	671	0.0253	3.74
1003	0.0298	7.22	1.07	967	0.0211	4.35
1250	0.0213	7.76	1.07	1205	0.0151	4.68
1481	0.0181	8.06	1.05	1428	0.0129	4.86
1739	0.0165	8.63	1.09	1677	0.0117	5.20
1990	0.0168	9.17	1.05	1918	0.0119	5.53
2171	0.0149	11.14	1.09	2093	0.0105	6.72
2340	0.0148	11.14	1.08	2256	0.0105	6.72
2883	0.0165	16.81	1.09	2779	0.0117	10.14
3321	0.0174	19.25	1.07	3202	0.0123	11.61
4927	0.0159	28.39	1.06	4750	0.0113	17.12
7269	0.0140	39.60	1.08	7008	0.0100	23.88
10492	0.0141	58.07	1.04	10115	0.0100	35.02
13481	0.0140	73.80	1.04	12997	0.0099	44.50
19747	0.0136	106.13	1.02	19038	0.0096	64.00
29267	0.0140	160.22	1.01	28215	0.0099	96.63
38673	0.0141	221.02	1.02	37284	0.0100	133.29

TABLE 2.33 Data summary for the Y-22 passage.

Re	f	Nu	$\Delta p_{wh}/\Delta p_w$	Re_m	f_m	Nu_m
692	0.0488	9.42	1.23	523	0.0304	3.68
1068	0.0385	10.34	1.27	807	0.0240	4.04
1161	0.0283	9.75	1.24	877	0.0176	3.81
1595	0.0283	11.98	1.17	1205	0.0176	4.69
2033	0.0230	13.26	1.18	1536	0.0143	5.19
2194	0.0182	12.95	1.07	1658	0.0113	5.06
2550	0.0180	12.56	1.05	1927	0.0112	4.91
2770	0.0160	15.71	1.21	2093	0.0099	6.14
3318	0.0179	16.60	1.11	2507	0.0112	6.49
4622	0.0142	21.78	1.04	3492	0.0088	8.52
4996	0.0142	27.74	1.05	3775	0.0088	10.85
7085	0.0129	37.72	1.09	5354	0.0080	14.75
9551	0.0117	50.50	1.02	7217	0.0073	19.75
14252	0.0116	70.94	1.10	10769	0.0073	27.74
14260	0.0117	81.97	1.11	10775	0.0073	32.05

TABLE 2.34 Data summary for the Y-23 passage.

Re	f	Nu	$\Delta p_{wh}/\Delta p_w$	Re_m	f_m	Nu_m
679	0.0661	7.31	1.04	599	0.0369	3.49
984	0.0383	8.39	1.08	869	0.0214	4.01
1221	0.0324	10.47	1.05	1078	0.0181	5.00
1552	0.0238	9.68	1.10	1370	0.0133	4.62
1951	0.0194	9.92	1.09	1723	0.0108	4.74
2431	0.0173	13.05	1.09	2146	0.0097	6.23
3059	0.0167	16.65	1.10	2701	0.0093	7.95
4135	0.0171	22.31	1.02	3650	0.0095	10.66
4958	0.0177	28.03	1.03	4377	0.0099	13.39
6784	0.0164	39.49	1.02	5989	0.0092	18.86
9680	0.0148	55.68	1.03	8545	0.0083	26.60
14914	0.0131	85.06	1.03	13165	0.0073	40.63
19101	0.0127	108.68	1.06	16862	0.0071	51.91
23480	0.0119	130.38	1.03	20727	0.0066	62.28

END

DATE FILMED

8/21/92